



Università
Ca'Foscari
Venezia

Master's Degree programme in
Conservation Science and Technology for Cultural Heritage

Final Thesis

*Identification strategies for textiles based on non-invasive
analyses for the application on historical museum artworks*

Supervisor

Eleonora Balliana

Graduand

Francesca Regnotto

870674

Academic Year

2022/2023

Table of Contents

Introduction	4
The tradition of silk in Venice	4
The renaissance of the Venetian textile industry	6
The recovery of an ancient art.....	7
An introduction to textile fibers	9
The composition of fibers	10
Natural fibers	10
Protein fibers	10
<i>Wool</i>	11
<i>Silk</i>	14
Cellulosic fibers	16
<i>Seed fibers: cotton</i>	17
<i>Bast fibers: linen and hemp</i>	19
Synthetic fibers.....	20
<i>Polyester</i>	21
Aim of the research	22
Materials and Methods.....	23
Optical microscopy	24
<i>Sample preparation</i>	25
Infrared spectroscopy.....	25
Raman spectroscopy.....	27
Fiber Optics Reflectance spectroscopy.....	28
The samples	29
Results and discussion.....	31
Optical microscopy	32
Animal fibers	32
<i>Wool</i>	33
<i>Silk</i>	47
Cellulosic fibers	51
<i>Cotton</i>	51
<i>Linen</i>	55
<i>Hemp</i>	59
Synthetic fibers.....	62
<i>Polyester</i>	62
Spectroscopic analyses.....	65
Animal fibers	65
<i>Wool</i>	65

<i>Silk</i>	69
<i>Cotton</i>	72
<i>Linen</i>	74
<i>Hemp</i>	Error! Bookmark not defined.
<i>Polyester</i>	76
<i>Appendix XX</i>	90
<i>Bibliography</i>	97

Introduction

The words “Venice” and “textiles” have been intertwined since long before the city reached its most flourishing period. Before the foundation of Venice, in fact, the neighboring city of Altino, and later the island of Torcello, were the first urban areas of the Venetian lagoon to produce and trade fine wool to the near Roman provinces since the II century b.C (Tessitura Luigi Bevilacqua, 2016). It is thanks to the surrounding water streams, the direct opening on the lagoon, and the proximity to the Annia way, which connected this area to other important Venetian cities such as Padua, Adria, and Aquileia, that Altino owes the success of its textile business activity. Unfortunately, the V century was the scenario of the harsh barbaric invasions that hit the cities of the Roman Empire, including Altino, and of the phenomenon of rising waters in the Venetian lagoon. For these reasons, the population of the mainland decided to move to the many islands of the lagoon, forming what will become the city of Venice. But not all the land cities in the Venetian area underwent the sudden mass relocation; Altino, in fact, endured until the VII century, before the population moved to the island of Torcello in the year 639 by order of the bishop of the city. Despite its downfall, the altinian textile-making tradition was carried on in Torcello, where artisans continued the production of fine wool at least until the XIV century before being completely surpassed by Venice, which had, in the meantime, discovered and mastered the art of producing and trading silk.

The tradition of silk in Venice

We often associate the Middle Ages with a somber era ruled by deadly diseases, famine, conflicts, and oppressive religious convictions. However, it is unfair to consider the Middle Ages as an untamed era, but instead one should think of it as a period of enrichment and discoveries despite the many difficulties that characterize this time. In particular, the business relations between today’s Europe and the Eastern land significantly contributed to the extension of many aspects of the culture of the Western world. A fitting example of these commercial exchanges is the Silk Road, namely all the itineraries by land, rivers, and sea, that linked the western and eastern lands for commercial purposes. The name derives exactly from the significant exportation of silk textiles from China and Venice, being one of the most important commercial harbours of the time, benefited from this situation.

Historians are not exactly sure about how silk first came to Europe. Some suggest that in the year 53 b.C. the Romans first met this material during the battle of Carre, the today’s Harran (Turkey), against the Parti. The roman enemies, in fact, marched hoisting their silk banners, which dazzled the roman soldiers. From that moment on, Rome begun the import of silk textiles using the Silk Road. The provenance and manufacturing process of silk was still unknown since the Romans used to buy this fibre not directly from China. Pliny the Elder, for instance, described silk in his treaty *Naturalis Historia* (I century a.C.) as “lanicium silvarum,” yarn from the woods, because the widespread belief attributed the provenance of silk to plants. (Tessitura Luigi Bevilacqua, 2020b). The European production of silk started with the work of the

emperor Giustiniano (VI century), who ordered secret expeditions to China to discover the secrets of the silk-making tradition; in this country, in fact, the silk industry had been an exclusive activity since the 2700 b.C. (Tessitura Luigi Bevilacqua, 2020b). The import of silk into the western continent was, therefore, already affirmed in the Christian Era (I-V century a.D.) and, during the reign of the emperor Giustiniano, it also involved Byzantium. This city had a consistent commercial connection with Venice, which was the only marine power that had total liberties in the export of Asian goods (Tessitura Luigi Bevilacqua, 2020a). The expeditions to China conducted by the Polo brothers in the XIII century contributed to the expansion of the knowledge about silk and its potential. In 1265, for example, the Art of Samiteri started the production of the finest silk textile of the time, the *sciamito*, which is the precursor of the famous Venetian velvet (Tessitura Luigi Bevilacqua, 2016). Venice became one of the few cities that imported luxury materials such as spices, ivory, and foreign textiles, and soon became a crucial centre in Italy to produce fine silk textiles, reaching its peak in the XVI century (Tessitura Luigi Bevilacqua, 2020b).

The silk production in Venice is known as *auroserica*, consisting of the braiding of silk, gold, and silver threads. The tight connections with the culture of the export countries, Chinese and Arabic, affected the way the venetian weavers learned the art of silk threading. For instance, Antinope, a Greek weaver expert at the service of the emperor Henry IV (XI-XII century), is a key figure in the history of the auroseric production in Venice since he passed onto the venetian artisans some of the fundamental procedures for the implementation of auroseric textiles. As previously mentioned, another valuable contribution was given by the Polo brothers who, in 1269, returned from their first trip to China with innovations such as the phytomorphic and zoomorphic motifs to decorate silk textiles. This improvement marks the beginning of the transformation of the decor tradition of venetian textiles that developed in the XIV century: from now on, eastern allegoric symbols like flowers, lotus leaves, peonies, and imaginary animals encountered the symmetric naturalism of the venetian tradition, along with the Christian symbolism that included calves, parrots, and peacocks. The development of the Venetian textile making industry was also affected by another textile power of the peninsula; the expert weavers from Lucca, for instance, came to Venice between 1307 and 1320 to share their skill and knowledge about velvet, a key artifact in the Venetian textile heritage. Velvet became, indeed, the most refined and requested fabric produced in Venice and, towards the end of the XIV century, it was commissioned and used by the wealthiest families and the prominent characters of the political scene of the time as a statement piece of wardrobe (Tessitura Luigi Bevilacqua, 2020a).

The production of velvet and the prestige it brought to the city became so important and settled in the Venetian culture that, at the end of the XIV century, the Court of the Paragon was established in Venice. This institution had the duty to collect, preserve, and catalogue patches of every textile of the Venetian production to guarantee the respect of the quality standards of the newly produced fabrics before being commercialized. The court mandated that every textile artisan should bring their creations to the *Offizio* to be compared with the ones there preserved. If the fabric failed the test they were destroyed because fabrics with a quality level inferior to the standards were not allowed to be sold, especially outside Venice (Campagnol, 2007).

Further preventive protective measures for the art of silk-making were taken, such as the import ban regarding auroseric textiles except from the ones acquired from the East; or the prohibition towards the master weavers to work outside Venice, along with the fact that it was absolutely prohibited for slaves to learn the art of textile making. These precautions led to the official regulation of the textile production to maintain the highest quality levels of each product. In 1366 the commission of vigilance for the silk production was nominated to establish the Sazo, namely an institution with the aim of administrating the dyeing procedures. The production of velvet was also under strict control and regulations thanks its prestigious. For example, both manufacturing techniques and tools were under constant examination and the dimension of each patch was predetermined before being branded. This strict control behaviour will reveal itself, as time goes by and as the economy changes, as counterproductive for the local textile industry of the lagoon area (Campagnol, 2007).

Towards the end of the XVI century a new typology of textile made its way through Venice's textile industry: furnishing fabrics. The differentiation between clothing and furnishing products was a consequence of the evolution of the necessities in the fashion world of that time; walls, draperies, backrests, and canopies needed to be adorned with fabrics with specific motifs inspired by wall paintings, sculptures, and stained glass decorated with grotesque fantasies. This new fashion design trend significantly surpassed the silk production in Venice in the XVII century, but the annual revenue of the textile industry, instead, improved thanks to the increasing demand of new kinds of fine fabrics required in the décor field.

The renaissance of the Venetian textile industry

The art of textile making in Venice kept its primacy until the XVIII century, when the prestigious French manufacture, specifically the extravagant and cheaper silks of Lyon and the newly introduced "simple" style influenced by the fashion statements of the queen Marie Antoinette, started to overtake this position in the European market. Therefore, the heavy and precious silk brocades, typical of the Venetian production, adorned with intricate metallic broderies, were completely banned from the international fashion market in the second half of the XVIII century. Most of the weaving companies in Venice were forced to shut their production also due to the severe protective restrictions exerted by the Venetian government on the silk industry that, instead of preserving its commercial power, put to disadvantage the Venetian textile economy against the ever-growing foreign competition. Many technological deficiencies also worsened the already difficult scenario. This situation was destined to deteriorate with the fall of the Serenissima Republic in 1797, decreed by the Main Council of Venice, under the Napoleonic army. This event led to a further crisis in the local social, political, and economic structure of the Venetian society which, eventually, passed onto the traditional textile arts (Campagnol, 2007). Thankfully, the venetian silk business managed to survive thanks to some historical weaving companies who, by combining their historical knowledge with the modern creative vision of the contemporary artisans, brought back the antique splendour of the Venetian industry back at the beginning of the XX century. Among these there are the Tessitura Luigi Bevilacqua, founded in 1875, the newly settled Fortuny,

which started its textile production in 1907, and Rubelli, founded in 1889 (Tessitura Luigi Bevilacqua, 2020).

The recovery of an ancient art

To revive the economic situation in Venice at the beginning of the XIX century the government decided to put in place a specific plan. At first, the idea of renewing the economy through the substitution of the textile business with the modern chemical industry was the most popular. The main goal was to modernize the old crafts, that characterized the Venetian economy, following the models of a better-organized and cheaper industry that was spreading through the northern European countries such as France, England, and Germany. Thankfully, these drastic changes were avoided thanks to a few determined local realities that deeply cared for the heritage tradition of the weaving industry of Venice. New institutions were established to preserve and study all those Venetian works of art that had been seized by Napoleon after the surrender of the Venetians. Although most of them were shipped to France, many remained gathered in the city and, thanks to the dedication of Pietro Selvatico, a Paduan architect and art historian, the *Gallerie dell'Accademia* were formed. His vision of salvaging the local art works and crafts later expanded to the island of Murano, where the first school of applied and industrial art was established, and which included the first *Glass Design School* founded by the priest and glass expert Vincenzo Zanetti. This preserving phenomenon gave life to other many institutions and schools that aimed at producing the traditional crafts, such as the glass production, the study of textile arts, and woodwork, and the training of future artisans who could pass on to the future generations the Venetian craftsmanship. An example is the *Burano Lace School*, established in the lagoon island of Burano in 1872. Here, women had at the opportunity to learn the art of lace making and this, other than raising the economy of the fishing island, gave them international recognition to be displayed at the Paris International Exhibition in 1925. This event launched the Venetian lace into the fashion system, becoming a statement symbol of European nobility.

What about the classical Venetian textiles in this time of rebirth? The textile production at the beginning of the XIX century was still struggling. The active weavers producing silk brocades and velvets in the city in 1831, according to the documents of the Venetian State Archive, were only three. The technological instrumentation of these industries, who were still working with manual looms as in the sixteenth century, was obsolete compared to the modern factories used in the other European countries. In fact, for example, the Jacquard loom, an intricated invention by Joseph-Marie Jacquard (1801) and which allowed for the weaving of complex designs, was absent in Italy despite being extremely popular in France and Germany. However, the incorporation of Venice into the newly formed Italian kingdom in 1861 led to an improvement of both the political and economic scenarios, which eventually passed onto the textile industry. A key figure of this renovation is Lorenzo Rubelli, who in 1889 acquired the G.B Trapolin weaving mill, later known as “Giovanni Battista Trapolin successor Lorenzo Rubelli”, one of the few still operating in Venice (Campagnol, 2007)).

Lorenzo Rubelli was born in 1847 in Venice. Grandson of Giovanni Paolo Rubelli, who was a member of the Art of the Silk Merchants of Venice since 1781 and owner of a fabrics shop, Rubelli continued the luxurious production of silk textiles of the late Trapolin Industry, earning already in the early days of his activity the title of the most renowned weaving company in Veneto. The fame and prestige of the Trapolin-Rubelli craftsmanship was so appreciated that it led them not only to satisfy the commissions of high-profile characters such as Queen Margaret of Savoy, but also to broaden their business and open a branch in other important Italian cities like Florence, Rome, Milan, and Turin. But Rubelli not only follows and perseveres with the traditional Venetian weaving work by still using original looms from the XVII century, but it is also attentive to the modernity and the changes it brings. Within the XX century, in fact, Rubelli developed many collections designed by relevant Italian architects and designers, among which there are Gio Ponti, Vittorio Zecchin, and Alfredo Carnelutti; these collections were often exposed to important exhibitions such as the international Biennale of Arts in Venice in 1934. The elegance of the Rubelli products also landed in the fashion universe in the 1950s with the first collaboration with the famous Venetian brand Roberta di Camerino, who wanted to use Rubelli's velvets to produce bags. During the 1970s the brand opened several international branches in Paris, New York, London, and Dubai, affirming its production at global level, and in the 1980s begun its contract division, supplying technical textiles for public spaces such as hotels, cruise ships, and theaters (Rubelli, 2023). Thanks to the collaboration between Ca' Foscari University and Rubelli, we were able to characterize and study a set of modern industrial samples provided directly by the company and, for this reason, I would like to thank Mr. Alberto Pezzato for taking interest in our activity and Mr. Marco Martinuzzi for his availability, kindness, and his exhaustive explanations of the processing steps of the fabrics.

An introduction to textile fibers

Textile fibers exist in a plethora of kinds and their variations consist in chemical composition, origin, and physical characteristics. They are mostly associated with fashion and domestic use, but textiles are also studied and applied in the industrial field where, when needed, their characteristics and properties are implemented according to the required purpose.

The best way to classify textiles is by chemical type. Above the chemical classification, they are broadly grouped in natural and human-caused fibers. Naturally, the textile market has been dominated for centuries by natural fibers, wool, silk, and later cotton. It is not until the end of the XIX century that the first artificial fibers started to develop, for example viscose. It is not entirely right to denominate these materials as synthetic since they were regenerated fibers, that is reworked textiles derived from natural matrixes such as cellulose. Real synthetic polymers, instead, renewed the textile industry and commerce starting from the 1930s with the aim of improving specific features of textile materials, an action that was not completely possible with natural fibers; nylon and polyesters are among of them (Mather & Wardman, 2015).

Textile fiber is a material characterized by a long and thin body. Many are the fibrous structures present in nature, but only the ones that can be worked into yarns are useful in the textile industry, both fashion and technical. Natural fibers usually exist as staple fibers that can be twisted to produce yarns through a spinning process, which relies on the surface roughness of the fibers required for them to adhere to one another. The lengths of the filaments range from 2-50 cm and their thickness from 10-40 μm . Synthetic fibers and silk are, instead, produced in continuous strand yarns and are sometimes cut to meet the required length. These yarns appear softer, fuller, and are used for knitwear and to be blended with natural fibers to improve their characteristics (Mather & Wardman, 2015).

The geometry and morphology of fibers are key factors to consider when characterizing fibers. In fact, as we shall see in the results section, a first general differentiation between several fiber types is made through the observation of their morphologies under optical microscope.

In the following paragraphs the chemical composition and class of belonging of each fiber type characterized in this project will be briefly introduced.

The composition of fibers

Natural fibers

Among the natural fibers there are three chemical classes:

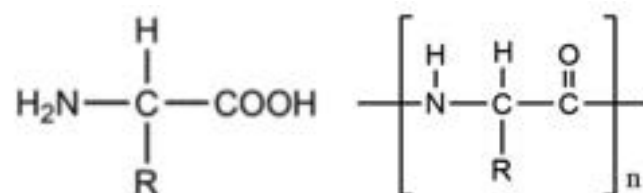
- *Protein*, obtained from wool, hair, and silk;
- *Cellulosic*, obtained from plants including stems, leaves, and seeds;
- *Mineral*, this class includes only one typology of fiber, namely asbestos, which is banned from a variety of countries due to its high toxicity.

The natural fibers studied in this work are wool, silk, cotton, linen, and hemp.

Protein fibers

Animal, or protein, fibers derive from animal hair and secretions. Animal fibers are composed of protein molecules, which are biomolecules made up of chains of amino acid residues. The main proteinaceous component, responsible for the hair's known strength, is keratin (Markova Ivana, 2019). Another excellent feature of keratin is its elevated content of cystine, a sulphur-rich amino acid, which is a differentiating factor between wool and silk, which derives from animal secretions and whose main protein component is, instead, fibroin that does not contain cysteine (Mather & Wardman, 2015). The keratin in wool and hair fiber and the fibroin in silk are structural proteins (Timar-Balazsy & Eastop, 2011).

But, more precisely, what is a protein? Proteins are polymeric materials present naturally in mixtures that vary considerably according to their source. Their linear polymer chains are known as polypeptides, the name coming from the peptide bonds (-CO-NH-) that link the amino acid units together (Timar-Balazsy & Eastop, 2011). Proteins are built from 20 different amino acids. Although being chemically different, there is a consistent resemblance within the molecules of this family. In fact, at the basic end of every amino acid unit (1) there is the amino group (-NH₂), while at the other extremity, the acidic end, is located a carboxyl group (-COOH); it is the composition of the side-chain R that differentiates one amino acid from another.

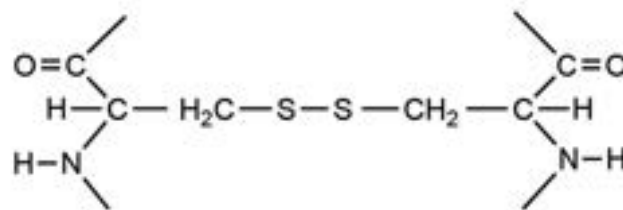


(1)

Due to the presence of these two functional groups of opposite chemical character, amino acids are to be considered as amphoteric, namely having a dual basic-acidic behaviour based on the pH of the solution to which the amino acid is added. We refer to the isoelectric point of the amino acid as the pH at which the basic and acidic contributions of the molecule are in

equilibrium. When the positive and negative charges are in equilibrium, in fact, the molecule is electronically neutral and takes the name of zwitterion. If the pH is below the isoelectric point, so if the value is acidic, the positive charge of the basic character is dominant and vice versa. Amino acids existing in living organisms are, apart from proline and hydroxyproline, α -amino acids, where the amino functional group is linked to the α -carbon next to the carbonyl group. For this reason, α -amino acids, except from glycine, whose R group is made of an H atom, are optically active compounds, meaning that they rotate polarized light to the left or to the right (Timar-Balazsy & Eastop, 2011).

Amino acids can be classified based on a variety of factors, such as pH, the polarity of the R groups, the aliphatic or aromatic behaviour of each, and the absence or presence of Sulphur. Cystine, for example, which is an important amino acid in wool chemistry that links adjacent keratin chains through covalent cross links (Mather & Wardman, 2015), is among the amino acids containing this element (Timar-Balazsy & Eastop, 2011).



Wool

There are many animal species from which it is possible to obtain wool; the most common is sheep, whose yarn is derived from shearing. The varieties coming from goats, Angora rabbit hair, and camels, instead, are considered luxury breeds due to the difficulties in obtaining their wool, which include the collection of the animal's fur (Markova Ivana, 2019). This luxury group also includes cashmere, mohair, alpaca, and yak hair and whose distinctive properties are remarkable softness, handling facility, resilience, and luster (Notayi et al., 2022a). There is, therefore, a very wide range of fiber structures when talking about wool, and their distinctions depend on the quality and provenance of each fiber. Different fiber morphologies are detectable even within the same animal species. Sheep wool, for example, exists in a great diversity depending on the single fleece of each animal, which is an aspect strongly affected by genetics, physiological, and nutritional conditions in which the animal was raised in (Mather & Wardman, 2015). Wool is classified according to the average length and diameter of the individual fibers: coarser wool fibers, for example deriving from Lincoln, Leicester, and Romney sheep, with larger lengths and diameters are less comfortable to wear due to their hardness and are used for rugs and carpets. The finest sheep wool, instead, is derived from Merino sheep, which is a breed originally developed in Spain, and now associated with Australia (Mather & Wardman, 2015).

Raw wool fibers contain impurities that can constitute from 30% to 70% of their total mass. These impurities include wool grease secreted from the sebaceous glands of the animal's skin,

consisting of esters formed by the combination of sterols with aliphatic alcohols and fatty acids, sweat, made of potassium salts of organic acids, dirt, and sand, whose amount gives information about the breeding conditions of the animal. Vegetable substances up to 5% can also be included in the list of impurities (Mather & Wardman, 2015).

Despite the differences among the numerous typologies, each wool fiber consists in three main structural regions: cuticle, cortex, and medulla.

The *cuticle* is the outer non-fibrous layer of the fiber that contains scales, also known as epidermis; the scales are covered in a thin membrane called epicuticle (Markova Ivana, 2019). Animal fibers are the only fiber type existing with an external layer of scales; therefore, this peculiarity allows a first distinction between animal and vegetable fibers under preliminary analyses under optical microscope.

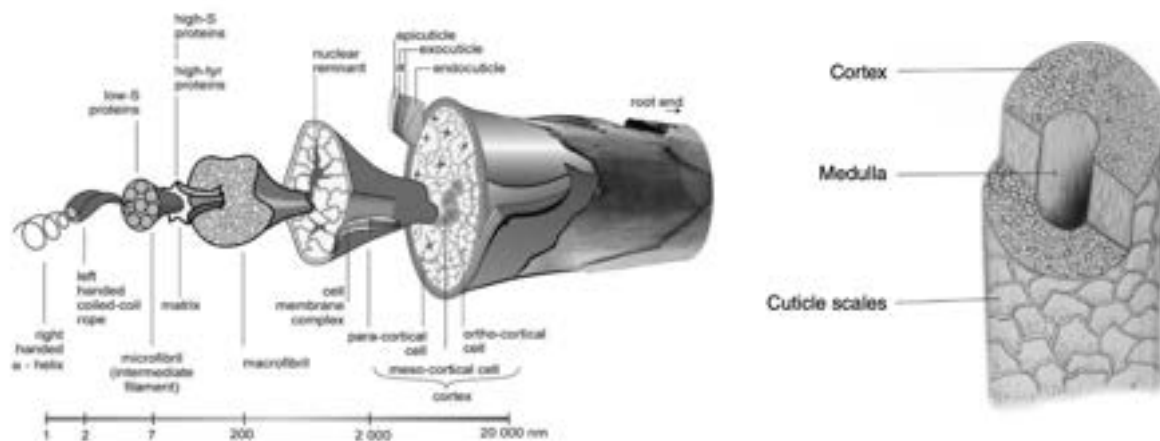


Figure XX: diagram of the morphology of a wool fiber by Mather & Wardman, 2015 and Markova, 2019

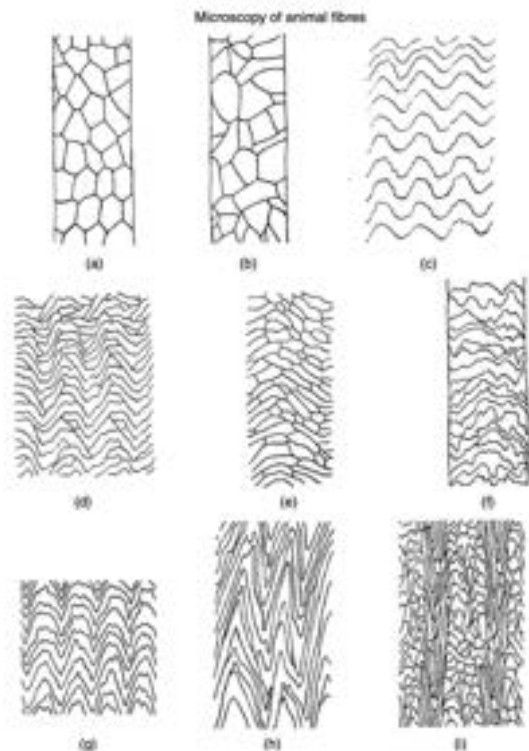
Cortical cells are responsible for the surface properties of wool and constitute circa 90% of the overall fiber and are separated from the underlying cortex by a cell membrane layer which also keeps the cuticles together. The cuticular cells, each of them approximating a rectangular shape with ca 30 μ m of length, ca 20 μ m of width, and ca 0.5 μ m in thickness, overlap each other creating a squamous surface. This orientation produces the directional frictional effect that allows wool to be extremely adequate to felt. Felting is an important property in the world of textile fibers and consists in the progressive entanglement of wool fibers when they are being subject to a mechanical action, that could be agitation in water. With felting, although becoming thicker and bulkier, the fabrics are more prone to undergo shrinkage during washing (Mather & Wardman, 2015).

Each cuticle is subdivided into three layers, namely epicuticle, exocuticle, and endocuticle (Fig XX). The *epicuticle* is a thin but resistant surface membrane containing keratin chains and a small quantity of lipid, which surrounds all the cuticular and cortical cells. The *exocuticle* constitutes the 60% of each cuticular cell and is divided into two subcomponents, which are not precisely defined: the A-layer, laying adjacent to the epicuticle, contains higher contents of cystine compared to the B-layer. Finally, the *endocuticle* is set below the exocuticle and

consists in a well-defined layer with low levels of cystine, being therefore a non-keratinous component of the wool fiber. The endocuticle constitutes the weaker component of the animal fiber; when rugs become worn out, for instance, it could be due to the fracturing of the endocuticles (Mather & Wardman, 2015).

The *cortex* is the main component of the wool fiber, and from which derive all the mechanical properties of the fabric, such as crimping, a property that helps wool fibers to better cling together for an improved strength of the overall yarn (Markova Ivana, 2019). It has a complex structure, consisting in spindle-shaped cells aligned along the fiber axis, and it is differentiated between two types of cortical cells: the orthocortex and the paracortex, distinguishable from each other by the allocation of the non-keratinous material within each cell. In the paracortical cells, for instance, the non-keratinous matter is in the nuclear remnants. Cortical cells are made of macrofibrils, which are cylindrical units with a diameter of ca 0.3 μ m, consisting of hundreds of microfibrils embedded in a matrix. Microfibrils are made of keratin chains divided into four sections of α -helix separated by three non-helical segments. The matrix, instead, consists in amorphous keratinous material, and is present majorly in paracortical cells compared with orthocortical cells (Mather & Wardman, 2015)

Lastly, the *medulla* is the central canal of wool fibres where the colour or pigment that characterize the breed is present; it is in the cortical layer and runs down to the centre of the fibre. The size and shape of the medulla varies widely, but it mainly consists in either continuous, interrupted, or fragmented line. This section contains air spaces that provide thermal insulation and confers wool of its light-weight properties (Markova Ivana, 2019). The components of the wool fibre are held together by the *cell membrane complex*, which is a continuous network diffused through the whole structure. The complex is made of three components: the intercellular cement, consisting of non-keratinous proteins, a lipid component, and a chemically resistant membrane, made of keratinous material. This latter component bonds each cell with the rest of the membrane complex (Mather & Wardman, 2015).



Wool fibers have a peculiar morphology that can be easily evidenced under an optical microscope. Their surface is, in fact, characterized by the presence of scales, or cuticles, which allow a fast differentiation between this specie and the other natural and synthetic fibers. In fact, the scaly surface of wool is the most characteristic feature among animal fibers. Fibers with angular and prominent cuticles, for example, will suggest the belonging to wool; while smoother surfaces are linked to luxury fibers, such as Cashmere (Greaves & Saville, n.d.). Scales are, in turn, classified in five groups (Figure XX) based on their pattern, namely mosaic, coronal, pectinate, chevron, and petal. The scale configuration varies based on the fiber specie.

Fine fibers, for instance, have overlapping scales that form a smooth surface, without sticking on the outer side. This gives the fiber the quality of being non-irritating on the skin. Coarse and medium fibers, on the other hand, are characterized by smaller and denser scales (Markova Ivana, 2019). Merino wool is a fitting example of fine wool, presenting the irregular mosaic pattern with smooth margins, in which the cuticles follow a coronal disposition where the scales are large enough to encircle the entire circular surface of the fiber. This characteristic is not present in coarse fibers (Markova Ivana, 2019).

With the optical microscopy instrumentation available in our facilities, therefore with the maximum available magnification of 63x, it was possible to identify the morphological differences between the fiber species, and to observe slight distinctions between fibers of the same species, for instance in the disposition of the cuticles in wool fibers. Further microscopic analysis at higher magnifications, with a Scanning Electron Microscope (SEM) for example, would allow an even more detailed morphological study, i.e., enabling the definition of scale margins among different wool fibers.

Silk

Silk derives from an off-white moth of various species, mainly *Bombyx mori*, but also the Indian Tussah moth *Antheraea mylitta*, and the Chinese Tussah moth *Antheraea pernyi* are among them, that secretes the protein in liquid form while preparing its cocoon. The substance discharged by the silkworm hardens into twin filaments of fibroin protein, cemented together with another protein, sericin (Timar-Balazsy & Eastop, 2011).

The life of a *Bombyx mori*, the most famous silk producer, may be short but intense. In fact, it lasts for about 50 days, where, in sericulture, the larva spends the first 30 to feed solely on mulberry leaves; this frenetic activity allows the complete filling of the silkworm's silk glands

with fibroin. The unsuspecting worker, after finding an adequate support, is now ready to spin its cocoon (Mather & Wardman, 2015). The silkworm completes the structure within a period of 3-6 days; it expels the protein through two openings on its head. The two filaments, as previously mentioned, are joined together by sericin, which is a protein gum extruded from two adjacent glands. The overall length of the filament in which the silkworm surrounds itself is of 1-2 km. When the cocoon is completed, the worm enters its chrysalis phase for about 3-4 days and then, after another 10 days, into a completely developed moth. To escape its silky cage, the silkworm secretes an enzyme able to soften the cocoon, however damaging the silk filaments. To avoid this natural situation, the cocoons undergo a treatment with hot air, at around 110°C, for a few hours. This process kills the chrysalis, maintaining the silk untouched. Sericin can also be removed from the threads by a degumming procedure, consisting in the isolation of the twin fibroin filaments. Degumming was traditionally performed using a soap solution for a several hours, but other procedures exist in which proteolytic enzymes are implied, along with hot water at high pressure with dilute solutions of alkali or acid. After the degumming process, silk is usually bleached in hydrogen peroxide and rinsed (Mather & Wardman, 2015). Silk that is not degummed is called, in the industry, raw silk (Markova Ivana, 2019). Silk exists in two main types: cultivated and wild. Cultivated silk, majorly coming from *Bombyx mori*, is finer and of higher quality and is, therefore, the most common. It is characterized by a triangular cross-section, whose edges allow light to be evenly reflected giving cultivated silk its peculiar luster. This silk variety has a small diameter and this, along with the smoothness of its rods, make it easier to confound it with synthetic fibers such as nylon. Wild silk, instead, since developing in an uncontrolled environment is not as uniform and valuable as cultivated silk. It includes two main varieties, Tussah and Anaphe. The first is the most used, and its longitudinal shape appears broader and with length wise striations, with a twisted and flat cross-sectional appearance shaped like a wedge. Anaphe, instead, presents cross-striations at intervals along the longitudinal shape of the fiber. The cross-section of this variety is triangular-shaped, but it shows some differences compared to the triangular section of cultivated silk. In Anaphe, in fact, the apex of the triangle is elongated and bent. (Markova Ivana, 2019).

An interesting alternative for silkworms is spiders. Spiders, as it is commonly known, produce silk to create their spider webs. Spider silk is known for its outstanding strength, five times that of steel, since its main objective is to trap and hold insects of a variety of dimensions; this property is now studied to be used in protection wear. Other than being impressively strong, spider silk is also very elastic, lightweight, and can absorb energy without breaking, characteristics that are also of interest in the technical wear field (Markova Ivana, 2019).

As previously mentioned, silk is composed of the protein fibroin and sericin; the latter, since being non fibrous, differs in the chemical composition with respect to fibroin.

Sericin contains mainly polar side groups rather than non-polar Rs. 60% of the polar groups are hydroxyl groups (-OH), making sericin soluble in water. Fibroin, instead, is the simplest among the structural proteins considering its amino acid sequence composition. The principal components of the protein are the amino acids glycine, alanine, and serine in a proportion of 3:2:1, forming up to the 60% of the crystalline areas of fibroin, in which the protein chains are completely extended into β configuration, acquiring the form of a β -pleated sheet where the

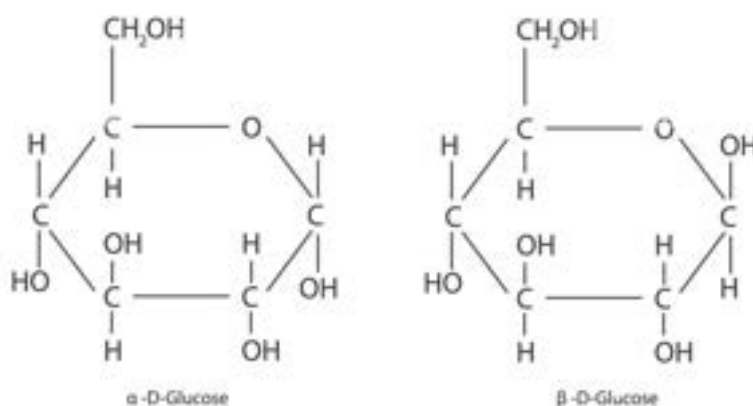
chains are held together by strong secondary hydrogen bonds. These crystalline regions in fibroin provide high tensile and tearing strength. The amorphous regions of the protein are, instead, formed by amino acids with hulking R groups like arginine, threonine, and tyrosine (Timar-Balazsy & Eastop, 2011).

Cellulosic fibers

Cellulosic fibers derive from plants and are classified into three categories according to their plant component of origin, namely the seed, the stem, and the leaf. The chemistry of cellulose started fully developing in the 1930s, even though the major chemical processes for cellulose have been in the research field since the late XIX and the early XX centuries. It is thanks to this previous research that cellulose variants were already present on the market, such as viscose and acetate fibers (Mather & Wardman, 2015).

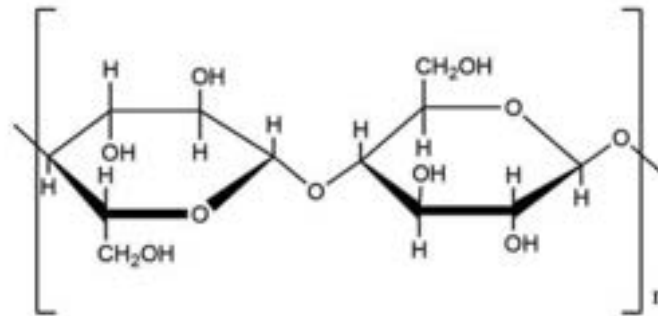
In this paragraph we will briefly discuss the chemical composition of cellulose and the characteristics of the typologies of cellulosic fibers studied in this project, namely cotton, linen, and hemp.

The main component of vegetable fibers is cellulose, the basic constituent of the cell wall (Timar-Balazsy & Eastop, 2011). Cellulose, whose empirical formula is $(C_6H_{10}O_5)_x$ (Mather & Wardman, 2015), is a polymer, a polysaccharide made of β -D-glucose units ($C_6H_{12}O_6$). The β -



D-glucose is a saccharide containing five hydroxyl functional groups and an aldehyde on carbon 1. The letter “D” in the denomination refers to the optical activity of the unit and it means dextrose, i.e. that the molecule rotates the polarized light to the right. Cellulose is produced in living plants through the process of biosynthesis, which involves the enzymatic catalytic action of some micro-organisms. During the biosynthesis, the glycosidic hydroxyl group on carbon-1 of one unit undergoes a condensation reaction with the same group located on carbon-4 of another unit, forming a $(1\rightarrow4)$ glycosidic ether bond. For the condensation reaction to occur, the two -OH groups must be close to each other. For this reason, one of the units must rotate, turning upside down, so that the hydroxyl group on carbon 4 is on the same plane as the hydroxyl on carbon 1. The mechanical properties of cellulose-based fibers strongly depend on their degree of polymerization, which in turn depends on the degree of maturation of the cell wall, the processing, and ageing of the structure (Timar-Balazsy & Eastop, 2011).

Cellulose presents both crystalline and amorphous regions, the latter being easily accessible to water and chemical reagents along with the surface of the crystalline areas. For this reason, the



crystalline parts of the cellulosic fibers are more prone to deterioration; for examples, wrinkles and creases in textiles lead to breaks in the cellulose chains in these spots (Timar-Balazsy & Eastop, 2011). Cellulose-based fibers contain, other than cellulose, several components in different proportions. Among these we find non-cellulosic polysaccharides, such as hemicellulose and pectines, proteins, waxes from the protective layer of the cell wall, organic acids, like the oxalic acid, lignin, coloring materials, and minerals.

Hemicellulose is the set of low weight polysaccharides associated in the cell wall and in the lamella; these molecules are highly hygroscopic and, bonding a conspicuous amount of water, they improve the flexibility of the fiber. Hemicellulose is, therefore, more accessible to water and more sensitive to the deteriorating agents because of its branched and amorphous structure. *Pectin*, mainly composed of pectic acid, can be found in both the cell wall and the middle lamella. *Lignin*, instead, is present only in the cell wall of wood fibers. It is an amorphous cross-linked polymeric material, usually associated with the woody stem of plants and trees (Mather & Wardman, 2015). This component is highly acidic thanks to the presence of phenols in its chemical composition; it is also characterized by a rigid hydrophobic amorphous matrix. Thanks to this property, lignin delays the penetration of deteriorating agents despite the presence of capillaries and pores in the lignin-hemicellulose matrix present in the cell wall. Lignin also contains chromophore groups that give the compound its characteristic yellow shade. These groups absorb the electromagnetic radiation in both visible and near ultraviolet regions; lignin is, therefore, highly photoreactive and its photo-oxidative deterioration results in discoloration of the material to yellow/brown and an increase in its acidity, making the cellulosic materials containing lignin photosensitive (Timar-Balazsy & Eastop, 2011).

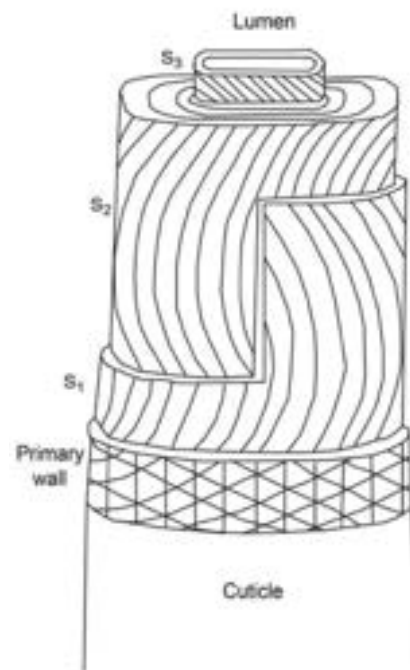
Seed fibers: cotton

Seed fibers generally come from the flower or the seed of a plant (Markova Ivana, 2019). The fiber of cotton is contained in the seed of a plant of the genus *Gossypium*, belonging to the *Malvaceae* order. This specie of plant is common in several regions of the world. In fact, the use of cotton for textile making has been in vogue for millennia and for centuries it has been a characteristic activity primarily in China and India; in the XVIII century cotton was, then, imported to the UK. Now, cotton bushes are cultivated globally with the main producers being India, China, USA, Pakistan, and Brazil. All these countries satisfy the requirements needed

for cotton to grow, since it is a specie that is quite sensitive to the environmental conditions of growth preferring warmer climates (Mather & Wardman, 2015).

How does a cotton fiber grow? After the blossom falls off, dark green triangular protuberances called bolls start to form, containing ca 20 seeds each. The seed hairs correspond to the cotton fibers. They gradually develop and, when the maturity of the boll is achieved, it bursts open releasing the seeds covered in cotton fiber, which must be collected in a short period of time to avoid being damage by the weather.

Cellulosic fibers consist in four parts within the fiber structure (Figure XX), namely the cuticle, primary wall, secondary wall, and lumen. The *cuticle*, characterized by a waxy appearance and a hydrophobic behavior, is the outer layer of the fiber that functions as a protective covering. The cuticle is very thin, being only a few molecules thick, and lays directly upon the *primary layer*, which is around 200nm in thickness. This stratum is made of fibrils of cellulose arranged in a spiraling network along the fiber length. Then, the *secondary wall* constitutes the bulk of the cotton fiber, being made up of numerous layers of cellulose fibrils that too spiral along the fiber axis. The secondary wall layers are three: from the outside S₁, S₂, and S₃, which is the closer to the lumen. The difference between each of them is the angle of spiraling of the fibrils, which is of about 20° in S₁, and 45° in S₃. The fibrils in the secondary wall show a characteristic twist from the S to the Z direction, which is contrary to the fibrils of the primary wall that, instead, present a consistent direction. The peculiar orientations of the fibrils belonging to the secondary wall confer high strength to the cotton fibers. Lastly, the *lumen* is the preliminary form in which a cotton fiber develops before fully opening, consisting in a tubular segment inside the boll. The lumen is, in fact, the major pore through which the sap, a diluted solution made of sugars, proteins, and minerals, flows during the fiber's growth. The lumen grows smaller when the boll opens, leading to the drying of the sap and the consequent deposit of proteins and minerals on the cotton fiber. This leads to the collapsing of the fibers from a circular to a bean-like



shape, which presents a hollow center. The cotton fibers also appear flatter and convoluted along their length; this conformation is the responsible for the peculiar ribbon-like morphology of cotton fibers (Mather & Wardman, 2015). This fiber twist allows the fibers to cling together more tightly, making the spinning of yarns of shorter fibers easier. The twist also gives elasticity to the fabric and an uneven surface, which enables only a random skin contact making cotton textiles comfortable for wearing (Markova Ivana, 2019). The ribbon-shaped convolutions can be either frequent and close to each other or more separated according to the age and chemical application of the single plant. For example, in cotton harvested from immature buds, the fiber will have minimal convolutions or no twists at all. The convolutions could also be affected by industrial chemical processes, such as the mercerization treatment used to impart greater affinity for dyes and chemical finishes in cotton-based textiles. In this

case, the twists would become more flattened and difficult to recognize under microscope (Markova Ivana, 2019)

Bast fibers: linen and hemp

Bast fibers include flax, hemp, jute, ramie, and nettle; these fibers have very similar characteristics and are therefore difficult to distinguish under optical microscope. However, they are well distinguished by other cellulosic and protein fibers (Markova Ivana, 2019). Bast fibers derive from the plant's stem and are generally characterized by long lengths. Flax fibers, for example, reach 1m of length, but they include the so-called ultimate fibers which are shorter fibers, adhered to one another thanks to the resins in the stem, to form the longer fiber. Bast fibers are naturally stiff because the stem keeps the plant up straight during the growth stage (Mather & Wardman, 2015). The longitudinal view of bast fibers shows cross marks, also known as nodes or joints, called dislocations, which confer the peculiar bamboo-like look of linen and hemp. The cross marks are used as a primary distinction feature between other cellulosic fibers (Markova Ivana, 2019).

Flax

Flax, or linen, has been used even before cotton, having the first evidence of used dating back to the 8000 B.C. Apart from being the oldest textile fiber known, linen has always been highly valued and the populations that exploited its properties the most were Egyptians, Babylonians, and Phoenicians. The great respect that people had for this textile was so great that they used it to wrap the bodies of noble personalities in burial chambers. For the Romans, instead, linen became a symbol of divine purity thanks to its whiteness. Later, during the Renaissance, this fiber was used by many elevated artists of the caliber of Leonardo Da Vinci as canvases for their artworks. During history, linen was widely used also to make sail cloths for sailing ships due to its renowned strength and durability; but its use drastically declined with the introduction of synthetic fibers, especially artificial rayons, during the XX century. Flax is now considered a luxury fiber (Mather & Wardman, 2015).

Flax is obtained from the stem of plants belonging to the *Linum usitatissimum* specie; the term "flax" is used specifically to indicate the fiber before processing it into yarns, while "linen" indicates the worked fiber which will be later woven or knitted into finished fabrics. The flax plant requires a mild climate to grow, and it is, therefore, cultivated in many regions of Europe such as France, Belgium, and the Netherlands. During the growing stage, flax plants can reach 1m of height with stems of about 2-3mm in diameter. The fibers lie at the surface of the stem and cover its length; flax fibers are therefore notably longer than cotton fibers (Mather & Wardman, 2015).

Due to the structure complexity of flax fibers, which are surrounded by tissues, waxes, and pectines binding them together with the woody central body responsible for the stem's mechanical strength, their extraction requires numerous steps. Firstly, the fiber structure requires to be softened through the retting process; the most common retting process is called dew retting and consists in the spreading of the stems on the ground for about 3 to 12 weeks.

During this period, the enzymatic action of bacteria dissolves the cellular tissue, aided by the temperature cycles that take place during day and night. After retting the stems are dried and, finally, the wood components are mechanically removed. The bundles of fibers obtained are then combed to make them progressively finer. Since the flax fibers in the bundles are held together by a natural gum solution, they are degummed in alkaline baths at 65-90°C. In some types of linen, the creamy original color of the fibers is removed by bleaching (Mather & Wardman, 2015).

For what concerns the chemical composition, the cellulose content in flax fibers is not as pure as it is in cotton. In fact, linen contains only 60% of cellulose, the remaining 40% consisting of other components such as hemicellulose and lignin, waxes, pectines, natural pigments, and water-soluble materials. Linen, like other bast fibers such as hemp, forms bundle that act as a straight structure in the fibrous layer that help to keep the plant erect. The fibers are made of long and thick-walled cells that overlap one another; the bundles formed by multiple cells are called ultimate fibers. these units are held together by non-cellulosic materials, forming continuous strands that run through the whole length of the fiber. (Timar-Balazsy & Eastop, 2011). Flax fibers have peculiar physical characteristics. Distinguished by soft handle and a lustrous appearance, they are not as convoluted as the cotton fibers, but they also present a lumen in the center of their structure. This variety of bast fiber, like hemp, presents the characteristic nodes throughout the overall length of the filament (Markova Ivana, 2019). Flax fibers are considered the strongest fibers present in nature, even though elasticity is not among the features that characterize them. Speaking about comfort, linen is considered as a summer fiber since it easily absorbs moisture; this quality makes linen an optimal candidate for glass-cleaning cloths, removing water effectively (Mather & Wardman, 2015).

Hemp

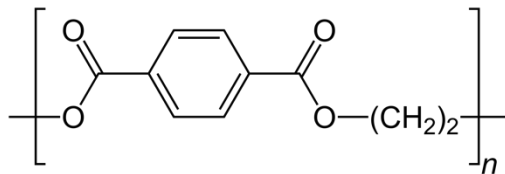
The production of hemp peaked in the XVIII century, especially in Britain. This fiber, thanks to its remarkable strength and length, was mainly used in the shipping field for the construction. Of ropes, sails, and sacking. Hemp manufacturing then decreased throughout the course of the XIX century due to the rising prices of both cotton, jute, and hemp (Mather & Wardman, 2015). The morphology of hemp fibers shows nodes, here called dislocations, on their longitudinal structure. This characteristic makes this fiber very similar to linen, although if studied under magnifications higher than 1000x, for example with SEM microscope, these dislocations appear less visible (Markova Ivana, 2019).

Synthetic fibers

Synthetic fibers are petroleum-based specimens (Markova Ivana, 2019) produced by polymers chemically synthesized from monomeric compounds (Mather & Wardman, 2015). The monomers undergo polymerization, polycondensation, or polyaddition to form the final polymer, a material suitable for extrusion, spinning and stretching processes (Timar-Balazsy & Eastop, 2011). Synthetic fibers have the advantage of being specifically engineered with detailed

properties based on their use and field of application and can be manufactured both as staple and filament (Markova Ivana, 2019).

Polyester



The synthetic fiber under study in this project is polyester. Polyesters are a family of polymers, whose monomeric units are joined by ester linkages -O-CO-; the most commercially important compound of this category is polyethylene terephthalate (PET) (FIGURE X) (Mather & Wardman, 2015). The production of polyester fibers began in the 1930s at the DuPont laboratories, a worldwide know research and development center where, by the condensation of octadecandioic acid (HOOC-(CH₂)₁₆-COOH) with propane1,3-diol (HO-CH₂-CH₂-CH₂-OH), the researchers obtained a product of molar mass of ca 12000, from which fiber filaments could be pulled out. Despite the success of this discovery, the new material, which was firstly synthetized from aliphatic comonomers, was not suitable for the textile use since its melting point was too low, causing premature dissolution already in dry cleanings. Further developments of this research led to the production of a fiber-forming polyester variety from ethane-1,2-diol (ethylene glycol; HO-CH₂-CH₂-OH) and terephthalic acid (Mather & Wardman, 2015).

PET fibers in the textile industry are used for several purposes, such as apparel, household, medical, and industrial scopes. In the clothing field, PET fibers are usually blended with other textiles to improve the fabric's softness. For example, PET is blended with cotton for the making of shirts, dresses, sportswear, bedsheets, and pillowcases. PET-wool blends are also common but are usually employed in formal-wear. PET is used in the medical field for sutures, heart valves, and artificial tendons and ligaments; the industrial applications of this compound, instead, include vehicle tire reinforcement, ropes, tents, and sailcloth. (Mather & Wardman, 2015). The dominance that this fiber holds on the market is due to its valuable properties, such as its great versability, easy care, and fast drying; this latter property is not present in natural fibers, and it gives PET great affinity in the sportswear field (Markova Ivana, 2019).

The production of polyester, and generally of synthetic fibers, starts from pallets of raw materials, which is melted into a dope or spinning solution. The compound is extruded through the openings of a peculiar object called spinneret, which is a device used in extrusion processes of polymers through which the melted material exits in the form of filaments. These filaments, or fibers, harden when emerging from the tool. The holes of the spinneret can be modified according to the desired shape and size, such as cylindrical or triangular; this, of course, influences the final shape of the polymer filaments. This procedure guarantees the uniformities in the morphology of synthetic fibers, including PET. For this reason, differentiating synthetic fibers by the observation of Optical microscope photographs is a quite challenging task; despite this premise, the study of the morphology of synthetic fiber is useful for the understanding of the fiber performance and its mechanical and physical characteristics (Markova Ivana, 2019). The longitudinal view of synthetic fibers is linked to their cross-sectional shape; Polyester, in fact, appears as smooth and cylindrical rod which probably means that its cross-section is

circular (Markova Ivana, 2019). Synthetic fibers are characterized by a variable luster that depends on the cross-sectional shape of the fiber; the amount of luster is proportional to the quantity of light reflected by the fiber. A high degree of luster corresponds, in fact, to round, trilobal, or oval cross-sections. To decrease the luster, a delustering process is carried out usually using titanium dioxide (TiO₂) applied during the manufacture of the synthetic textile; these agents work by absorbing the light instead of the fiber itself. Under optical microscope, delustering agents appear as colored grains which, despite diminishing the luster, weaken the fiber by affecting its mechanical properties (Markova Ivana, 2019).

Table XX summarizes the different fiber varieties and their chemical composition that will be analyzed in this study (Greaves & Saville, n.d.).

Table XX: fiber varieties studied in this research with their type and principal chemical component.

<i>Generic Name</i>	<i>Type</i>	<i>Principal Component</i>
Cashmere	Natural, animal	α -keratin (protein)
Cotton	Natural, vegetable	Cellulose
Flax	Natural, vegetable	Cellulose
Mohair	Natural, animal	α -keratin (protein)
Polyester	Man-made, synthetic	Polyethyleneglycolterephthalate
Silk	Natural, animal	β -keratin (protein)
Wool	Natural, animal,	α -keratin (protein)

Aim of the research

Textiles and art make up for a solid partnership in history and, for this reason, fabrics of all kinds are a constant item in cultural heritage. This link leads to the need of conservation strategies for these objects, which include the study of their chemical composition and behavior to allow a safe and conscious preservation plan. Properly identify textile materials and understanding their chemical composition is fundamental not only in the historical and archaeological field, for example for the study of the mummies' bandages (Oras et al., 2020), but also in the forensic field (Śmigiel-Kamińska et al., 2020) and in the industrial-quality control area (Peets et al., 2017a). In particular, the study of the chemical characteristic and peculiarities of textiles is a challenging topic due to the high variability of fiber types and because often fibers of the same class, for instance linen and hemp both cellulosic fibers, may have very similar morphologies and composition. Additionally, when studying textile such as archaeological or even modern ones, the need of employing non-invasive techniques and in-situ methodologies may become fundamental in force of their cultural and historical value and fragility (Peets et al., 2017a). The analytical techniques proposed in this study, namely Attenuated Total Reflectance ATR and ER FTIR, Raman, and FORS, satisfy the in-situ requirement and allow a safe and non-invasive approach for understanding the chemical composition of the specimens. The physical principles of each technique will be later discussed, along with their specific application in the cultural heritage field. An interesting aspect must

be pointed out, that is the advantage of thinking of the above-mentioned techniques not as single tools giving separate answers, but instead as union of different knowledges, each giving its specific response that, when added and confronted with the others, constitutes the result of the analysis. To do this, it is necessary to understand the strong and weak points of each technique to balance the confrontation of the different analytical outputs. The use of complementary techniques can be considered a valuable approach in the study of the composition of cultural heritage materials, included ancient textiles.

The aim of this research is to evaluate the contribution and the potentiality of non-invasive diagnostic techniques here proposed to identify and study textile fibers commonly present in historical artworks in Venice. The project focuses on the analysis of the chemical composition of two sets of textiles. The first, which will be called reference (REF) set, contains raw textile specimens belonging to both animal and cellulosic fibers; the second set, instead, was kindly given by the Rubelli (Venice), and contains several fabrics made of animal, cellulosic, and synthetic fibers. The spectral responses of the two sets of samples will be confronted to detect the spectral matches between the reference and unknown fibers. The spectral information of each technique will be then tested with statistical methods, namely Principal Component Analysis and Cluster Analysis, to observe how the spectral results of each technique gather based on the spectroscopic tool used. The final goal is to test the capabilities and limitations of each technique, considering also the possible differences between raw material and final product, for selecting then the most promising in the study of textile-based artworks.

Materials and Methods

The following paragraph describes the techniques employed for characterizing and studying the textiles object of this study. The aim of the research is to identify which non-invasive analytical technique allows to best discriminate each fiber type, by also means of statistical methods such as Principal Component Analysis (PCA) and Cluster analysis.

Here, the techniques will be displayed alongside a brief description of their physical principle and a few examples of their use in the Cultural Heritage field. The present study represents a first step to evaluate the best diagnostic approach to be then applied on historical textile.

Optical microscopy

Optical microscopy is a quick and essential tool for the preliminary identification of a broad range of materials, including minerals, metals, ceramics, paint, hairs, and textile fibers. In fact, through the magnification of the object, this technique allows the observation of the morphological characteristics of each specimen (Stuart H. Barbara, 2007).

The first uses of microscopes, which at first consisted in the use of simple glass lenses like glasses, dates to the late 1600s and some of the scientists that contributed to their invention and development are Galileo Galilei, Zacharias Janssen, and Robert Hooke. Further improvements were made in the XX century, which included the development and adaptation of the lenses, with the main contributor being the German mechanic Carl Zeiss, who partnered with the physicist Ernst Abbe and the glass chemist Otto Schott. Their work led the way to further extensive improvements during the past 200 years. Today, microscopes are relatively simple instruments that can be found in any laboratory facility (Markova Ivana, n.d.) and are used in every scientific field.

Optical microscopy exploits the interaction of light with a sample to obtain magnifications from x2 to x2000. There is a variety of optical microscopes and operational modes depending on the purpose of each research; some of the most common are transmitted and reflected light microscopes, which use photons to create clear images, or electron scanning microscopes (SEM) which, instead, exploit electron beams for the same aim. Polarized light microscopy, for instance, is another sub-field of optical microscopy often used to analyze the structure of oriented samples, that uses polarizing filters on a standard microscope (Stuart H. Barbara, 2007).

As previously mentioned, optical microscopy is fundamental for the identification of textile fibers. This activity is not only necessary for diagnostic, and restoration works on Cultural Heritage artifacts, but it is also used, for example, in the forensic field (Bergfjord & Holst, 2010). Optical microscopy is often one of the first steps in the work pipeline. The preliminary information gathered from the microscopy photographic campaign is very useful for a better understanding of the nature of samples and eventually allow to gather details on the production and conservation state. For instance, in the study of (Luo et al., 2021) optical microscopy is used to depict possible differences in the morphology between cashmere and wool fibers.

In this research, the reflected light microscope used was an OLYMPUS BX41 U-CMAD D3 with magnifications of x4, x10, x20, and x40, while the transmitted light microscope was a Leica DMIL LED coupled with a Leica Flexa cam C3; the images were also acquired with the PH1 filter inserted in the set-up.

Sample preparation

The samples of the raw animal and vegetable fibers set (REF) and some of the Rubelli's set were prepared to be analyzed under optical microscope. Single representative fibers were withdrawn from each batch and mounted parallel to each other on glass slides (Greaves & Saville, n.d.). The fibers were then set under a micro glass slide, which was secured to the main slide with adhesive tape. This operation allowed for a more detailed identification of the fiber type under optical microscope.



Figure XX: samples prepared on the glass slides for the analysis under Optical Microscope

Infrared spectroscopy

Infrared spectroscopy here has been used in two different working modes: Attenuated Total Reflectance (ATR) and External Reflection (ER).

The Fourier Transform IR spectroscopy (FTIR) is a technique that allows the identification of the chemical composition of a variety of materials, including textile fibers.

IR spectroscopy uses infrared radiation to trigger the excitation of electrons that, thanks to this low-energy radiation, are the object of translational, rotational, and vibrational transitions. This technique exploits the fact that a molecule has unique and defined movements that are related to its structure, therefore their measurement allows the characterization of the specimen. The information gathered from IR spectroscopy can be read through an IR spectrum (fig XX) which depicts the extent of the interaction between the IR radiation and the sample, usually shown as Absorbance (or Transmittance %) on the y-axes and Wavenumber (cm^{-1}) on the x-axes (Derrick & Landry, 1999).

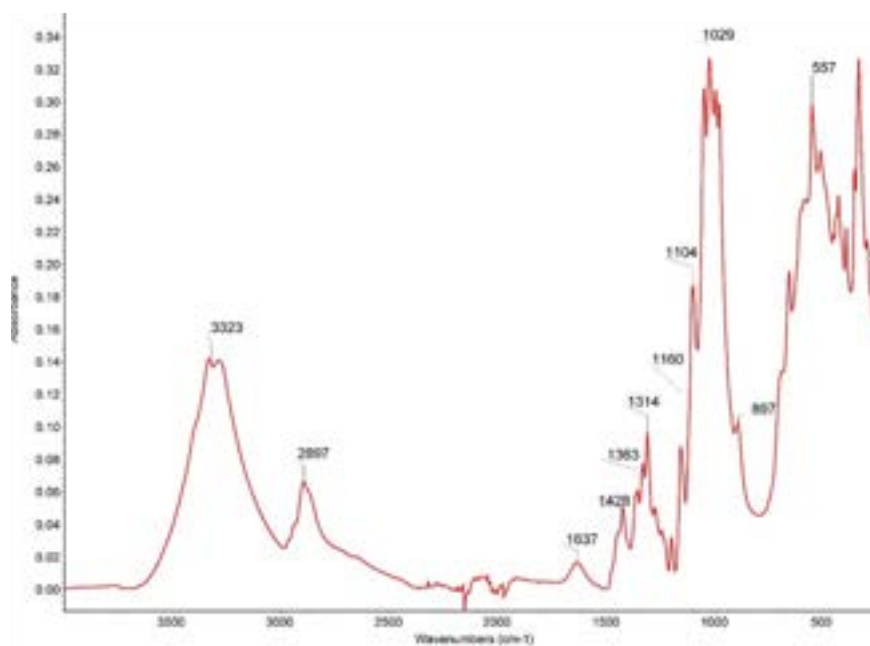


Fig. XX example of an ATR-FTIR spectrum of cotton (Peets et al., 2017b)

The Attenuated Total Reflection (ATR), also known as Internal Reflection Spectroscopy (IRS), was introduced in the 1960s as an additional working mode of FTIR spectroscopy and is based on the principle that the internally reflected IR radiation can penetrate the specimen only for a few micrometers, without leaving any damage to the sample (Derrick & Landry, 1999). This aspect makes the ATR-FTIR technique a non-invasive analysis tool, which, along with the portability of the instrument, is an almost essential requirement in the field of Cultural Heritage Diagnostics.

External Reflection (ER) is another reflectance working mode in the FTIR spectroscopy, in which the information acquired comes from the intensity of the radiation reflected by the sample, which is measured at a desired angle of incidence (Handke et al., 1990). Like in the ATR mode, the radiation penetrates only the external surface of the sample and can, therefore, be considered a non-invasive technique. When working with fibers, as in this very case, ATR and ER modes are preferred with respect to the normal IR spectroscopy since fibrous samples are often too thick and would absorb too much radiation (Derrick & Landry, 1999), giving unrealistic data difficult to interpret.

FTIR spectroscopy can be performed both in laboratory facilities, with workbench instruments, or in situ and is used in a variety of fields. This technique finds many applications also within the Cultural Heritage world, thanks to the wide range of materials it can analyze. For instance, (Nodari & Ricciardi, 2019) used ER-FTIR to identify paint binders on parchment-based works of art. Medieval illuminated manuscripts were also analyzed by (Vetter et al., 2019), (Vetter et al., 2021) using ATR-FTIR. The ER-FTIR technique is less common to find in Cultural

Heritage-related studies, especially in the textiles' domain, but a recent example of its use is given by Geminiani et al., whose aim was to differentiate hard silk from soft silk to gather useful historical information and for a better monitoring of the conservation of historical silk. A Bruker ALPHA II Fourier Transform IR Spectrometer was used for External-Reflection (ER-FTIR) and the Attenuated Total Reflectance (ATR-FTIR) analysis. ER-FTIR analyses were performed using an aperture of 6 mm and a 1-to-3 min of acquisition time. These measurements allowed for the registration of spectra in the range 7500 - 350 cm^{-1} , which comprises wavenumbers where combination bands and overtones are present. ATR-FTIR analysis were recorded in the spectral range from 4000 to 350 cm^{-1} , using a synthetic diamond crystal for the compression of the samples. Both background and samples were measured with 24 scans before each acquisition, with a resolution of 4 cm^{-1} .

Raman spectroscopy

Raman spectroscopy allows the study of the radiation scattered by the sample. The scattering phenomenon happens when, during the de-excitation of a molecule, the intensity of the radiation doesn't correspond to the intensity of the radiation absorbed (Stuart H. Barbara, 2007). The interpretation of the spectroscopic data is made by means of a Raman spectrum (fig. XX), depicting the Raman Intensity (or Absorbance) on the y-axes, and the wavenumbers (cm^{-1}) on the x-axes. This technique is widely used in the Cultural Heritage field thanks to its ability to detect both organic and inorganic compounds, as well as being a portable instrument (Rousaki & Vandenabeele, 2021). In fact, Raman spectroscopy, as previously mentioned for the FTIR technique, can be performed both in laboratory but also in situ allowing for analysis of artifacts that are not recommended for sampling.

Raman's applications include a variety of uses, from the in-situ analysis of pigments used in South African rock art (Tournié et al., 2011), to the identification of the composition of Limoges' enamels from the XVI-XIX centuries (Kirmizi et al., 2010), or to the study of medieval illuminated manuscripts belonging to the Indian tradition of the XVII century (Ravindran et al., 2011). In the textile's field, besides from the study of textile structures (Puchowicz & Cieslak, 2022a), Raman spectroscopy was employed for the investigation of cellulose fibers of paintings' canvases and linings (Kavkler & Demšar, 2011a), as well as for the detection of structural changes in wool's keratin after chemical treatments that improve wool's hydrophobic properties (Wojciechowska et al., 2004).

Raman spectra were collected with a Bravo portable Raman spectrometer by Bruker Optics, characterized by a dual laser excitation (two lasers at 758 and 852 nm working simultaneously). The Raman spectra were collected in the 3200–300 cm^{-1} spectral range between, with 10 cm^{-1} resolution, scan time from 1 s to 60 s.

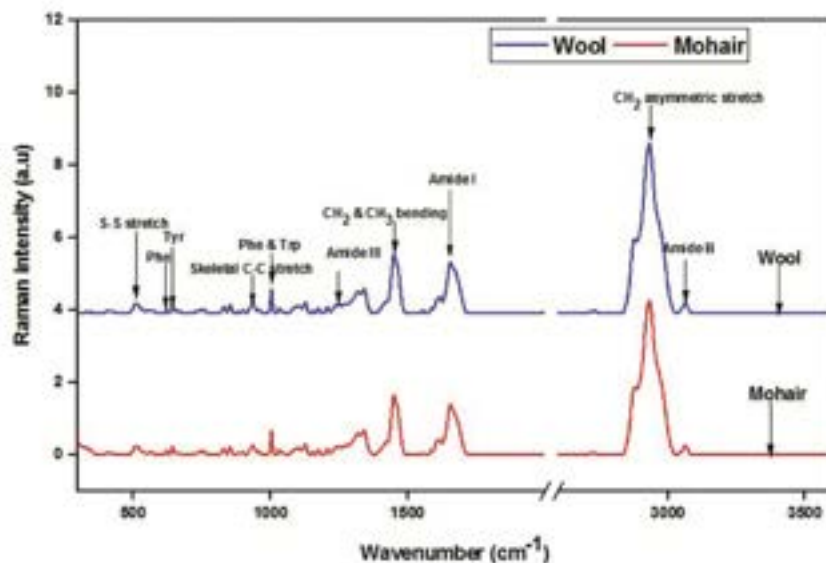


Fig. XX example of a Raman spectrum (Notayi et al., 2022b)

OPUS software managed the acquisition and elaboration of both the IR and Raman spectra. The data were further elaborated with Origin 8.5; the elaboration consisted in the normalization from 0 to 1 of the absorbance data of each measurement, along with the graphical processing of the spectra.

Only a single spot for each sample of the raw animal and vegetable fibres set (REF) was analysed with IR and Raman spectroscopy. The samples from the Rubelli set were, instead, tested in areas of different colours and textures. The measurements for both sets consisted in single acquisitions.

Fiber Optics Reflectance spectroscopy

Fiber Optics Reflectance Spectroscopy (FORS) is a valid non-invasive technique for the Cultural Heritage field, that can be used directly in situ and without the need of sampling. Thanks to the measurement of the light reflected by the sample's surface, it is commonly used for the identification of the artist's materials, including pigments, dyes, and lakes in a variety of types of artworks including textiles (Shahid et al., 2019). FORS also gives information about the molecular composition of organic compounds when used in the NIR region, thanks to the stimulation of vibrational, rotational, and translational transitions inside the molecules. Fig. XX shows an example of FORS spectroscopy used for the identification of different textiles. The spectrum is the result of the analysis performed on four materials, namely silk, wool, cotton, and hemp (Zhao et al., 2019a). The graph displays the amount of reflected light detected by the instrument (Reflectance, on the y-axis) against the wavelength (nm, on the x-axis) and, by observing the inflection points of each specimen and their absorption bands in the NIR and SWIR regions, it is possible to characterize and differentiate each material.

The Fiber Optics Reflectance Spectroscopy is a very versatile tool also used to analyze polychrome surfaces on paintings (Bacci et al., 2003) and illuminated manuscripts (Delaney et al., 2014), or again to identify organic colorants on Japanese paintings (Leona & Winter, 2013).

As previously mentioned, FORS has also been used in the study of textile structures by (Quintero Balbas et al., 2022a) and (Zhao et al., 2019a).

FORS analyses were performed using an ASD FieldSpec 4 Standard – Res Spectroradiometer equipped with three detectors, working in a range between 350 and 2500 nm (resolution of 3 nm in the Vis—Near IR range 350-1000 nm, 8 nm in the SWIR 1000-1800 nm and 1800-2500 nm) and endowed with a contact probe with an inner halogen light source collecting light scattered at 45° and a spot size of 1.2 cm². For the data elaboration, the ViewSpec Pro software and Origin 8.5 were employed. The FORS spectra in this research show reflectance values normalized from 0 to 1.

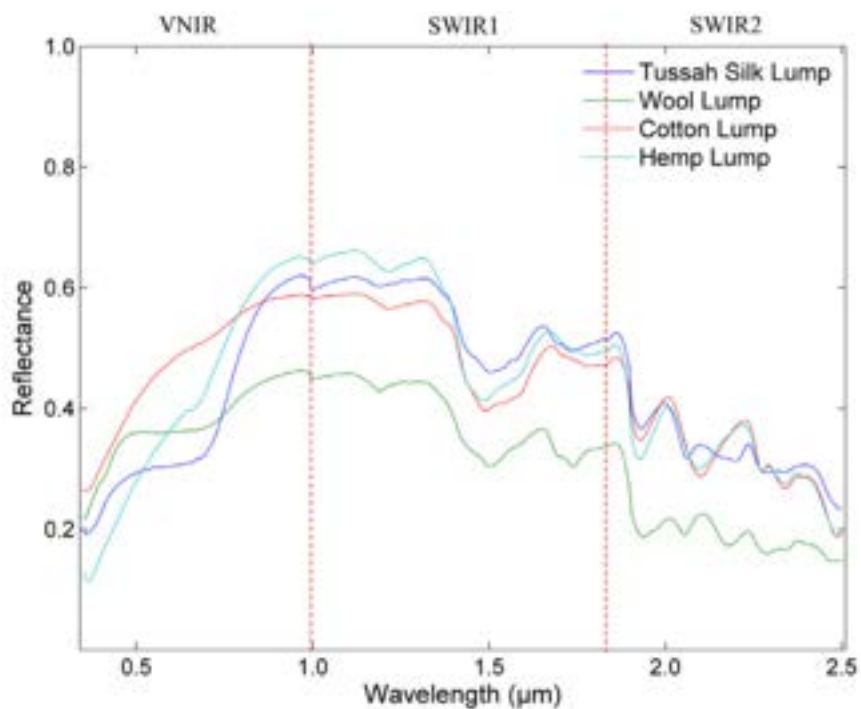


Fig. XX example of a FORS spectrum that allows the identification of the spectral features of silk, wool, cotton, and hemp (Zhao et al., 2019a)

After the elaboration of the spectral data of IR, Raman, and FORS analyses, the Past 4.0 software was used to build tables for each technique and for each set of samples, REF and Rubelli, containing the wavelength or wavenumber value of each peak for every sample. The numerical information contained in these tables was then used on the same software for the computation of statistical analyses such as Principal Component Analysis and Cluster Analyses that will be discussed in the following chapters.

The interpretation of the IR, Raman, and FORS spectra was made by comparing the obtained results with data found in literature. The reference tables with the key spectral features identified by each technique and for each type of fabric are shown in Appendix XX.

The samples

The samples analyzed in this research are divided into two separate sets. The first one (REF) consists of the coarse animal and vegetable fibers used to build the reference spectral dataset, in particular eleven wool types, silk, cotton, and two linen samples. The second set is made of industrial textile samples supplied by the historical textile company Rubelli and include both natural and synthetic fabrics.

Table XX shows the samples that make up the reference dataset.

<i>Name</i>	<i>Type</i>
ALP	Alpago – wool
ARG_CO	Argentina Corrientes – wool
AUS_MER	Australia Merinos – wool
AUS	Australia – wool
CAM_MO	Mongolian Camel – wool
MOH	Mohair – wool
N_ZEL	New Zealand – wool
SAR_P	Sarda Piemontese – wool
CACH	Cashmere – wool
MOR	Moretta – wool
MON_GOT	Mongolian Greyorn – wool
C1	Chinese Silk – silk
CO_G	Cotton
LINEN	Linen
LI_G	Linen

Table XX Sample identification name and description of the Rubelli set; in which only a few samples came with the description of their composition.

<i>Name</i>	<i>Type</i>
S1	Wool
S2	Wool
S3	Cotton
S4	Wool
S5	Silk
S6	Polyester
S7	Polyester
S8	Silk + Viscose
S9	Cotton + Viscose
S10	50% cotton, 20% acetate, 18% silk, 12% viscose
S11	Polyester
S12	64% viscose, 18% silk, 18% linen
S13	32% viscose, 25% acetate, 24% silk, 19% linen
S14	55% viscose, 24% linen, 23% silk
S15	Silk
S16	Silk
S17	Silk
S18	Silk
CAN_G	Raw hemp

CAN_T	Dyed hemp
LI_18	Linen 1/8 white
SAV_R	Saville Raw – combed wool
PL	Polyester (fire-resistant)
PL_R	Dyed polyester (fire-resistant)
CO_R	Dyed combed cotton
C3_S	Sdrucito – dyed silk
C2	Raw silk
L_PET	Raw combed wool

Results and discussion

Optical microscopy

The optical microscopy (OM) photographic campaign was performed for a preliminary identification of the fiber species based on their morphology (Greaves & Saville, n.d.). Here, only the longitudinal characteristics will be considered, such as the appearance of the surface of the fiber, and the possible presence of scales, nodes, and other elements.

Figure XX shows the flow-chart elaborated by (Greaves & Saville, n.d.) for the group classification of fibers based on their morphological appearance, which was used in this study as a guideline in the observation of the OM photographs and which will be referred to in the following descriptions.

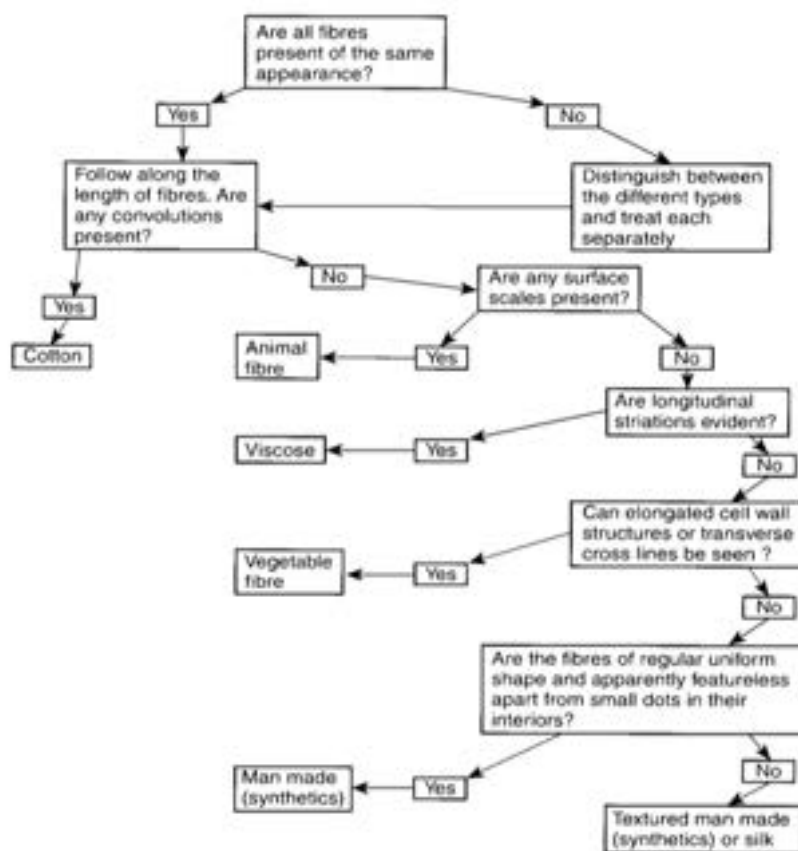


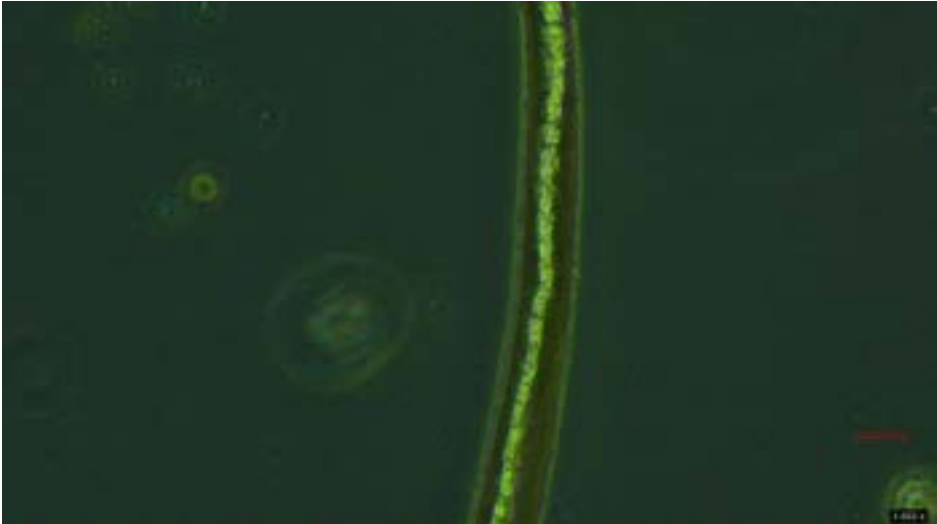

Figure XX: “Classifying fibers into groups by initial examination of longitudinal whole mounts” (Greaves & Saville, n.d.)

Animal fibers

Wool

In table XX the surface of the wool fibers under study is briefly described along with their relative optical microscopy images.

Table XX shows the OM pictures of the reference wool samples.

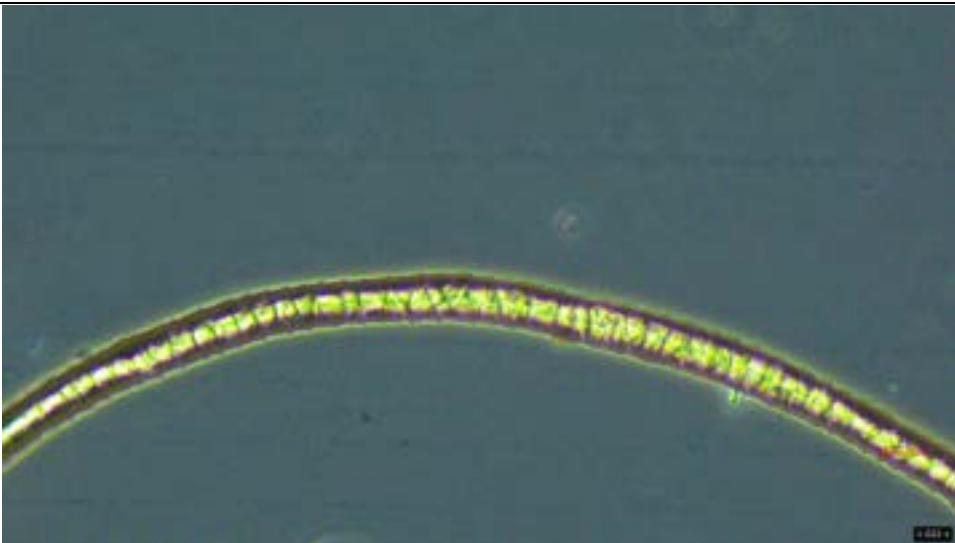
ALP	
	
	
ALP 20x PH1 filter / ALP 40x	
ARG_CO	



ARG_CO 20x PH1 filter / 40x

Wave – regular mosaic configuration. The scales are overlapping and slightly protrude outwards, the surface is not completely smooth. This behavior is typical of long and coarse fibers, typically sheep hair.

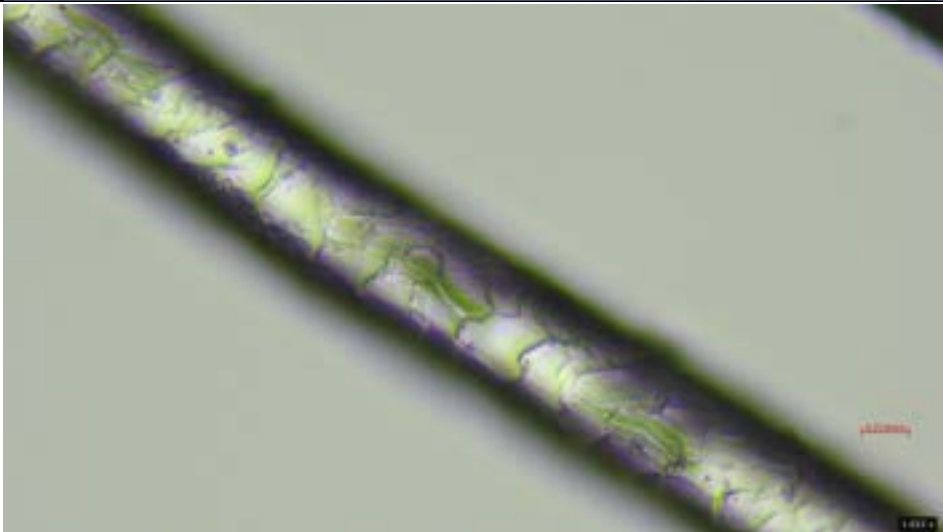
AUS





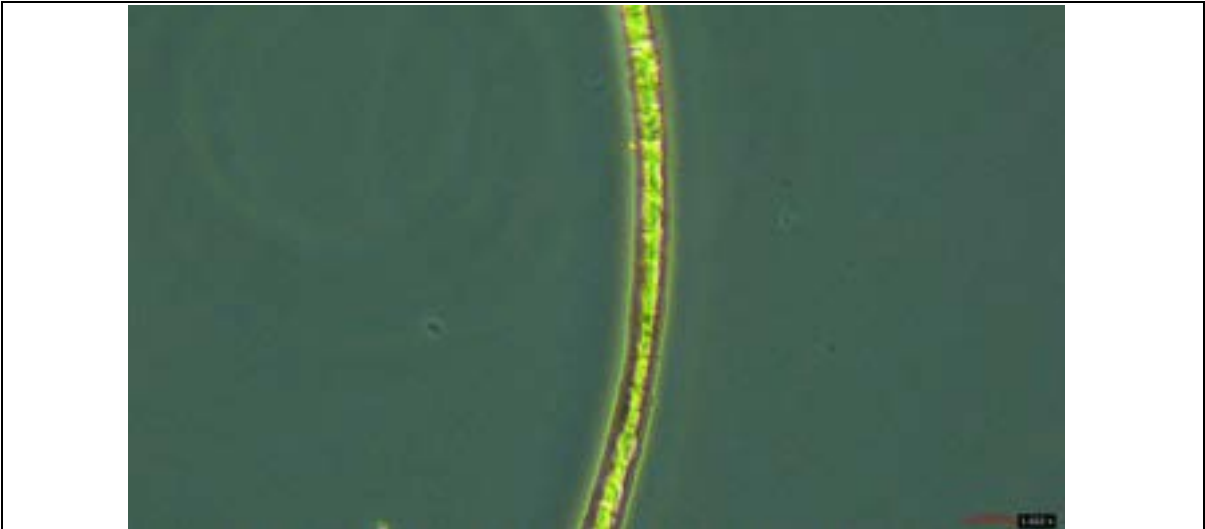
AUS 20x PH1 filter / AUS 40x

AUS_MER



AUS_MER 20x PH1 filter / AUS_MER 40x

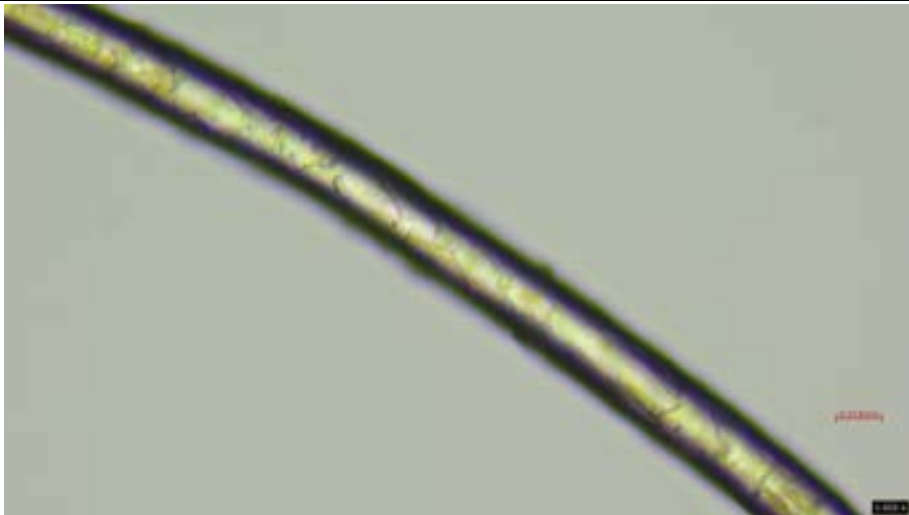
CACH



CACH 20x PH1 filter / CACH 40x
Simple regular wave configuration, smooth surface. Typical behavior of luxury fibers

CAM_MO





CAM MO 20x / CAM MO 40x

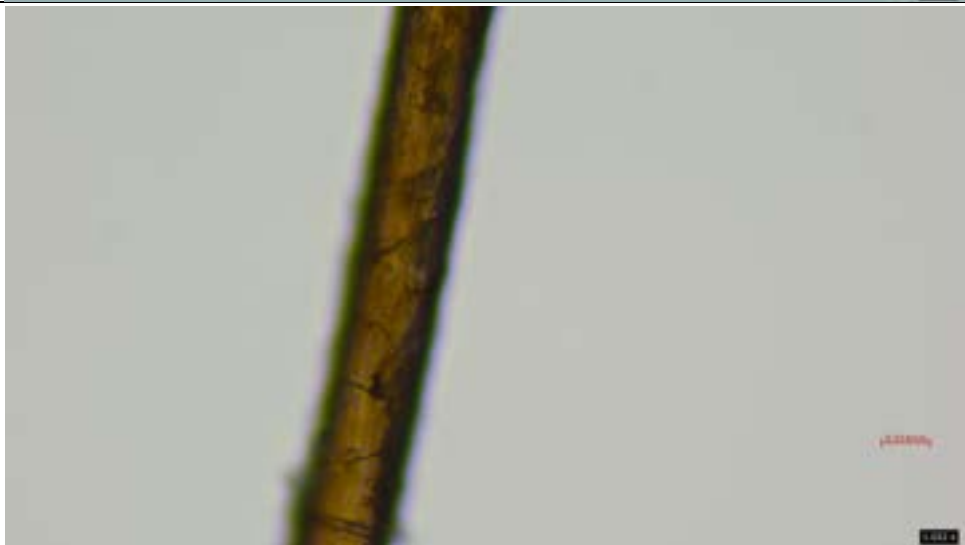
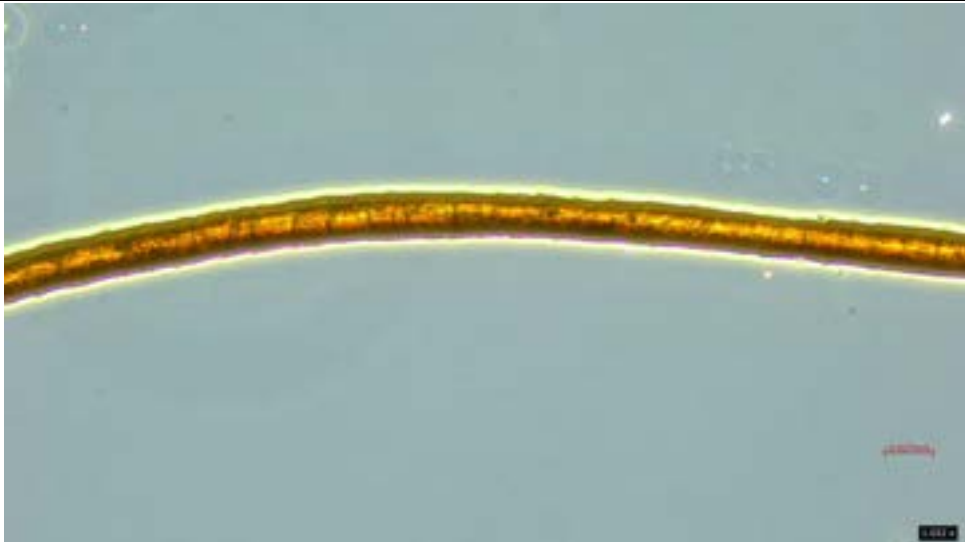
MOH



MOH 20x PH1 filter / MOH 40x

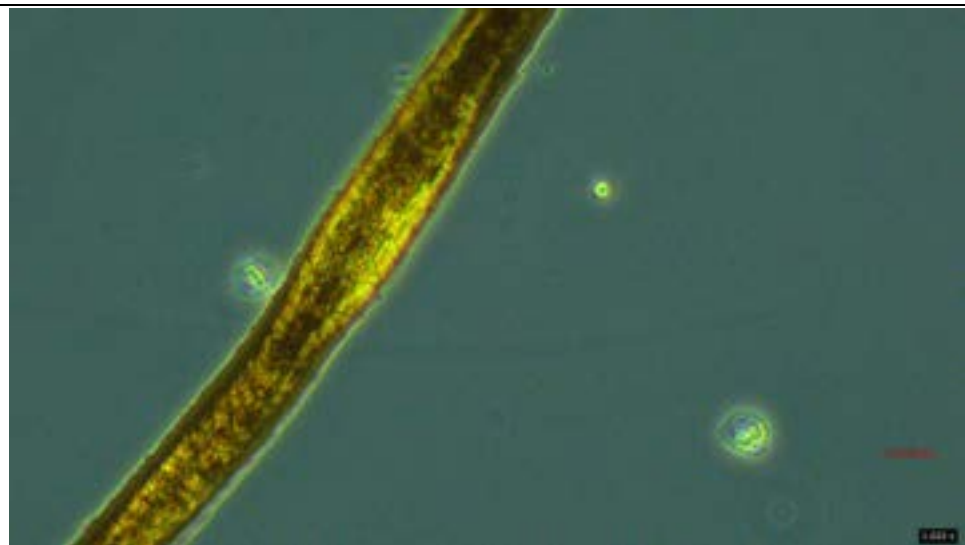
Wave - regular mosaic configuration that results in a smooth surface. This gives the fiber luster and low friction on the skin

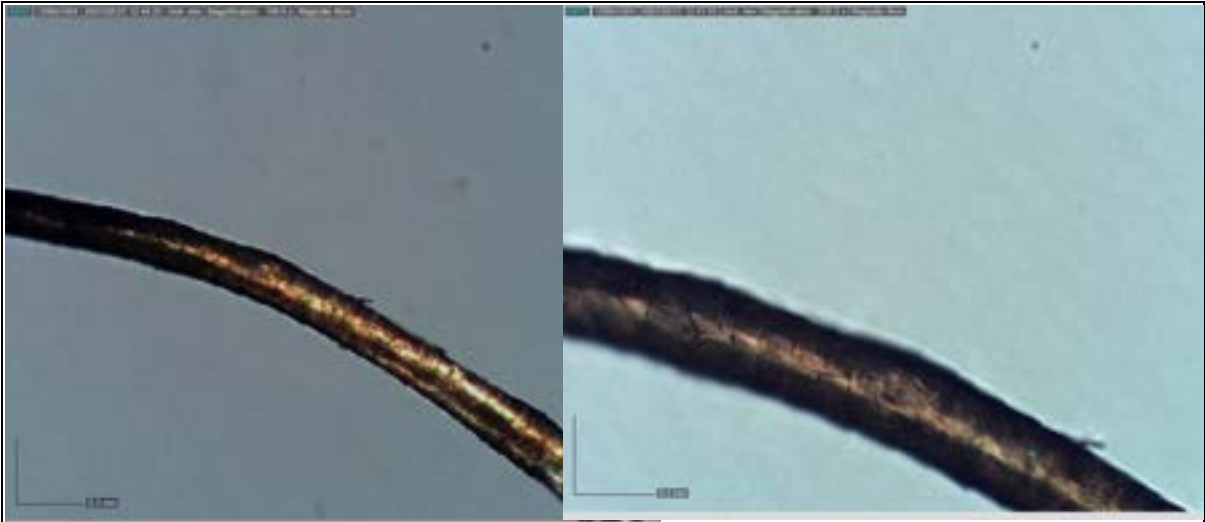
MON_GOT



MON GOT 20x PH1 filter / MON GOT 40x

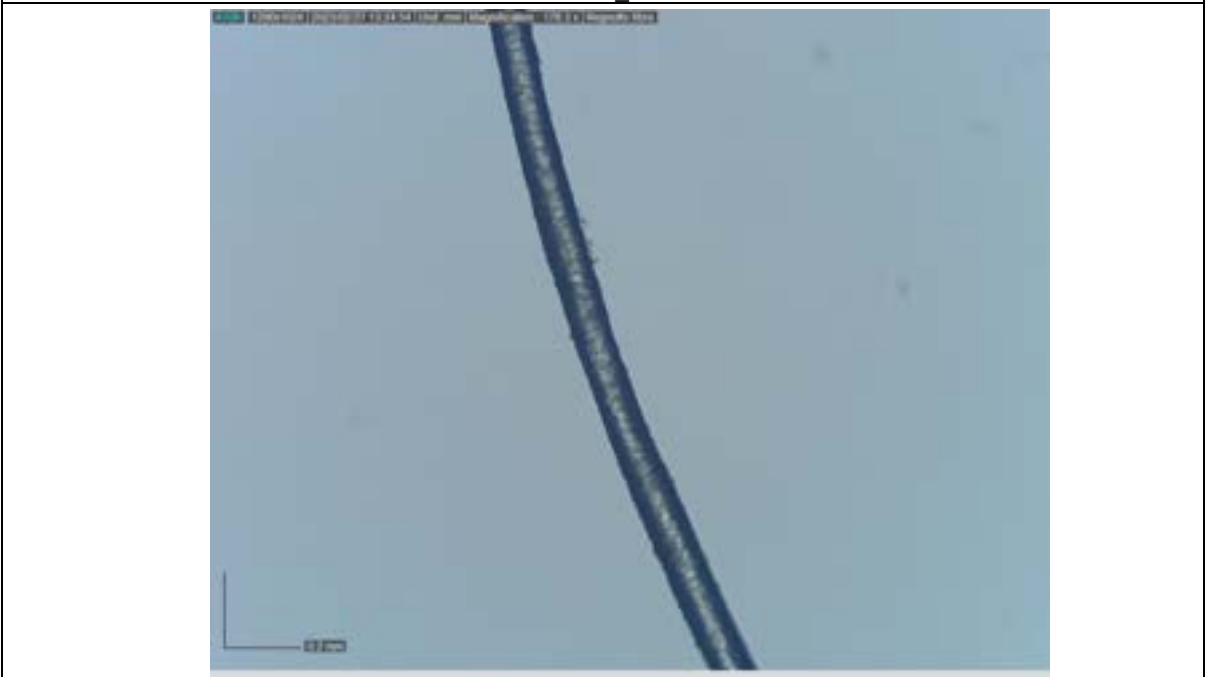
MOR

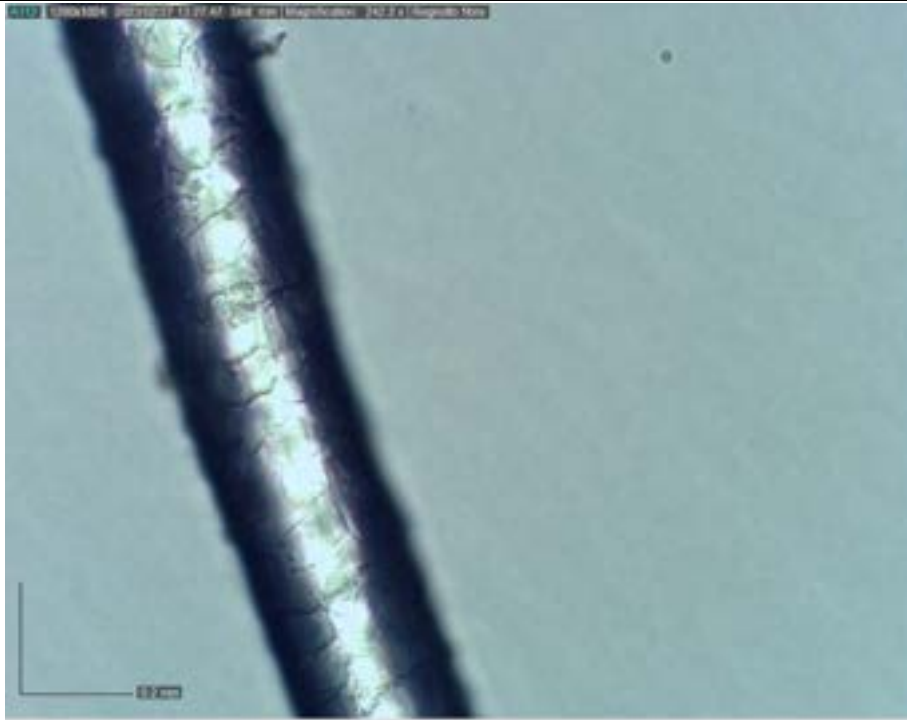




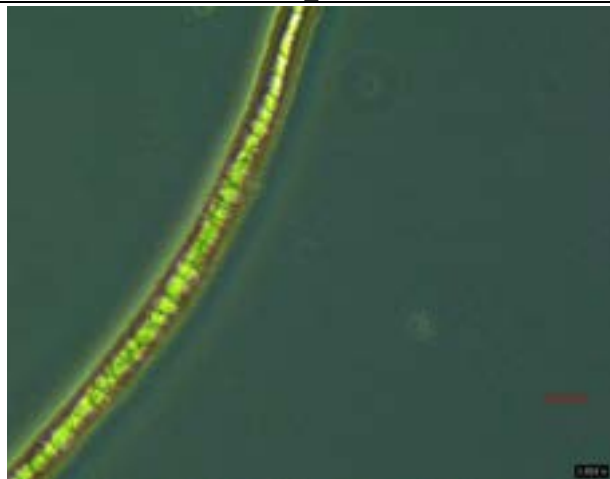
MOR 20x PH1 filter / MOR 20x/ MOR 40x

SAR_P





SAR P 10x/ SAR P 40x
N ZEL



Optical microscopy is a useful tool since it highlights the variability of the morphology of wool fibers depending on their provenance. Wool varieties, in fact, must be considered when studying the morphology of these fibers. Sheep's wool, for instance, presents several typologies based on the breed of the animal (Markova Ivana, 2019), this literature information was confirmed with the observation of wool samples in this study, namely. Generally, wool is divided into coarse, mainly used for interior design objects such as carpets, and fine wool, used as clothing base in the fashion industry (Markova Ivana, 2019). In this study, the fibers include wools belonging to both categories.

Firstly, no convolutions are observed in all the wool fibers, instead the presence of scales is clearly visible, and this confirms the animal provenance of the samples (Greaves & Saville, n.d.). By further observation of the optical microscope photographs, it is possible to classify as fine wools the following samples: N_ZEL, MOH, CAM_MO, ALP, MON_GOT, and of course CACH.

N_ZEL photo

The N_ZEL sample presents a tight disposition of the overlapping cuticles, which appear to have a wave - regular mosaic pattern (Markova Ivana, 2019), the surface can be considered smooth since the protruding of the scales is visibly minimal. Most of the scales also seem to have a coronal disposition, surrounding the entire diameter of the fiber. All these features allowed the classification of the N_ZEL sample as a fine wool (Markova Ivana, 2019).

MOH photo

The disposition of the scales in the MOH sample appear wave-like, both regular and irregular mosaic (Markova Ivana, 2019). The cuticles are also overlapping and adherent to the surface, without protruding outwards and, therefore, giving a smooth finish to the sample's surface; this feature is responsible for Mohair's luster and softness when in contact with the skin (Markova Ivana, 2019). Like the N_ZEL sample, most of the scales appear to have a coronal disposition. Following the observation of the OM photographs and the consequent considerations, MOH can, therefore, be included in the class of fine wool fibers.

CAM_MO photo

The scales disposition in sample CAM_MO appear slightly different from the other fine wool types, this could be due to the fact that this fiber is of camelid origin. Camel fibers are considered luxury fibers and, as it is visible in sample CAM_MO, present way less scales with respect to wool (Markova Ivana, 2019); the surface is consequently very smooth. This characteristic confers CAM_MO a hypoallergenic feature.

ALP photo

The ALP fiber presents scales that appear tightly layered on the surface and without protruding outwards, thanks to the coronal form of the scales. The disposition of the cuticles appears to be a wave-irregular mosaic. Although being well-adhered and despite the smooth surface of the fiber, which are characteristics that guarantee the inclusion of this variety within fine wools, ALP is not considered a luxury fiber due to the number of its scales, which is greater with respect to the amount observed in CACH and CAM_MO (Markova Ivana, 2019).

CACH photo

The sample CACH shows the wave-regular mosaic scale pattern typical of fine wools (Markova Ivana, 2019), being one of the most luxurious fibers on the market itself. Even without studying its cross-section, the diameter of CACH is visibly smaller than that of coarse fibers, such as AUS fiber (Table XX), and it should be around 5 μm according to the literature (Markova Ivana, 2019). Moreover, the scales of sample CACH are not prominent towards the outside, are less in number with respect to coarse fibers (Markova Ivana, 2019), and are also longer along the axis than most of other species (Greaves & Saville, n.d.). The cuticles' margins also appear more distant compared to the disposition of the scales in coarse fibers; this disposition gives Cashmere its characteristic smoothness (Markova Ivana, 2019).

MON_GOT photo

The sample MON_GOT presents a regular mosaic scales (Markova Ivana, 2019). Although not having a completely smooth surface, with the scales slightly protruding outwards, this fiber shows a low number of scales, which are big and at distance from each other. The diameter of the MON_GOT fiber also appears to be smaller than coarse fibers (Markova Ivana, 2019). So, despite the slithly rough surface, it is possible to hypothesize that the MON_GOT fbers belong to the fine wool category based on the information in literature (Markova Ivana, 2019).

The remaining wool varieties, namely samples SAR_P, MOR, AUS_MER, AUS, and ARG_CO, ca be considered coarse fibers after the observation of the OM photographs. Among the samples under study, it is possible to consider as coarse fibers the samples MOR, MON_GOT, ARG_CO, SAR_P and AUS. Coarse fibers, as observed in this study, other than having a bigger diameter (33-44 μm) than fine fibers, are characterized by a rough surface. In fact, they have a greater number of scales, which are in most cases protruding towards the outside. The scales' dimension is also greater than the one of fine fibers (Markova Ivana, 2019). These characteristics give coarse fibers less luster and a less soft feeling at touch.

SAR_P photo

From the photograph with the 10x magnification it is possible to observe the rougher surface of the sample SAR_P due to the protruding outward of the cuticles; this aspect already gives a hint about the coarse nature of this wool variety (Markova Ivana, 2019). The pattern of the scales in SAR_P appears to be irregular mosaic, they appear tightly overlapping and are way more numerous with respect to the above-mentioned fine fibers. The cuticles also appear to be smaller than the ones in fine wools, not allowing them to cover the circumference of the fiber; these factors provoke their protruding outwards and their consequent exclusion from the category of fine fibers (Markova Ivana, 2019).

MOR photo

The diameter of the MOR fiber is visibly bigger than the one of fine fibers previously observed, such as the sample CACH. The pattern of the scales appears to follow a wave-irregular mosaic trend; the cuticles do not have a coronal shape due to their shortness, which is a typical trait of coarse fibers, that leads the scales to protrude toward the outside making the surface not smooth. Moreover, the scales are very numerous and this excludes the possibility to consider MOR a fine fiber (Markova Ivana, 2019).

AUS_MER photo




By observing the photograph of the sample AUS_MER at 20x, it is possible to notice its irregular surface, due to the small size of the cuticles which, for this reason, do not have a coronal shape and, therefore, protrude outwards; the pattern of the scales appear to be irregular mosaic (Markova Ivana, 2019). Considering these aspects, along with the information in literature, the fiber AUS_MER could be considered as a coarse variety.

AUS photo

The AUS sample shows well defined scales that protrude outwards, depriving the surface of smoothness; the photograph at 20x magnification gives the idea of this observation. The diameter of the fiber also appears bigger than the above-mentioned fine wools. The scales pattern seems to follow a regular mosaic trend (Markova Ivana, 2019). Considering the diameter and the rough surface, it is possible to hypothesize that the AUS sample belongs to the coarse fiber category.

The wool samples given by Rubelli were also observed under OM. Two wool varieties were included in the gifted collection: combed wool (L_PET) and Savile Row (SAV_R), a plain satin textile made of pure combed wool. Table XX shows the results of this preliminary morphological study.

Table XX: OM images of the Rubelli wool samples L_PET and SAV_R

L_PET

L_PET 4x

L_PET 10x

L_PET 63x
SAV_R



SAV_R textile



SAV_R 4x: As for the sample L_PET, low magnifications (4x) allow the observation of the twisting of the single fiber that, when intertwined together, form the final yarn.



SAV_R 10x



L_PET photo

At low magnifications (4x) it is possible to notice how the single fibers of the sample L_PET are intertwined with one another to form the yarn. As the magnification increases (10x, 40x) it is possible to identify the morphology of the fiber. The scales appear to have a wave-regular mosaic configuration with a coronal disposition (Markova Ivana, 2019); the surface is smooth and the diameter of the fiber seems to be like those belonging to the fine fibers category. The photographs of L_PET at 63x confirms the before mentioned observations, in particular the coronal shape of the cuticles, their pattern, and the smoothness of the surface. The scales also appear to be less numerous and this, among the previous considerations, is a typical characteristic of fine fibers (Markova Ivana, 2019).

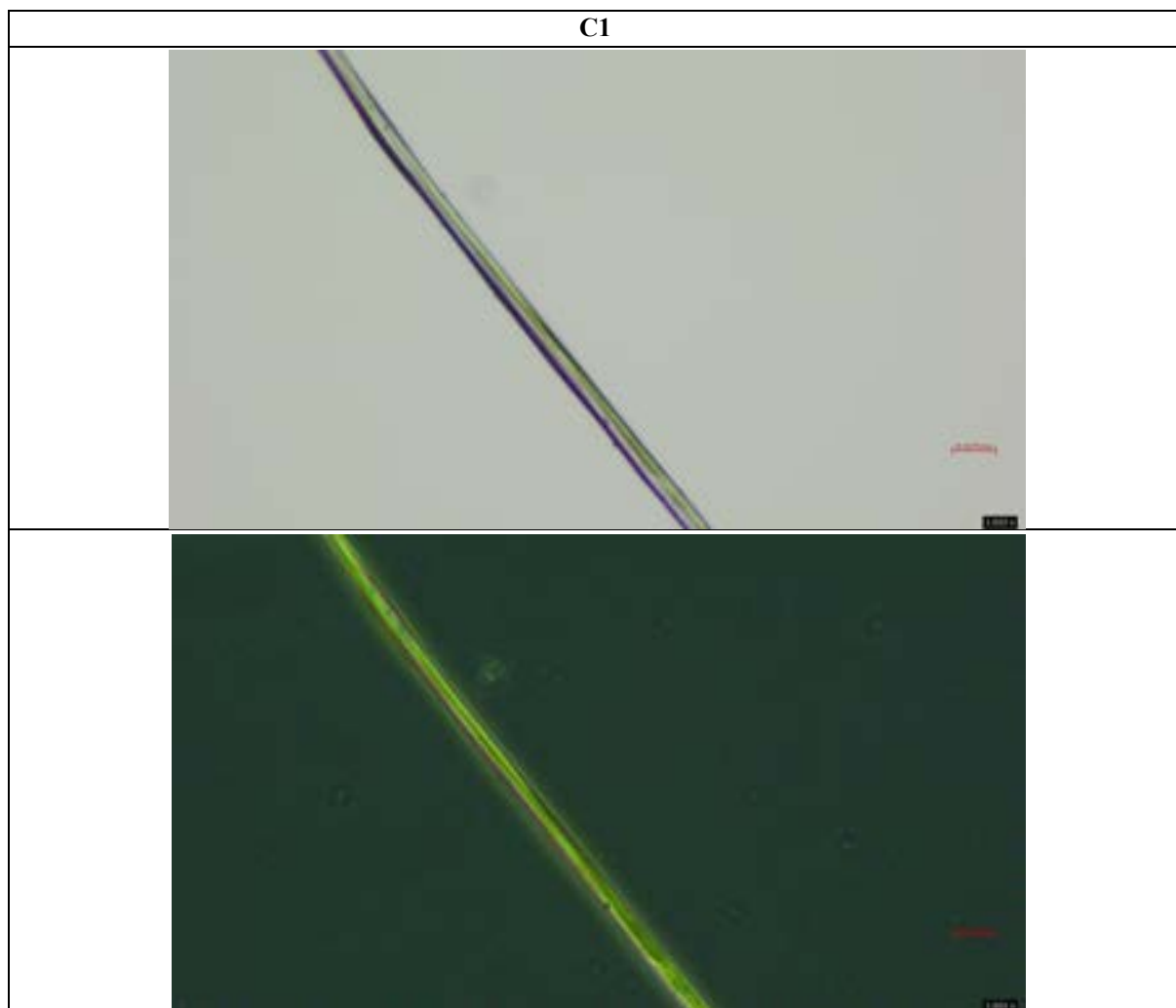
SAV_R photo

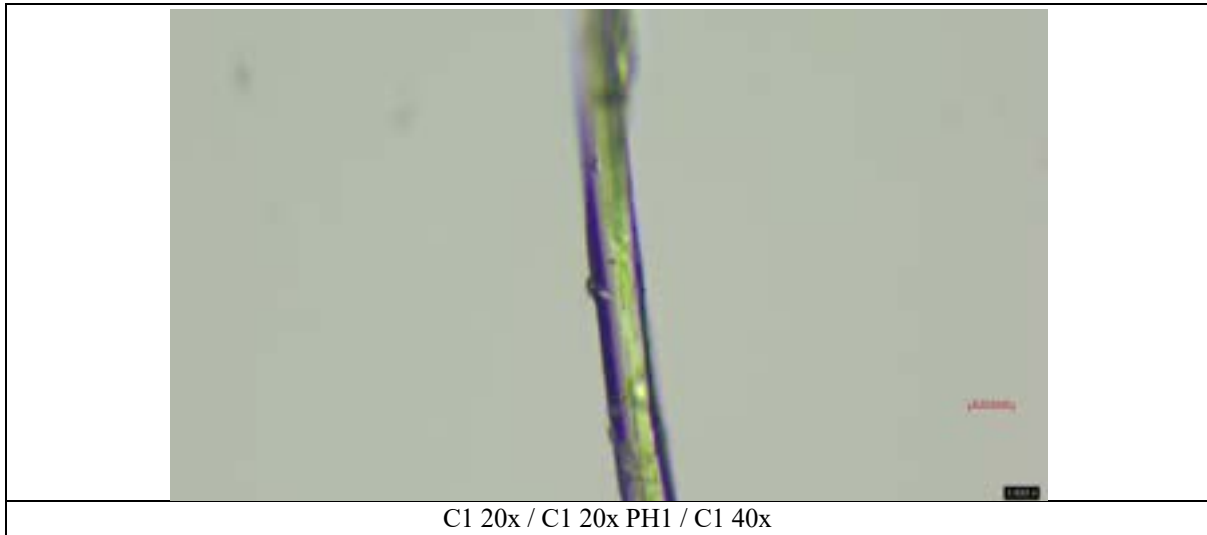
SAV_R is the first processed textile examined in this section; although being visibly dyed (Figure XX – picture of the Rubelli textile), no evident traces of dyes or color are visible in the OM photographs. The morphology of SAV_R is typical of animal fibers, since the presence of scales throughout the overall surface of the fiber is evident (Greaves & Saville, n.d.). The pattern of the cuticles, unlike L_PET, seems to follow a wave-irregular mosaic and does not present a coronal shape (Markova Ivana, 2019). Moreover, the number of the scales seems higher respect the L_PET sample. These considerations lead the observer to identify the fibers of the SAV_R textile as coarse fibers (Markova Ivana, 2019). This is an unexpected result since, given the information supplied by Rubelli, the Saville Row textile is made of combed wool, here L_PET; the morphology of the two fibers was, therefore, expected to be the same. The differences in the fibers appearances could be due to a simple misunderstanding with the information given by the industry, or it could be due to the **behavior of the textile following the manufacturing process, including dyeing** (Timar-Balazsy & Eastop, 2011).

Silk

The following table contains the pictures of the reference silk sample C1 and the two varieties of silk belonging to the Rubelli set, namely the silk yarn C2 and the *sdrucito* textile patch C3_S consisting of blue yarn-dyed silk.

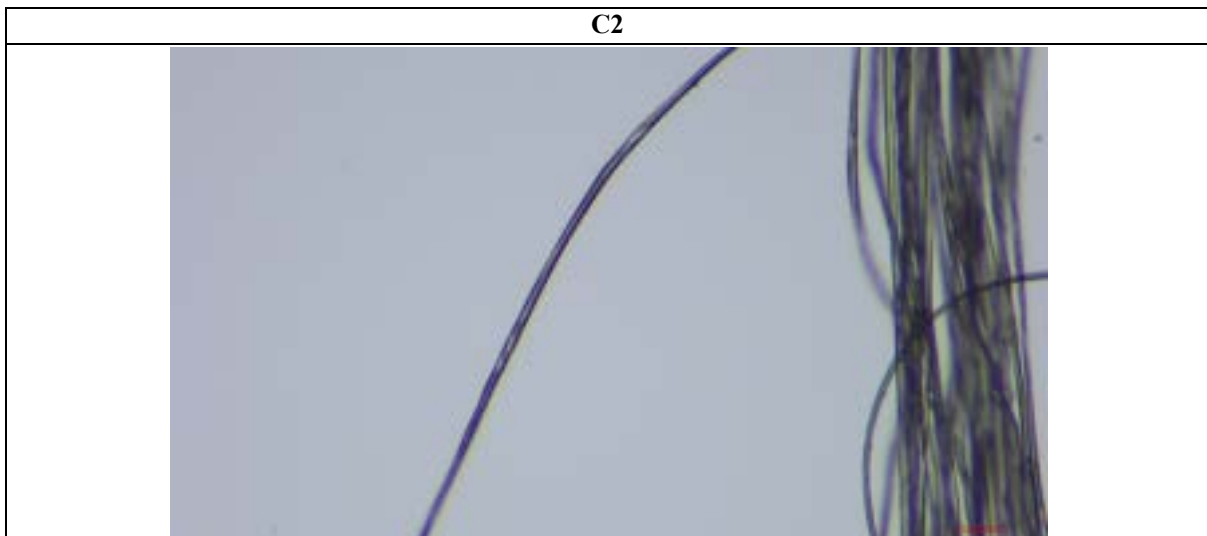
Table XX: photographic campaign of the reference and Rubelli silk samples.

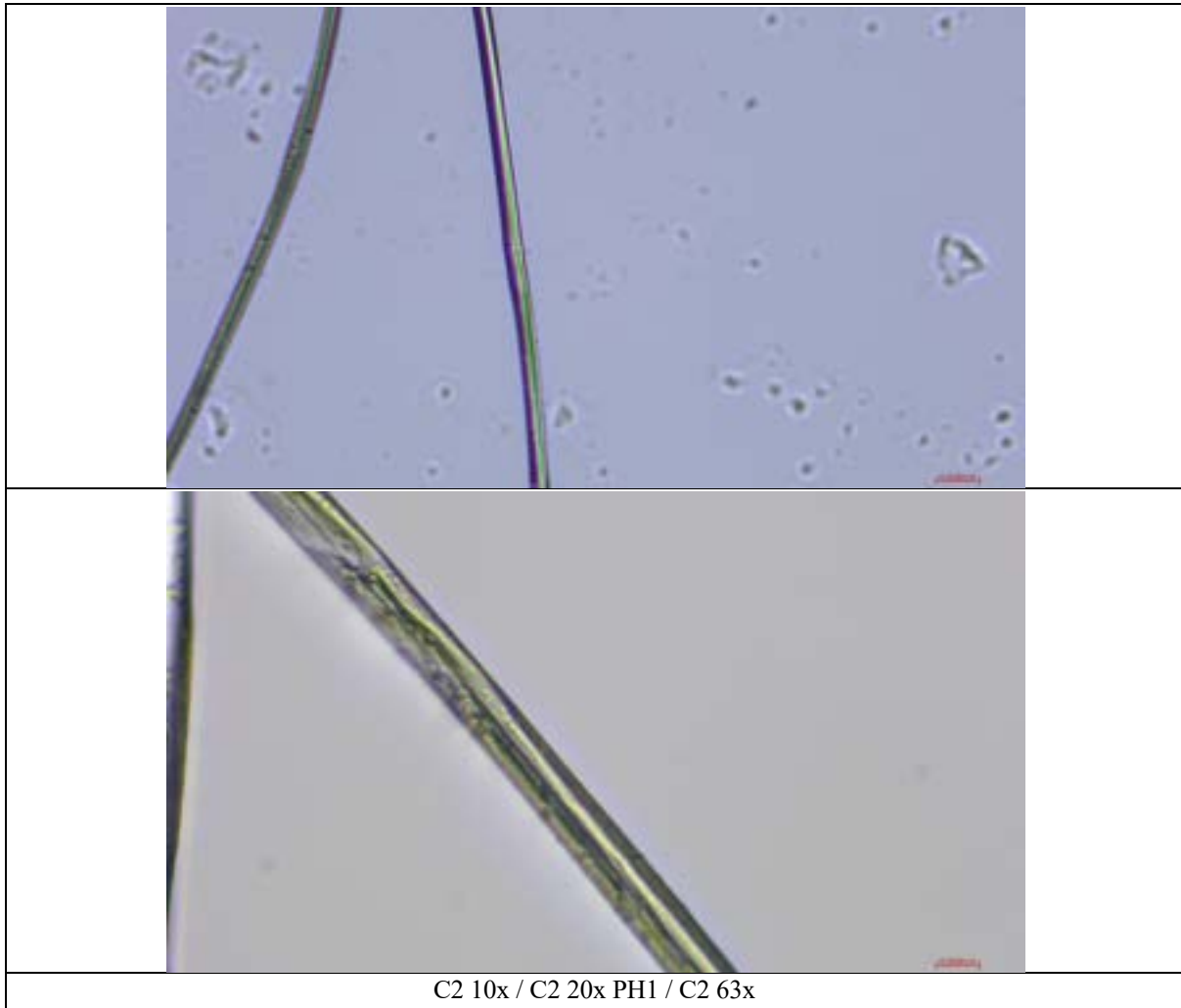




C1 photo

The photographic evidence of the sample C1, Chinese silk, shows that the fiber presents a smooth surface and a small diameter even at the 20x magnification, in concordance with literature (Markova Ivana, 2019) (Favaro et al., 2021). The surface of C1 presents **small protuberances** visible both at 20x and 40x where a few longitudinal striations are visible and could be attributable to wild silk, more specifically the Tussah variation (Markova Ivana, 2019).



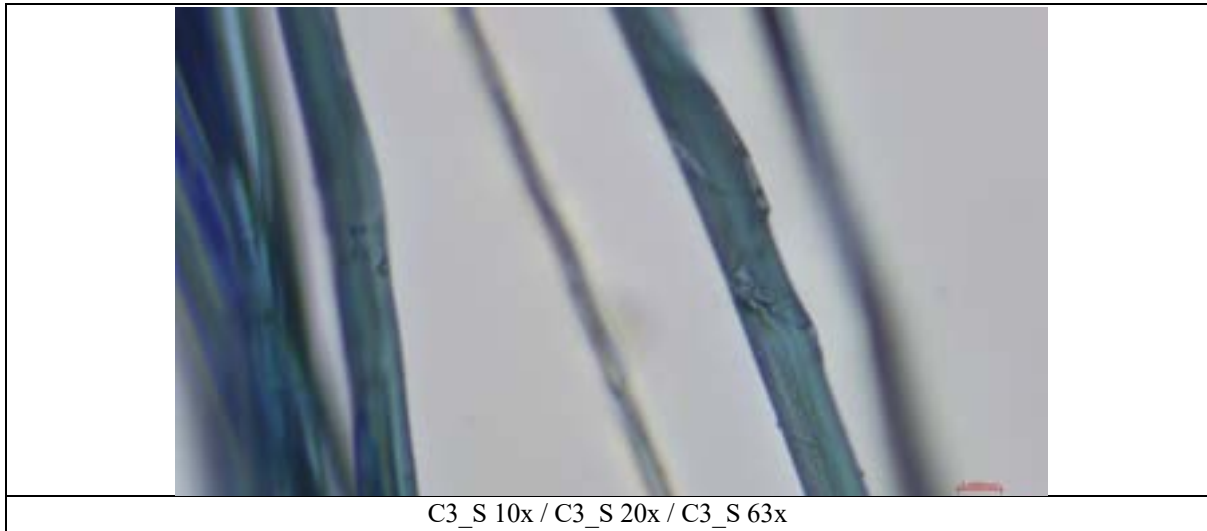


C2 photo

The morphology of the sample C2 appears smooth and with long cylindrical filaments, as according with the information in literature (Markova Ivana, 2019). By observing the photograph at 10x it is possible to notice some shrinkages in the filament structure. At high magnifications (63x) some inhomogeneities are visible on the surface of C2; the longitudinal striations typical of Tussah wild silk is here still recognizable (Favaro et al., 2021), but the area presents the above-mentioned shrinkages, which are here visible in detail. These deformations are conducive to the **manufacturing process of the yarn**.

C3_S





C3_S photo

The surface of sample C3_S appears in the complex smooth, even though it presents a few **protuberances**. The shape of the filament is not completely longitudinal, and at high magnifications (63x) the fiber appears quite damaged, but still presenting the straight striping of wild silk (Favaro et al., 2021)(Markova Ivana, 2019). Appreciable is the evidence of the blue dye of the C3_S textile which results very visible in the OM photographs.

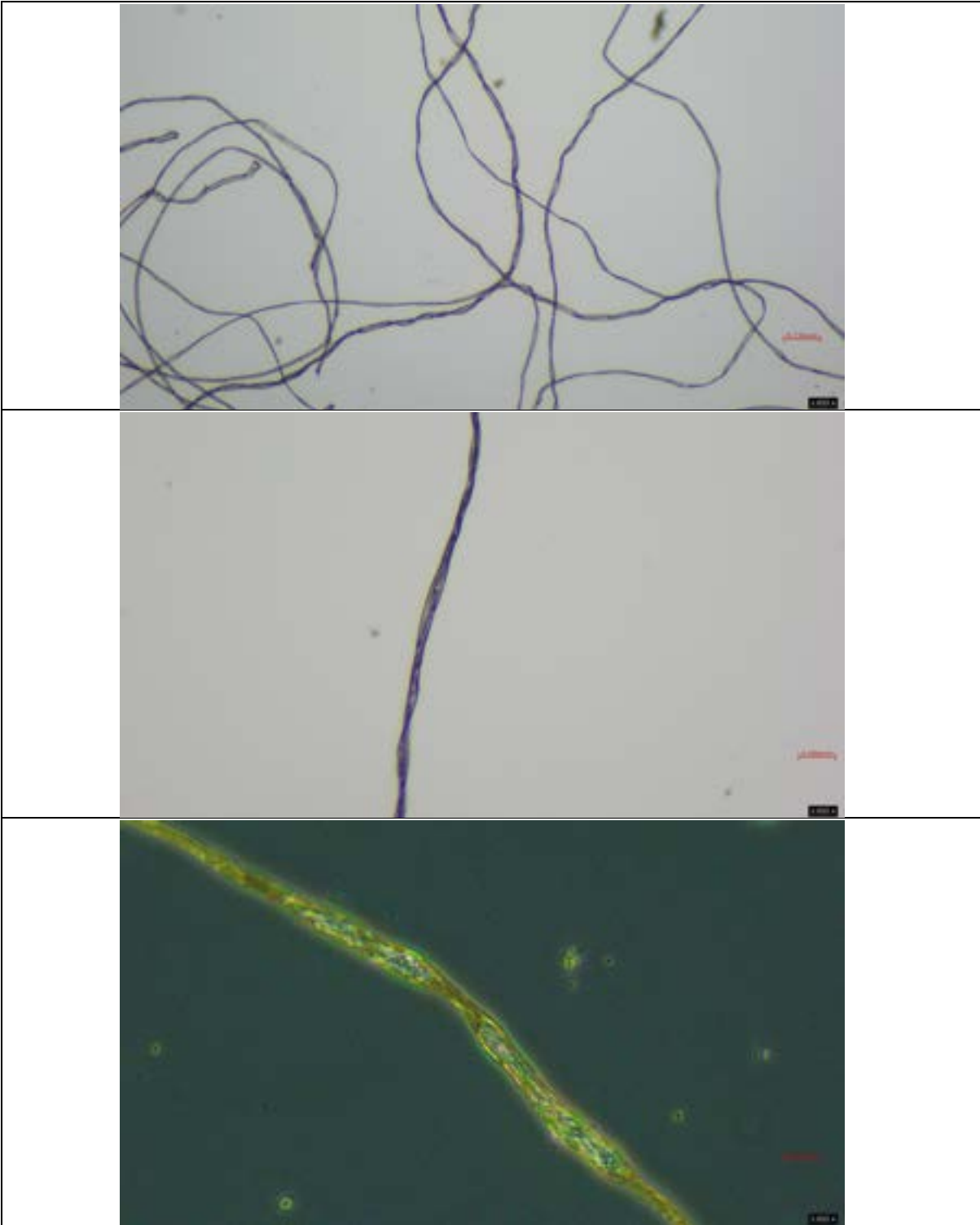
Cellulosic fibers

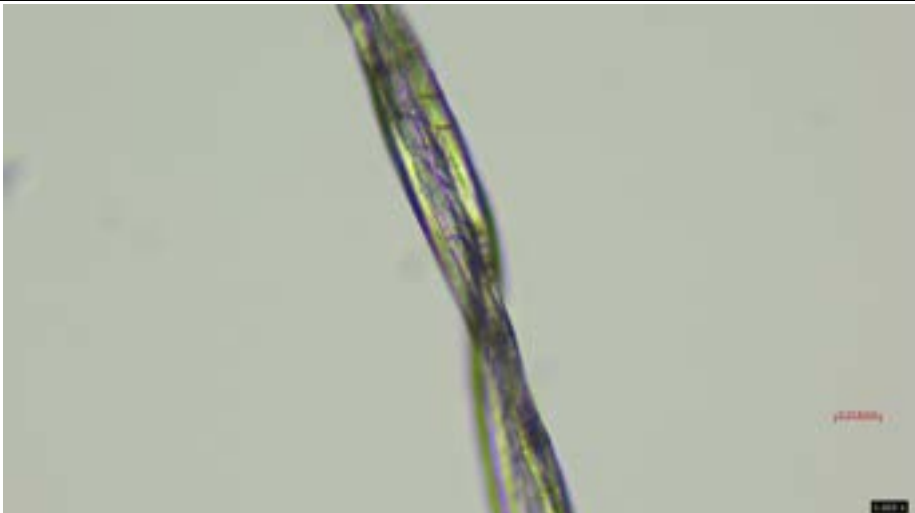
Cotton

Table XX shows the OM photographs of the reference cotton sample, CO_G, and the sample textile included in the Rubelli set, CO_R, that is a yarn-dyed fabric of combed cotton.

Table XX: photographic campaign of the reference and Rubelli cotton samples.

CO_G

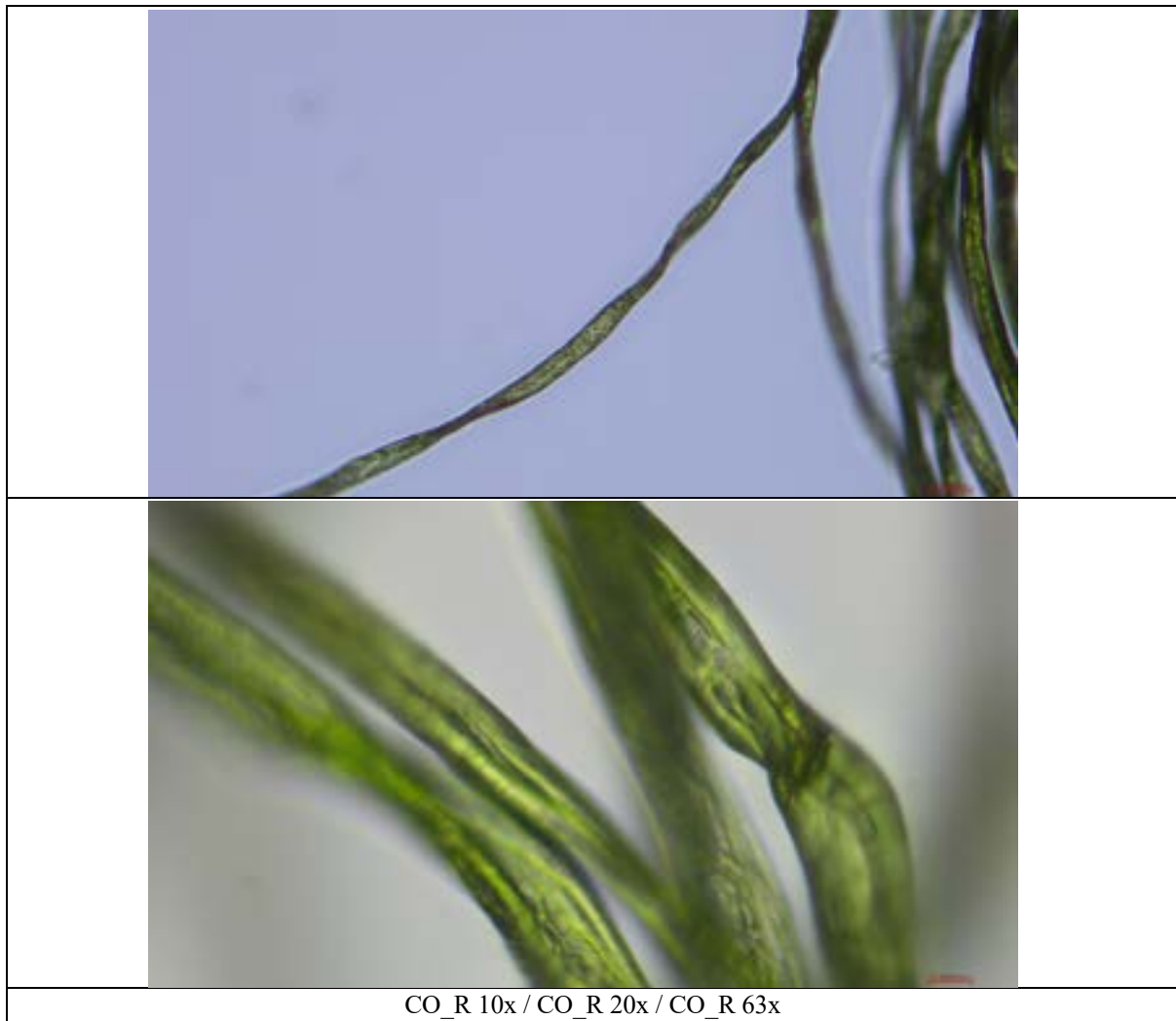




CO_G 4x / CO_G 10x / CO_G 20 PH1 filter / CO_G 40x

CO_R





CO_G and CO_R photo

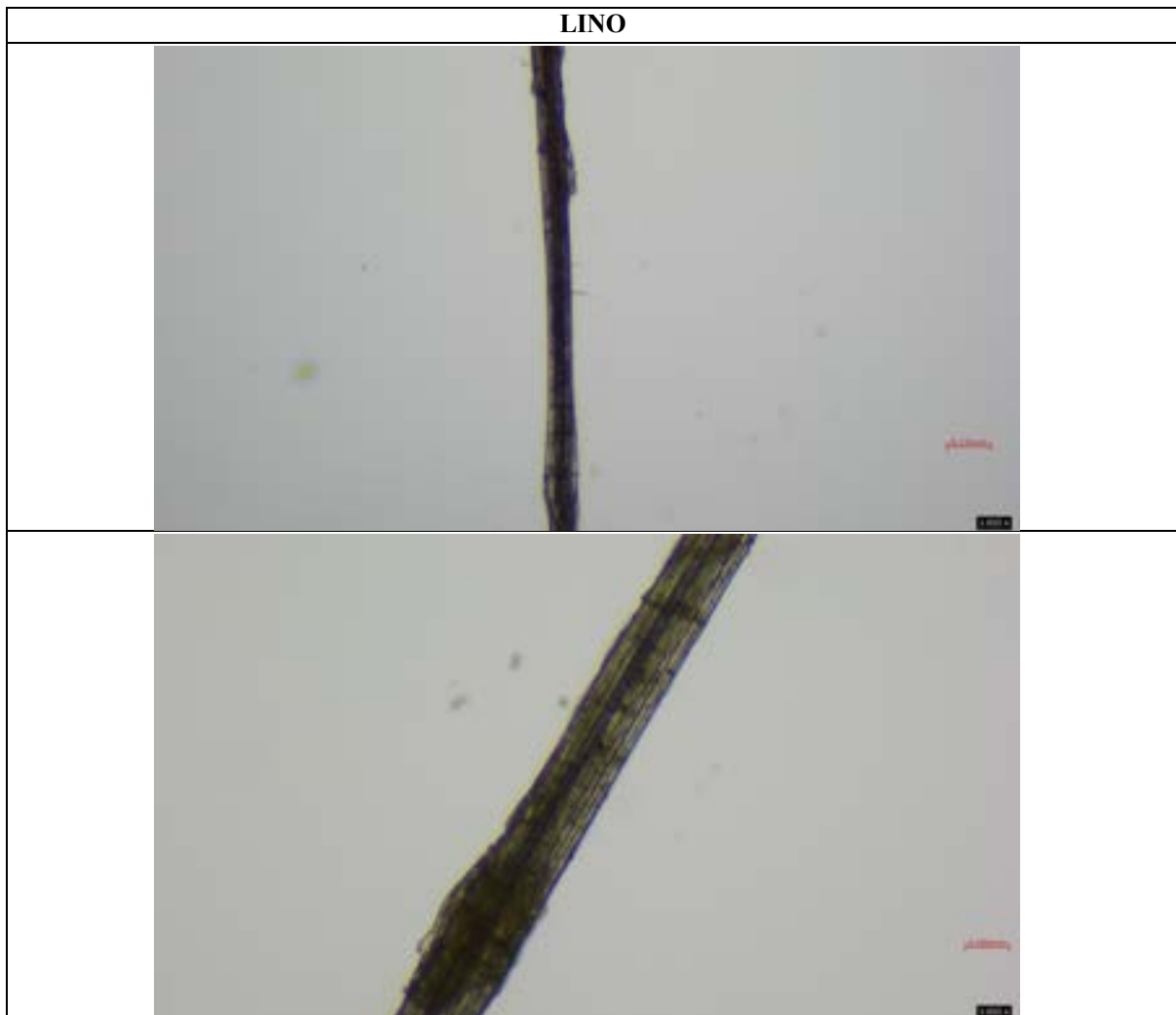
The cotton fibers under study show the characteristic ribbon-like convolutions of this cellulosic fiber (Markova Ivana, 2019) (Greaves & Saville, n.d.), which in this case are very well defined in both the untreated (CO_G) and dyed (CO_R) samples already at the low magnification of 4x. This would indicate that the chemical treatments for the dyeing and preparation of the CO_R textile, for example the mercerization treatment, did not affect the structural properties of the fibers, since the characteristic convolutions are intact and placed at a small distance between one another and the overall appearance of the fiber seems undamaged (Markova Ivana, 2019). The component of the green dye of the CO_R sample is very visible in the observed OM photographs.

Observing the 40x image of both CO_G and CO_R, a minor shrinkage is visible in the center of the fiber, between the longitudinal margins of the convolution; probably this shows that the fiber of samples come from an immature cotton boll (Markova Ivana, 2019). Further investigations of the cross section of the fiber would be required to confirm or deny this hypothesis.

Linen

Table XX shows the photographs of the two reference linen samples, LINO, and LI_G, and the fabric included in the Rubelli set, LI_18.

Table XX: photographic campaign of the reference and Rubelli linen samples.

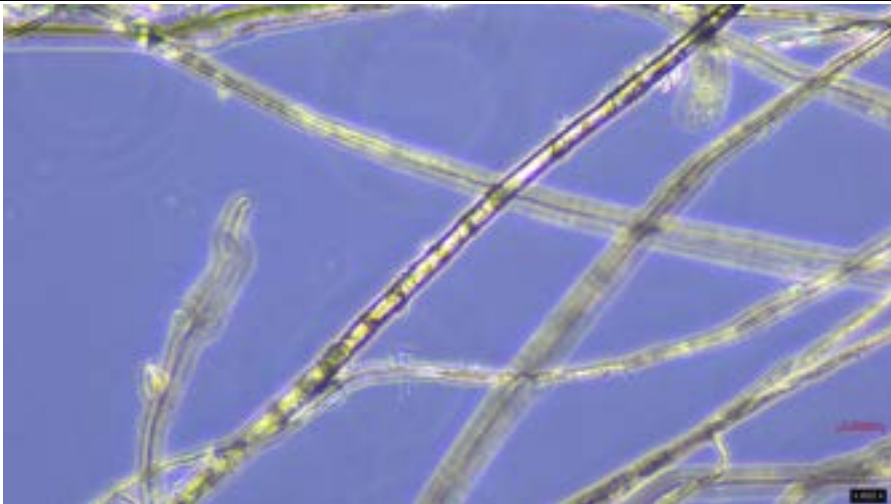




LINO 4x / 10x / 20x

LI_G

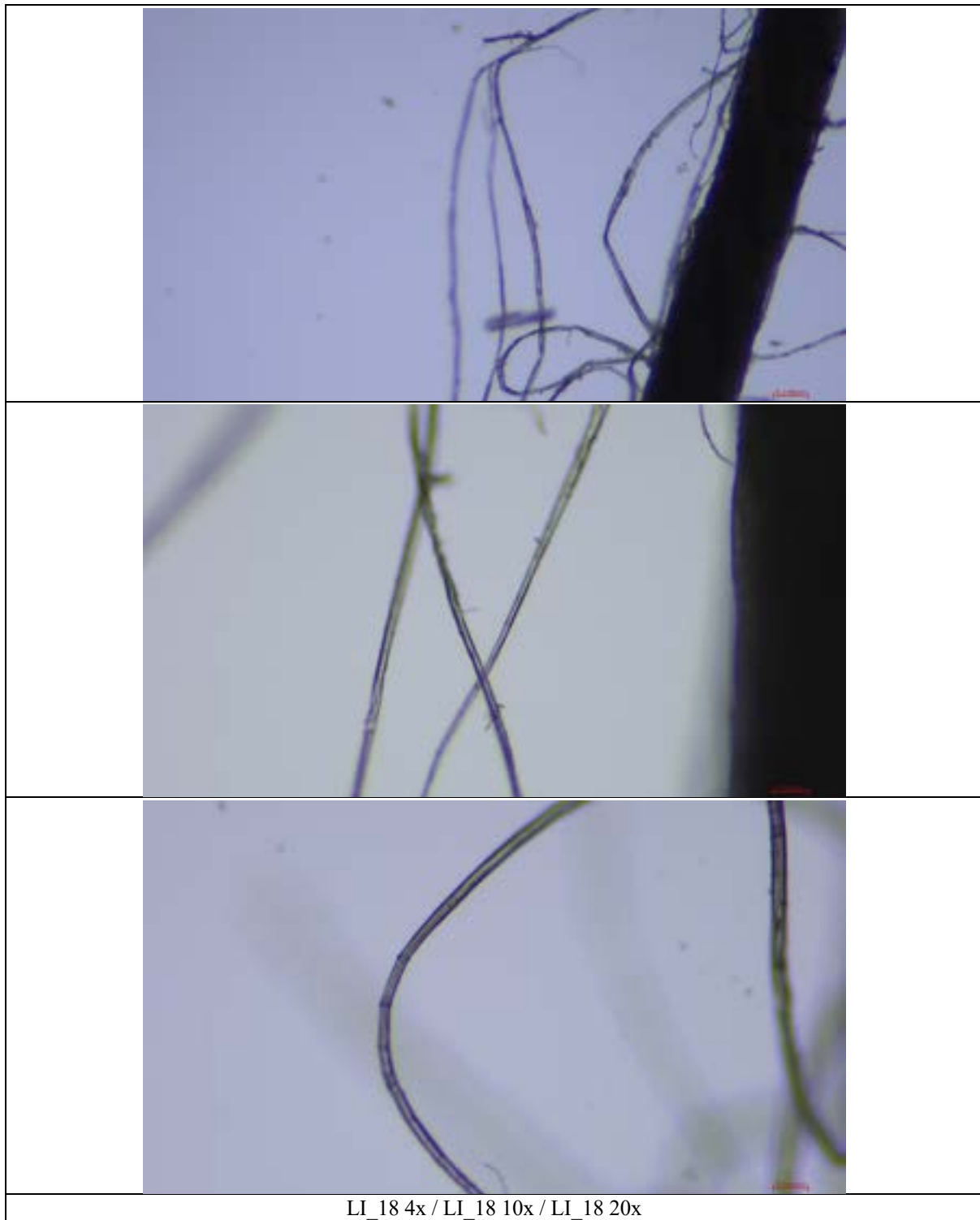




LI_G 4x / LI_G 10x / LI_G 10x PH1 filter / LI_G 40x

LI_18





LINO photo

The sample LINO, which at the naked eye appears brown and of rough texture, shows the typical characteristics of linen fibers: the straight course of the fibers and the bamboo-like nodes (Markova Ivana, 2019) (Greaves & Saville, n.d.), especially at 20x; in this case, also evidence of the ultimate fibers is clearly visible (Mather & Wardman, 2015). LINO, therefore, can be considered as a **virgin** fiber, also thanks to its healthy and compact aspect.

LI_G photo

The LI_G sample is another variety of raw linen but, since it appears white, it could be said that this specimen has **undergone some level of bleaching**, also given the fact that the fiber results frayed throughout its length, visible at both 4x and 10x, with slight shrinkage areas spread over the surface of the fiber visible at 4x. Despite this, it presents long fibers connected by the characteristic nodes (Markova Ivana, 2019), visible in detail at 40x magnification.

LI_18 photo

LI_18 is a variety of linen bleached by 1/8; according to the information given by supplier, this is a typical nomenclature system to indicate the level of whitening a linen batch has undergone. As in LI_G, the surface of LI_18 appears significantly frayed, as it is visible in the pictures a 4x and 10x. Despite this, the typical conjunction nodes are clearly visible (Markova Ivana, 2019), although seeming lesser in number with respect to LI_G.

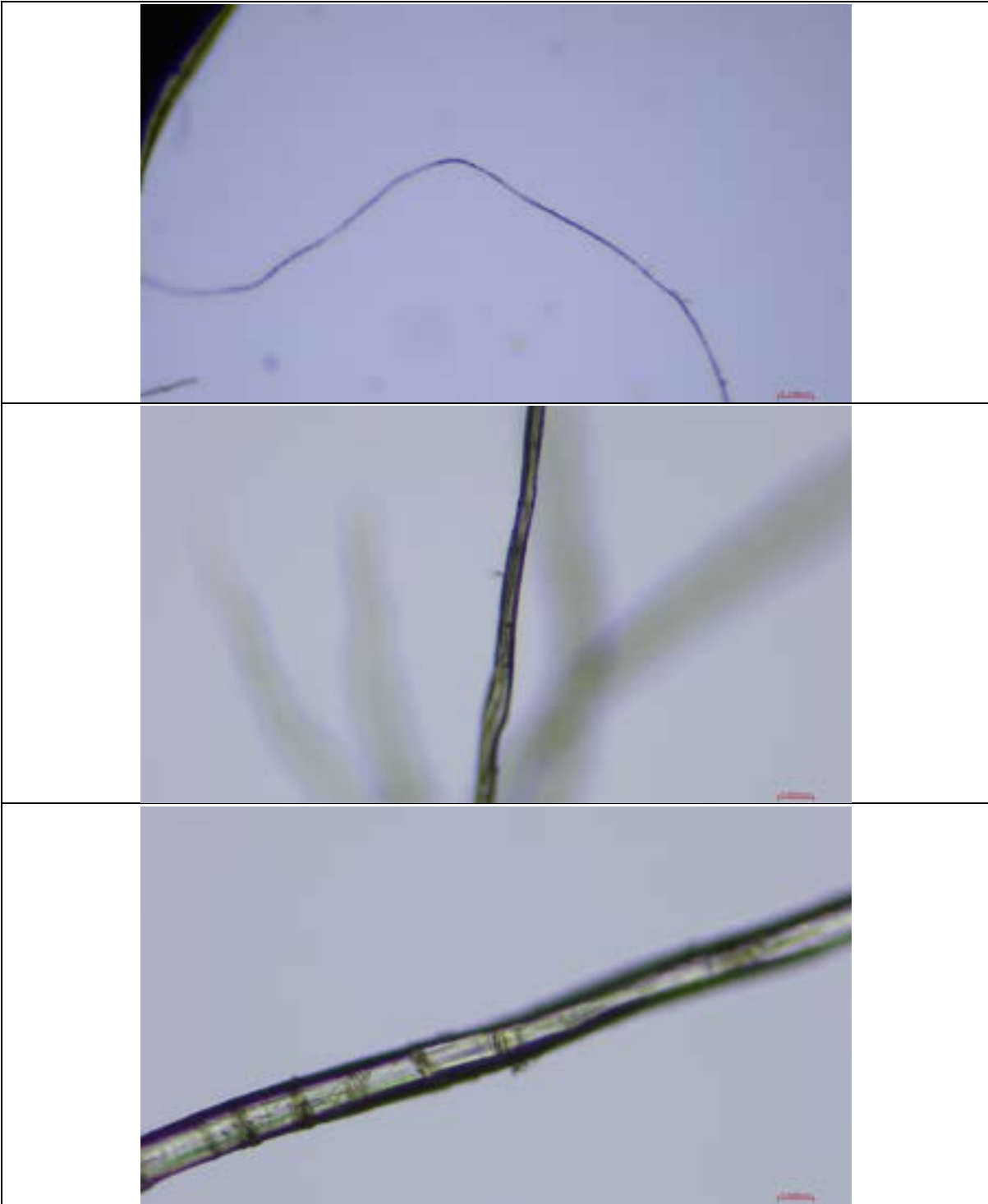
From the observation of the OM photographs, a common similarity that can be highlighted between LI_G and LI_18 is the smaller diameter of their processed fibers, which is greatly inferior with respect to the coarse and unprocessed fibers of sample LINO.

Hemp

When studied under optical microscope, Table XX table shows the photographs of the Rubelli hemp samples.

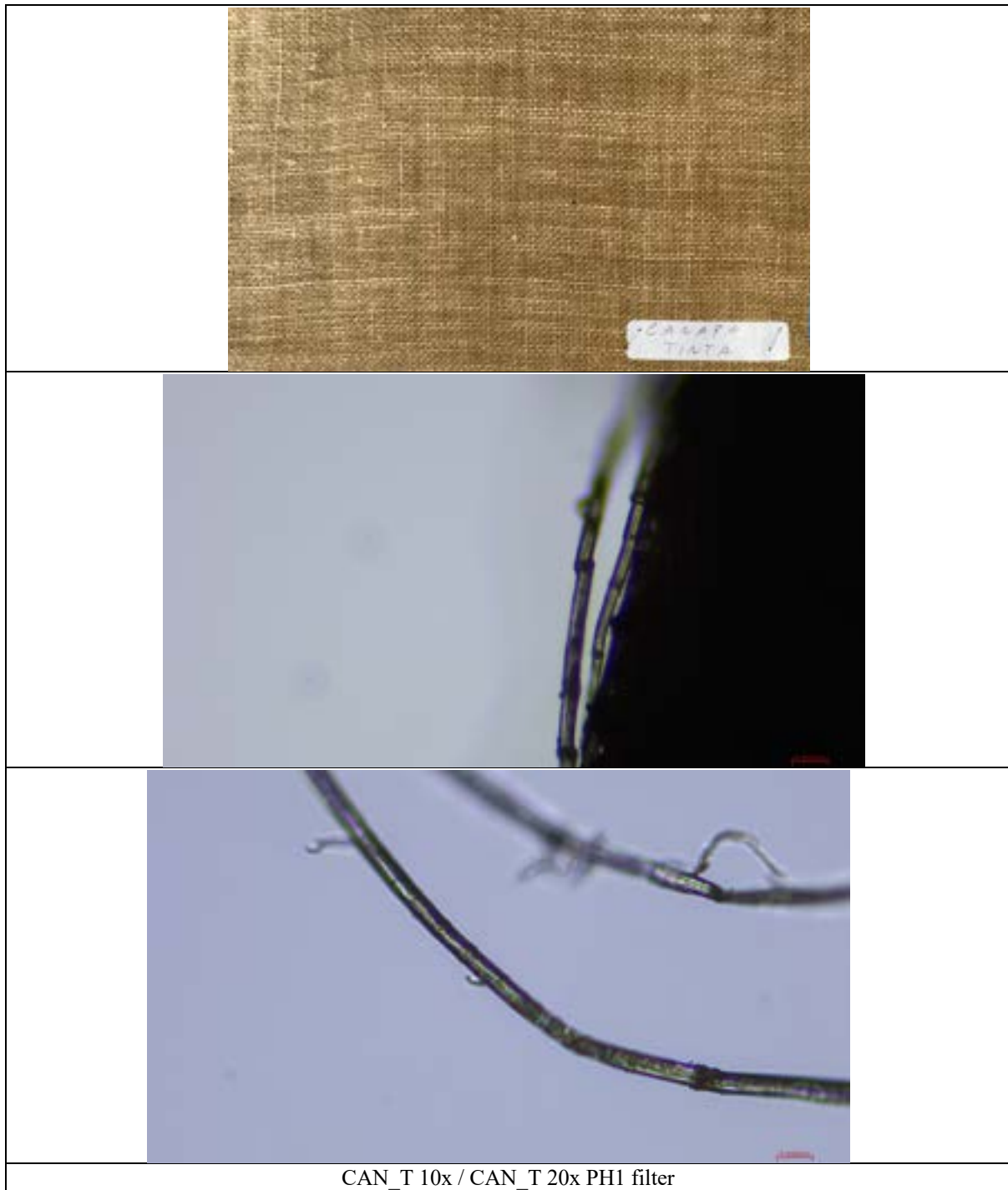
Table XX: photographic campaign of the reference and Rubelli hemp samples.





CAN_G 4x / CAN_G 10x / CAN_G 20x

CAN_T



CAN_G and CAN_T photo

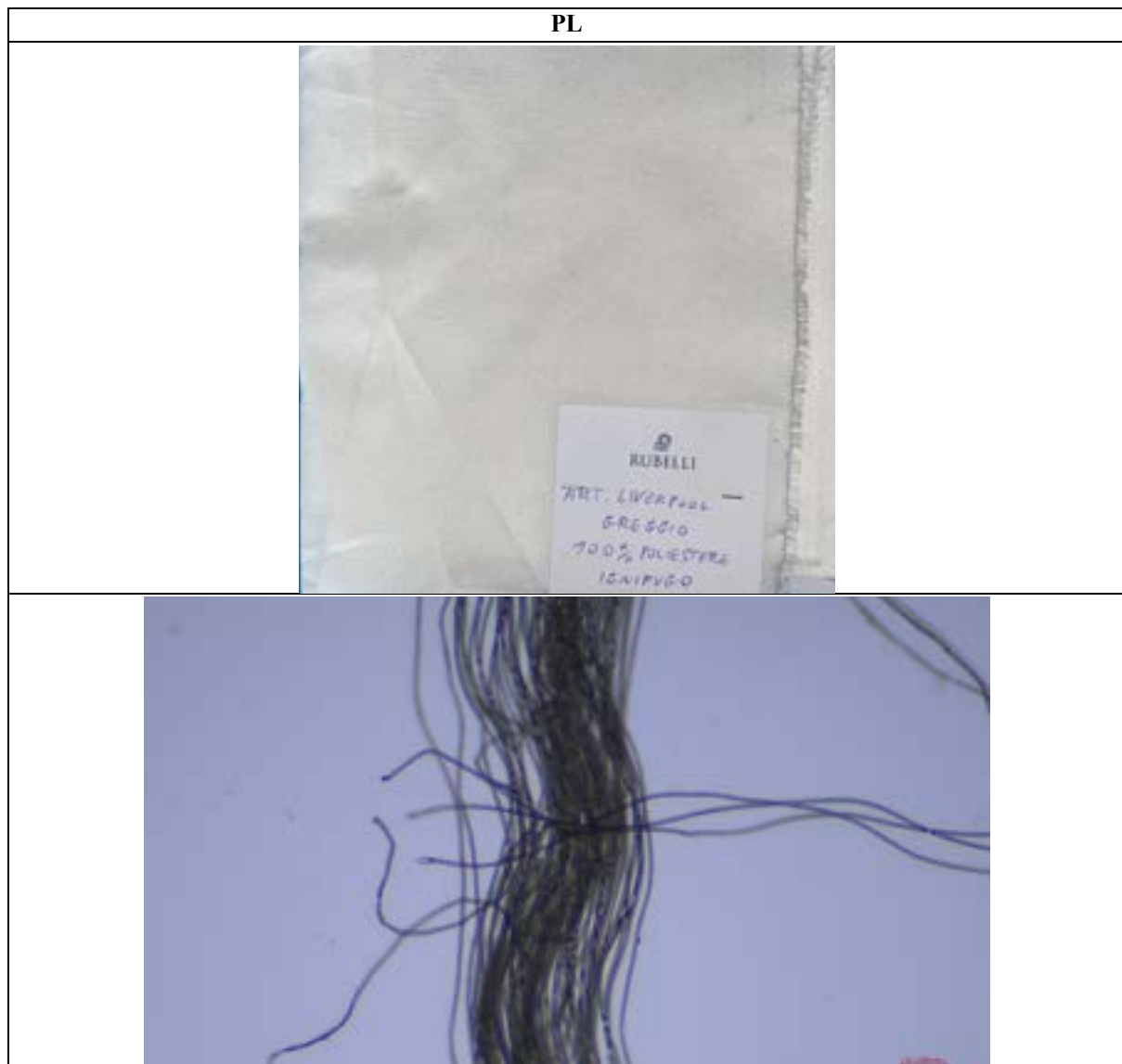
The samples CAN_G and CAN_T consist in row hemp and tinted hemp respectively. When observing the samples at low magnifications (CAN_G 4x) it is possible to observe the rough texture that characterizes hemp fibers, consisting of a longitudinal structure interspersed with conjunction nodes, like the ones found in linen fibers (Markova Ivana, 2019). The only visible difference between rough and tinted hemp varieties is the slightly dark color on the tinted CAN_T fibers.

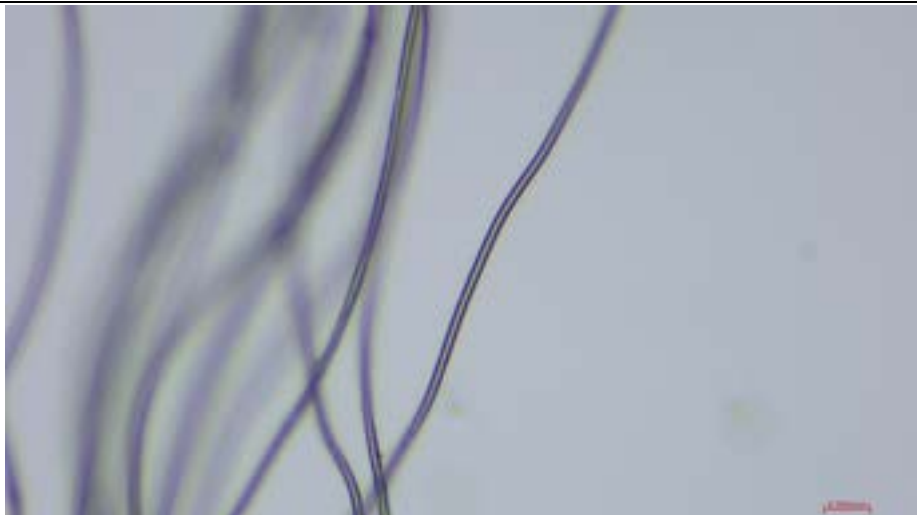
Synthetic fibers

Polyester

Table XX shows the two polyester samples belonging to the Rubelli set.

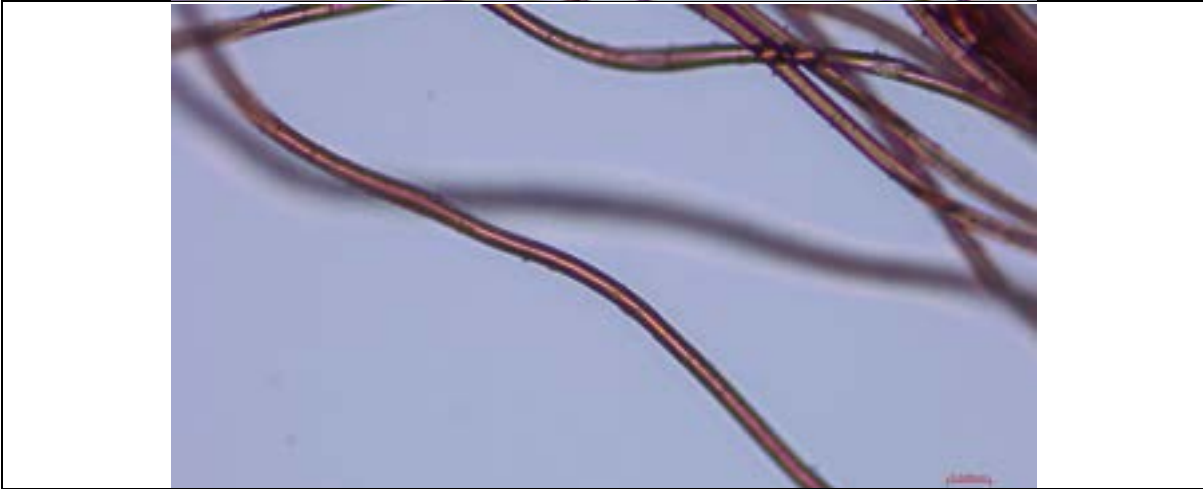
Table XX: photographic campaign of the reference and Rubelli hemp samples.





PL 4x / PL 10x / PL 20x PH1 filter / PL 63x /

PL_R





PL and PL_R photo

The two samples consist of two fireproof and tinted polyester textiles, namely PL (white) and PL_R (red). Both PL and PL_R show the characteristic polyester morphology at each magnification, consisting in a smooth cylindrical rod (Markova Ivana, 2019). At 20x some foreign small bodies appear attached to the surface of the fiber PL but, since they do not appear also on the fibers in the background, we could think of them as small dust particles on the microscope glass. This is not valid for the PL_R sample which, at the same magnification (20x) clearly shows the presence of small strands coming from the main fiber. This damaging of the fiber is probably due to the dyeing process the sample PL_R has undergone.

Spectroscopic analyses

Spectroscopic analyses were performed on the samples from both the reference and Rubelli sets to study the chemical composition of the specimens. The techniques used in this research were ATR-FTIR, ER-FTIR, Raman, and FORS, their use and physical principle are explained in the Materials and Methods chapter.

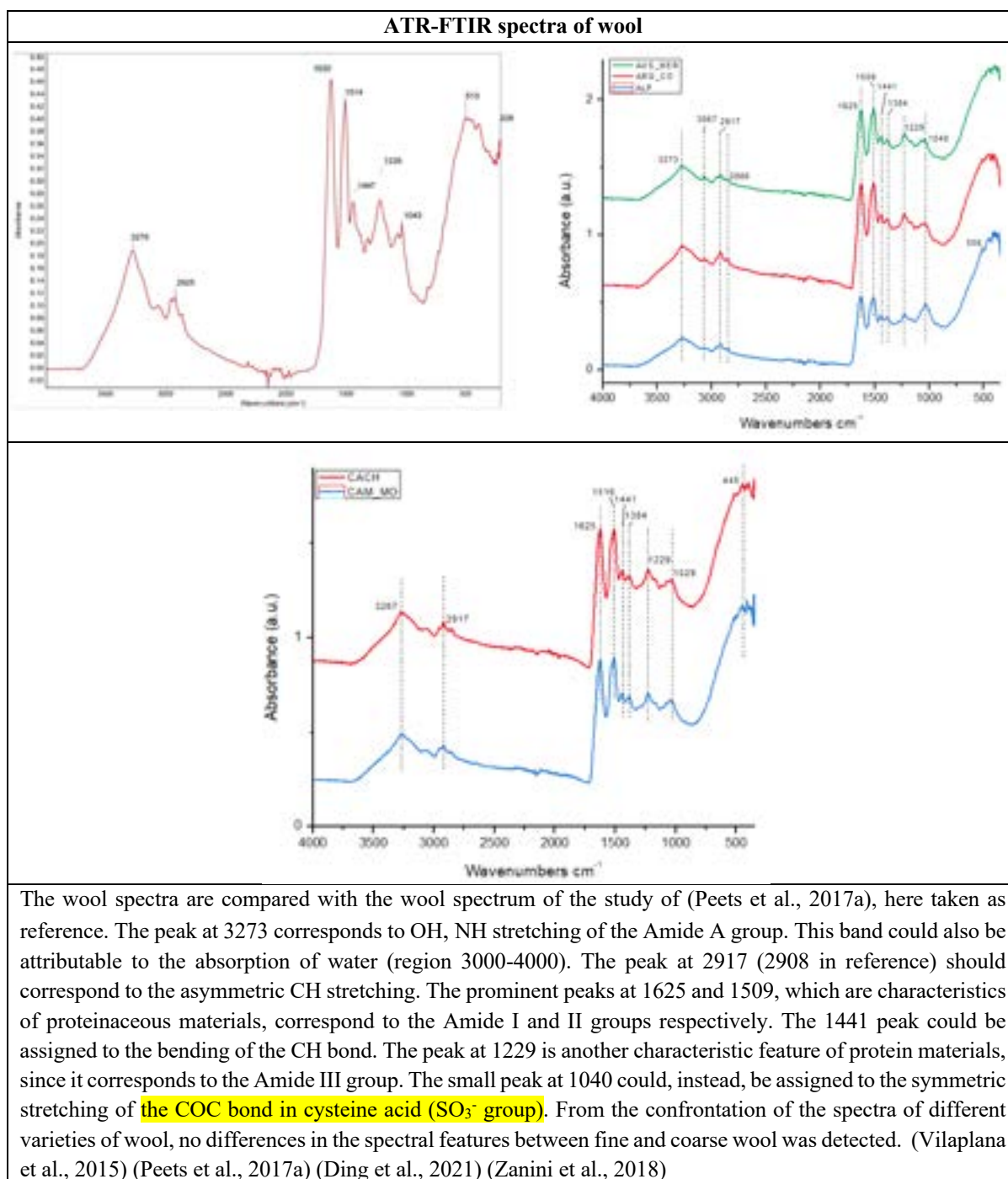
The set of reference textiles (REF), consisting of various wool varieties, cotton, linen, and silk, was first analyzed. The results were then compared to the spectra of the Rubelli set to confirm the chemical composition of each textile.

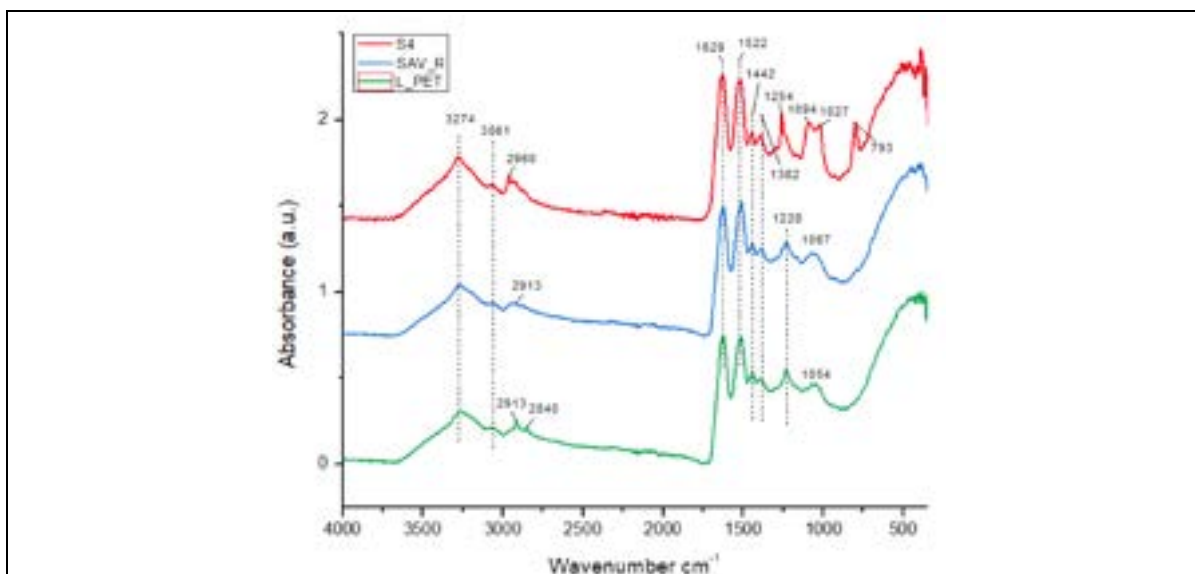
Animal fibers

Wool

The following table shows the most significant wool spectra acquired with ATR-FTIR. The following spectra belong to the reference set of textiles. For the interpretation, the spectral reference values in the Appendix XX were used.

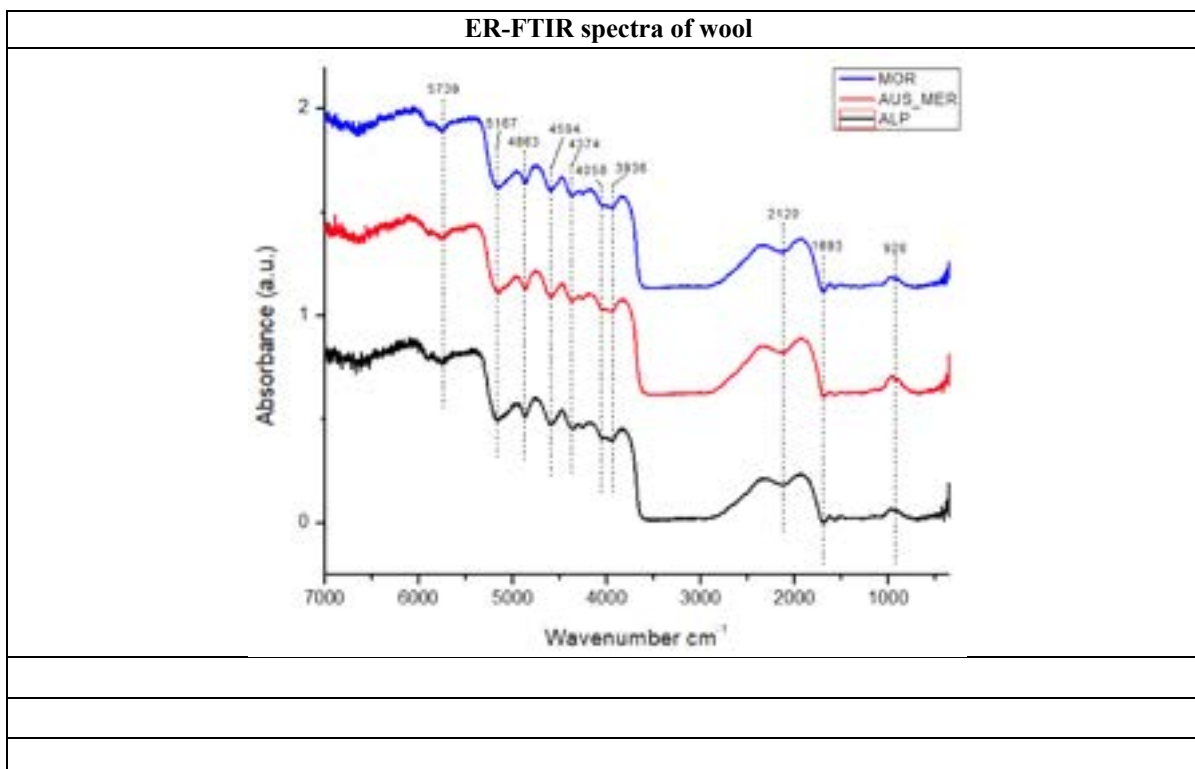
Table XX shows the commented ATR-FTIR spectra of the reference wool samples.



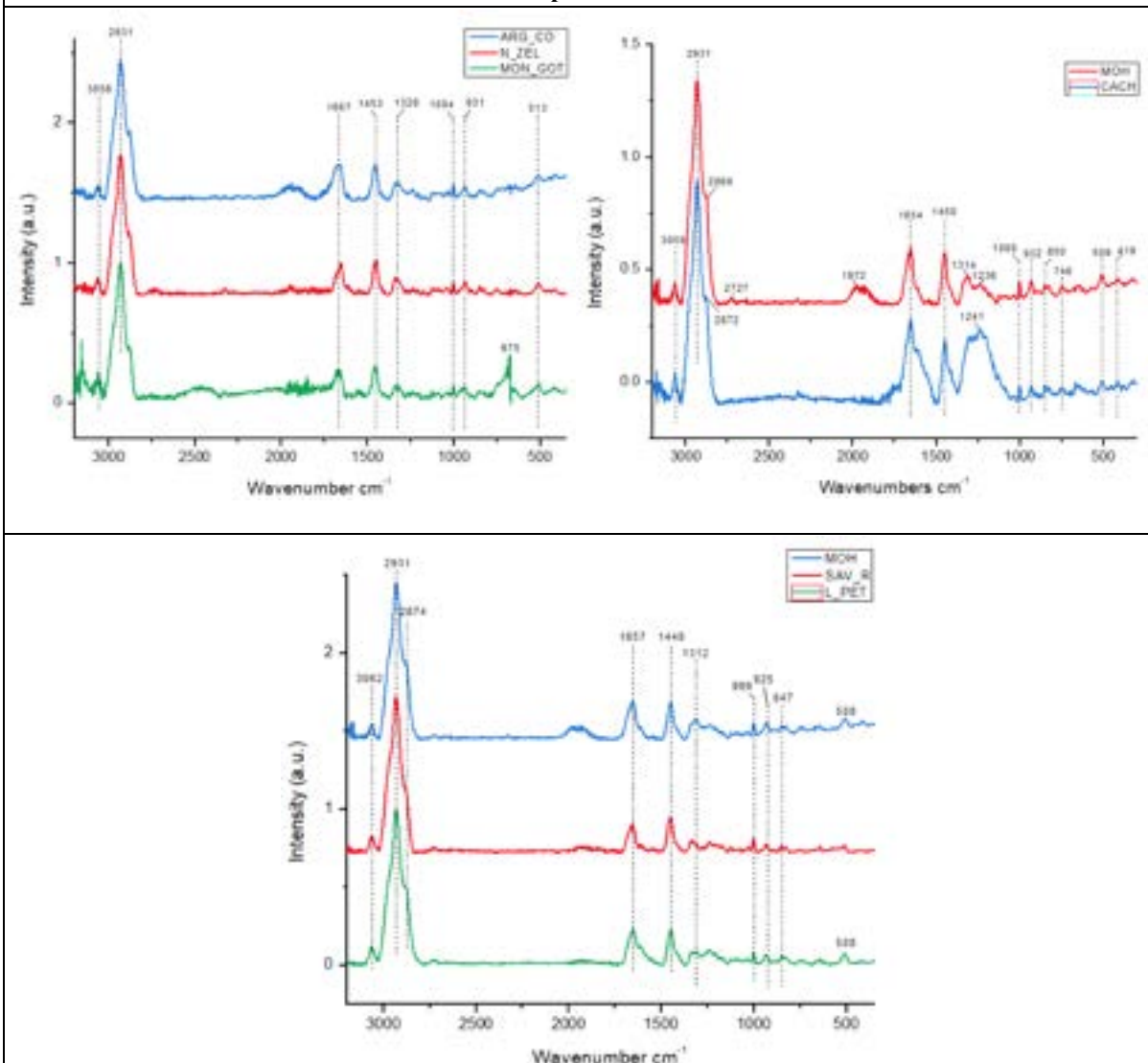


The above spectrum shows the spectroscopic features of some of the wool samples of the Rubelli set. The S4 sample comes from a woven textile made from a mixture of wools, SAV_R is a satin, yarn-dyed textile made of combed wool, and finally L_PET is the undyed combed wool in question. The overall trend of the spectra are similar, with the typical proteinaceous bands of the Amide groups at 1629, 1522, and 1228. This latter peak, appears shifted to lightly higher wavenumbers in the S4 spectra, it is in fact located at 1254. This samples also shows a prominent peak at 793; while the band at 1067 and 1054 in SAV_R and L_PET respectively, results split in the S4 sample, with two main peaks at 1094 and 1027. The SAV_R and L_PET peaks are very similar as one would expect, with the only difference in the peak at 2840 in the L_PET sample, that could be assigned to a CH stretching (Zanini et al., 2018)

The following table shows the ER-FTIR spectra of the wool samples.

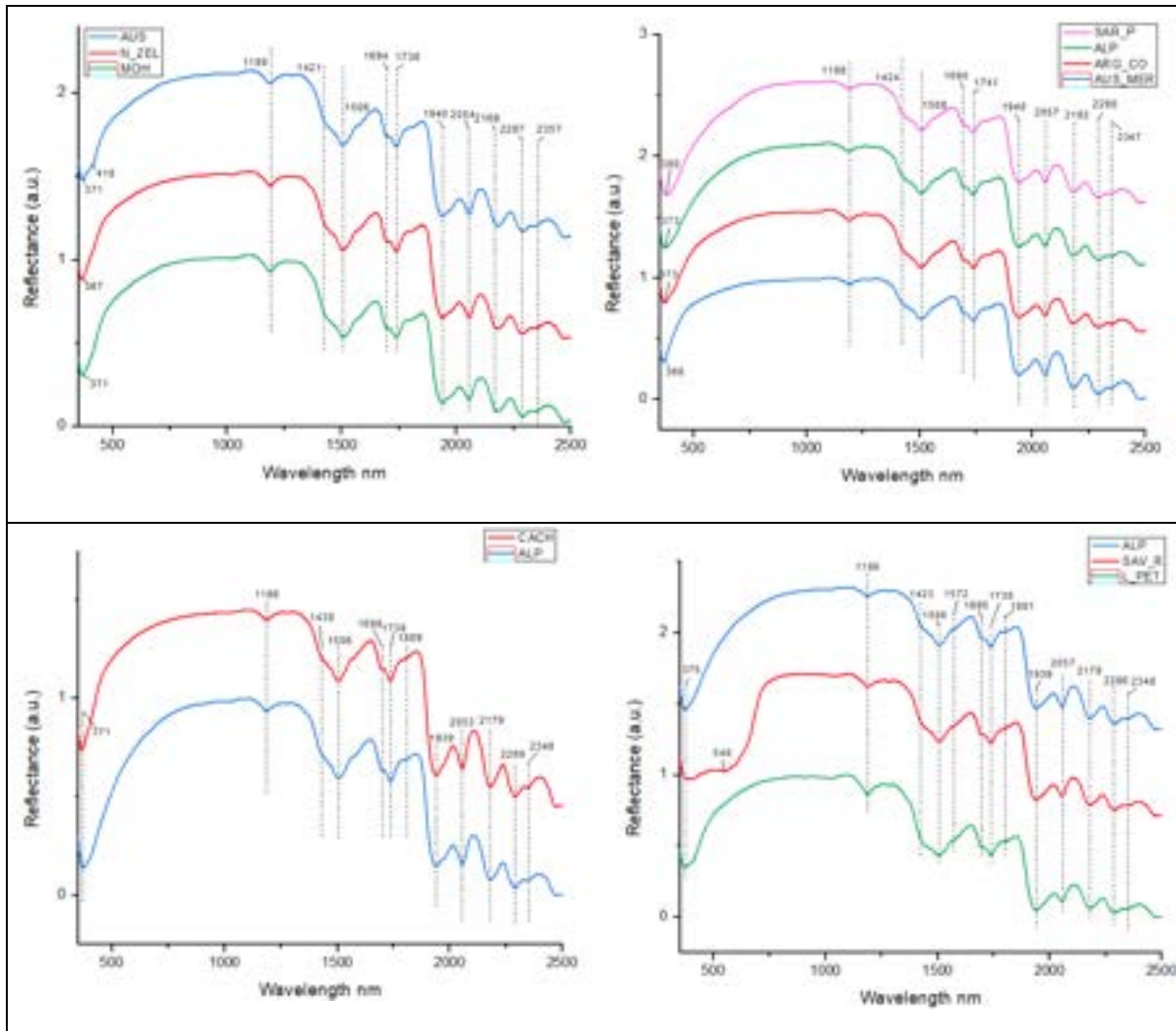


Raman spectra of wool



The prominent peak at 2931 could be assigned to a stretching vibration of a CH bond. The peaks at 1667/1654/1657 correspond to the Amide I group, precisely to the stretching of the C=O and COO bonds. The peak at around 1450 could be assigned to the bending of the COO, while the peak at around 1311 corresponds to a CH bending (Puchowicz & Cieslak, 2022b). These features are present in all the reference wool samples (ARG_CO, N_ZEL, MON_GOT, MOH, and CACH) and should, therefore, be considered as characteristic wool features identified by Raman spectroscopy. The differences between fine and coarse wool (CACH and MOH respectively) is not identifiable. Differences between treated (SAV_R) and untreated (MOH and L_PET) are, instead, detectable although being minimal. For example, in treated wool it is possible to see a slightly shift of the small peak at 1312, in untreated samples, to bigger wavenumbers; the peak at 509 also results attenuated.

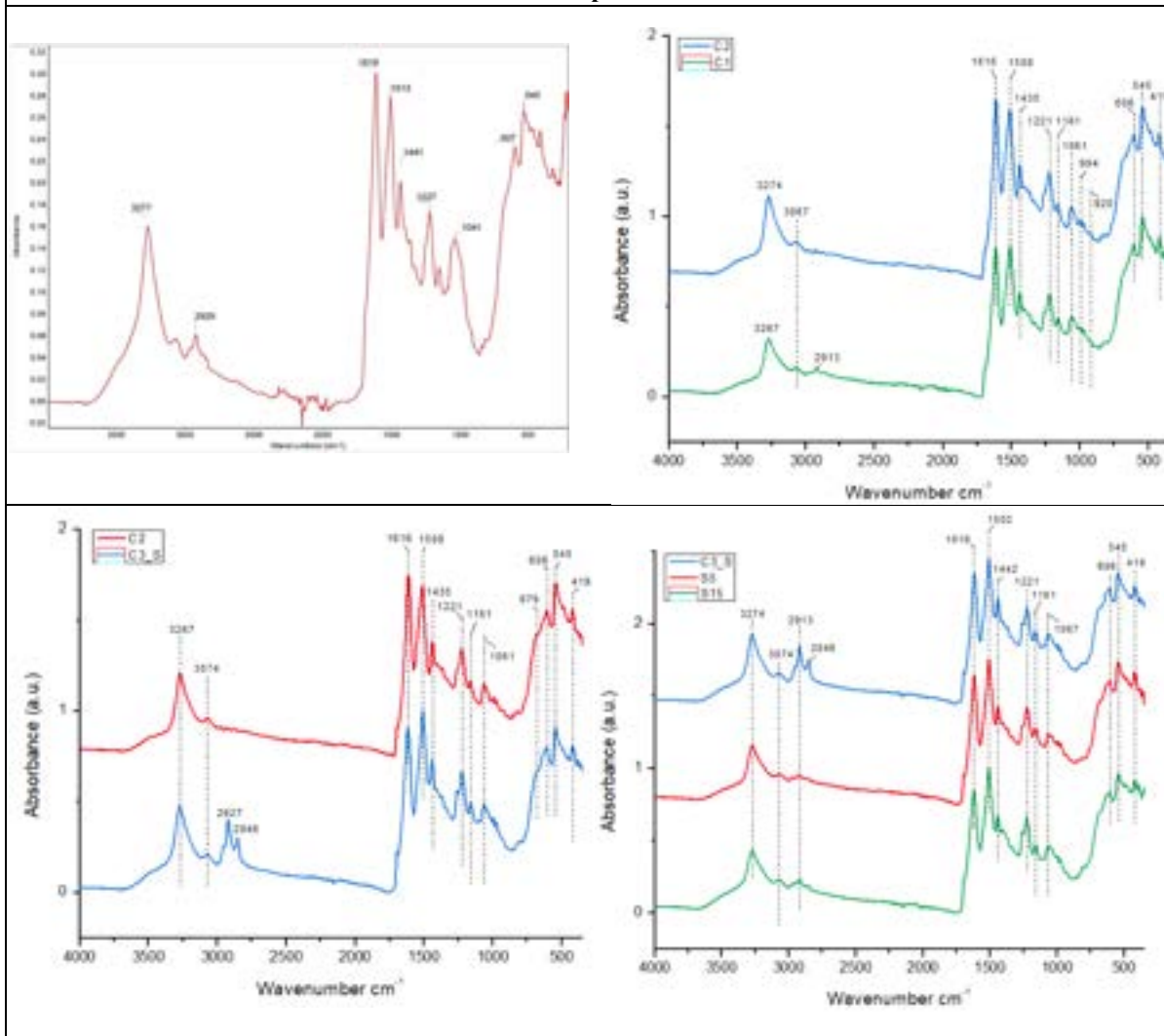
FORS spectra of wool



The peak at 1186 corresponds to the 3rd overtone of the CH bond of proteinaceous origin. The prominent band at 1506/1508 could be assigned to the OH overtone in the α -helix structure of wool. The bands around 2350 and 2179, instead, and generally the peaks included in the 2100-2400 region, correspond to the features of the α -helix structure of wool. The band at around 2289 could be assigned to the stretching of the CO and OH bonds, or to both the bending and stretching of a CH₂ group. All the wool samples are characterized by an inflection point around 370/400nm. (Zhao et al., 2019b) (Quintero Balbas et al., 2022b) (Delaney et al., 2016) (Maynez-Rojas et al., 2017a). Some differences appear comparing the SAV_R spectra and other reference and untreated wool types. SAV_R shows, in fact, another small peak at 548, right after the inflection point, shared with the other wool samples, at around 375. Therefore the overall trend of the region between 370 and 700 ca nm results different from the trend of untreated wool in the same region. This difference, being in the Vis range of the spectrum, could be due to the light brown color of the SAV_R textile.

Silk

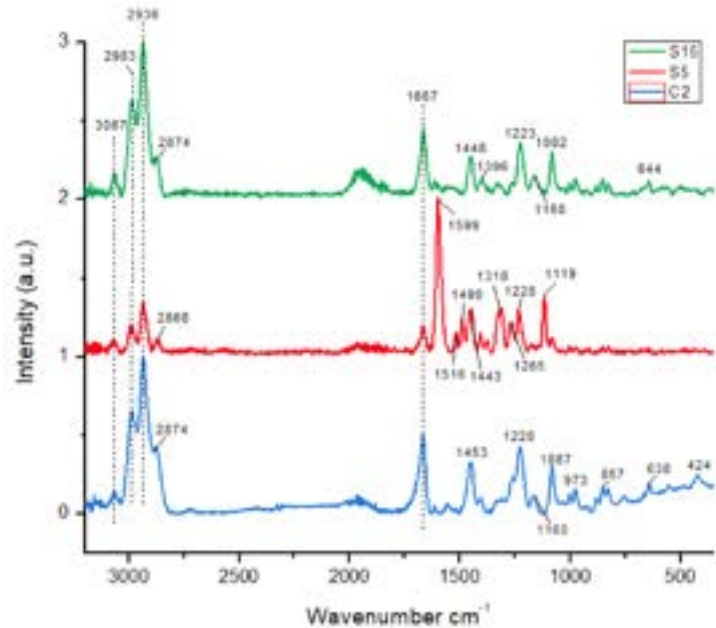
ATR-FTIR spectra of silk



The peak at 3274 appear less pronounced with respect to the reference spectra (Peets et al., 2017a), but still clearly visible. This feature corresponds to the NH/OH stretching of the Amide A group. The small peak at 2913, visible only in the C1 spectrum, corresponds instead to the stretching of the CH bond. As in the wool ATR-FTIR spectra, the characteristic features of proteinaceous materials are well-identifiable at around 1616 and 1515, and correspond to the Amide I (-CONH-, C=O stretching) and the Amide II (bending of the CNH bond) respectively (Ding et al., 2021). The peak around 1435 is attributable to the bending of the CH bond; the peaks at around 1220/1225 should correspond, instead, to the Amide III group, in particular to the CN stretching. The silk spectra also show a small peak at around 1161, which is not highlighted in the reference spectra of (Peets et al., 2017a), and which corresponds to the CH bending. The other small peak in this region, at 1061 corresponds to the COC stretching. The differences between dyed and un-dyed silk (C3_S and C2 samples respectively) is minimal but clearly visible: spectrum C3_S presents, in fact, two evident peaks at 2927 and 2846, which are not present in the raw silk C2. The peak at 2927 is present but poorly visible on sample S15, which is a light-pink colored silk. It could be hypothesized that this spectral feature can be reconducible probably to a dyeing agent present in the dyeing mixtures (Zanini et al., 2018) (Vilaplana et al., 2015)

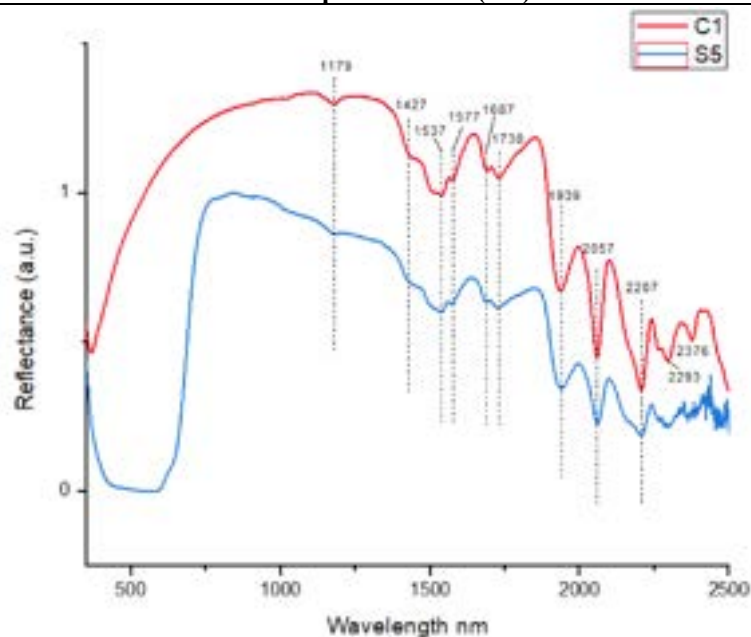
RAMAN spectra of silk

comparison with C3_S



The peak around 2935 corresponds to the stretching of the CH bond, while the peak at around 1667, which is smaller in sample S5 with respect to S15 and C2, should be assigned to the Amide I group, specifically to the C=O and COO stretching. The peak at ca 1450 refers to the bending of the CH₂ group, while the signal at 1223/1228 to the Amide III group, specifically to the CH₂ group. The peak at 1082 in S15 and 1087 in C2 could be assigned to the CC skeletal vibrations, in sample S5 this is a very small signal. The peak at around 976 is visible only in sample C2 and S15 and corresponds to the CH₂ group. Another spectral feature visible only in previously mentioned samples is at around 640 and corresponds to the Amide IV group, specifically to the NCH bending. (Puchowicz & Cieslak, 2022b)

FORS spectra of silk (nm)

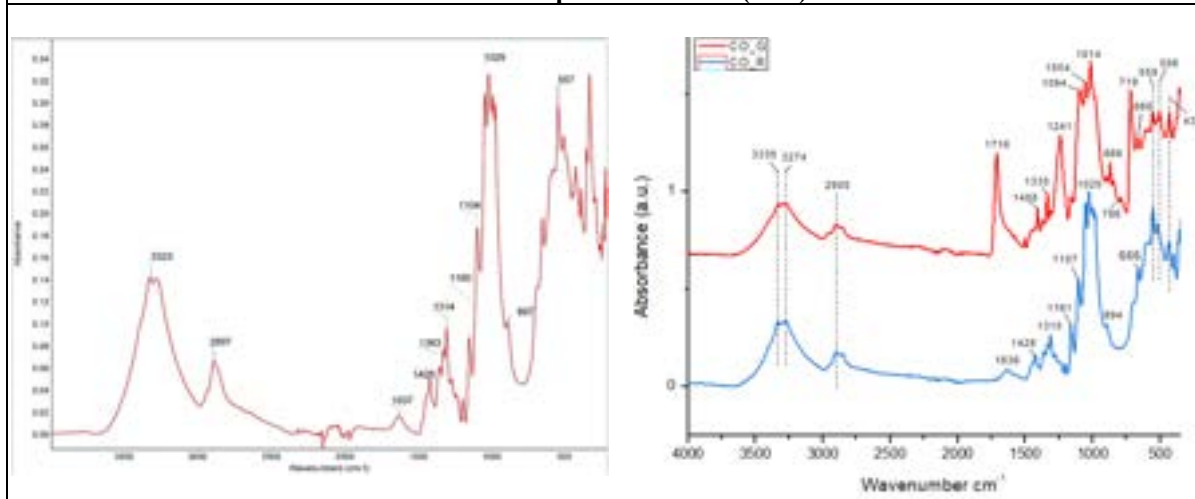


The main differences in the spectra of the reference raw silk C1 and the treated, Bordeaux-colored silk fabric S5 is very noticeable in the visible region, due to the color of this latter sample. Sample C1, in fact, presents an inflection point at around 370, while the spectrum of S5 shows the inflection point at around 650, with a shoulder at ca 700. Apart from a couple of very small bands in the region between 700-1000, the rest of the trend of the two spectra is almost identical. The peaks at 1537 and 1577, for example, corresponds to the

Amide group of silk's β -sheet, along with the OH and NH overtones. The peak at 2207 is also assigned to the vibrational features of the β -sheet. (Quintero Balbas et al., 2022b) (Delaney et al., 2016)

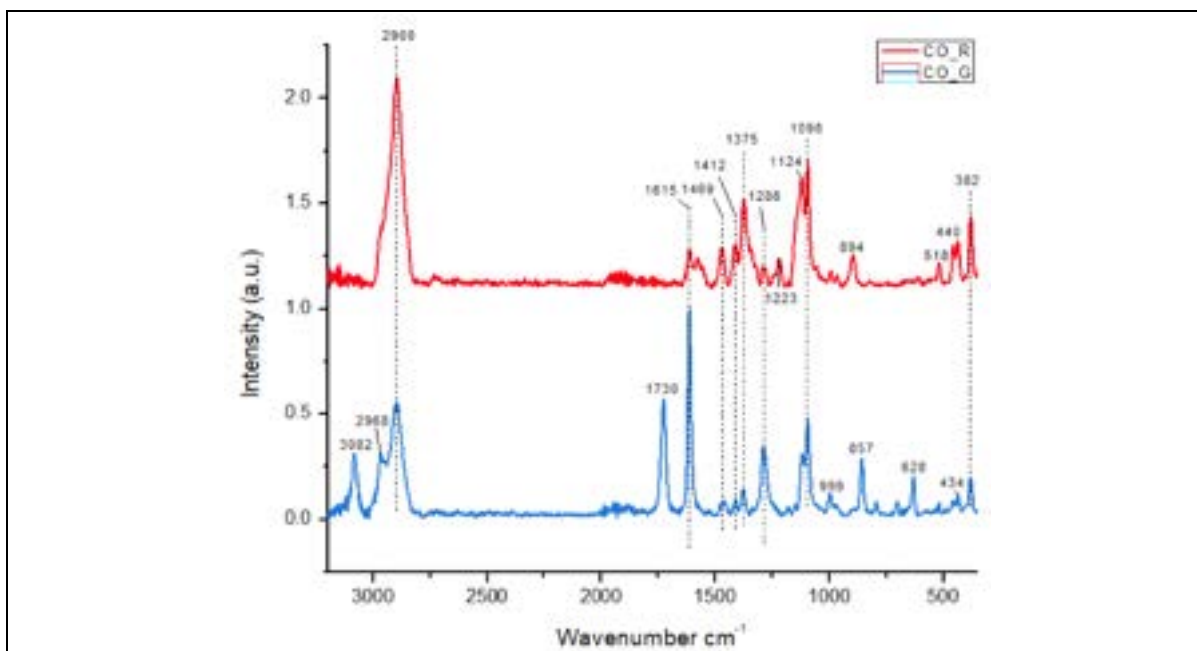
Cotton

ATR-FTIR spectra of cotton (cm^{-1})

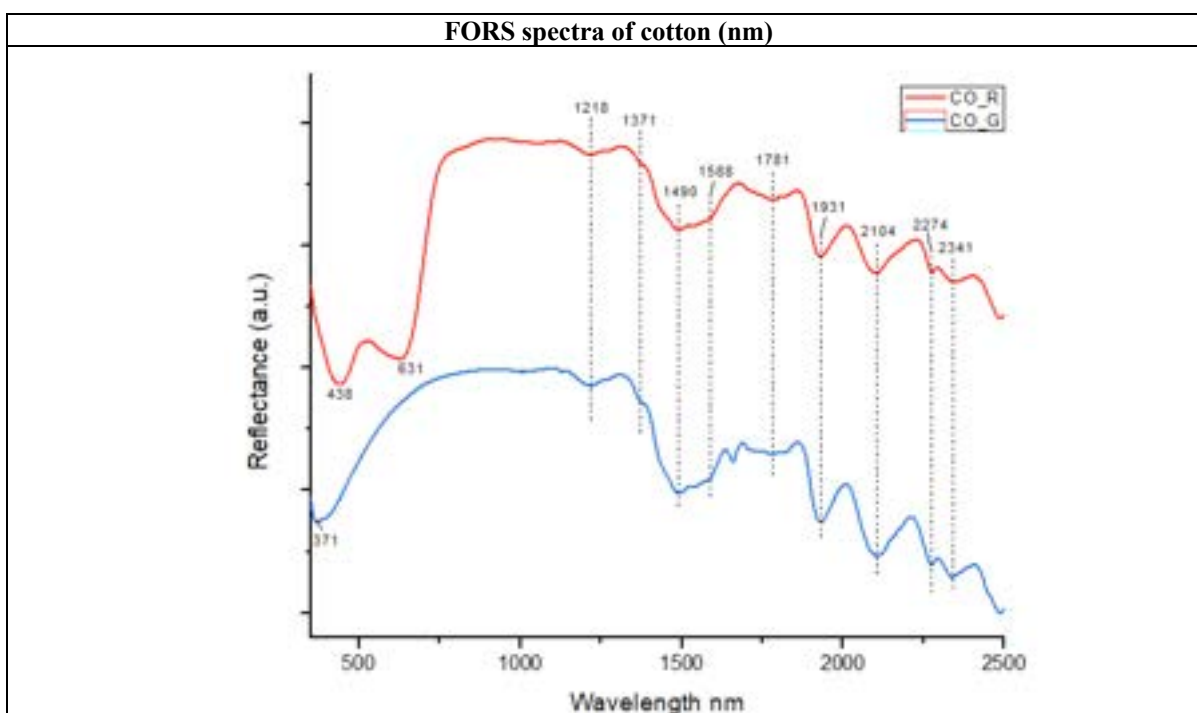


The cotton spectra are compared with the cotton spectrum of the study of (Peets et al., 2017a), here taken as reference. The first well-identified spectral features present in both samples CO_G and CO_R are the peaks at the at top of the band between 3335 and 3274, which correspond to the stretching of the OH group. The smaller peak encountered right after, at ca 2905, corresponds instead to the stretching of the CH group typical of cellulose. The well-defined peak in 1716 in sample CO_G represents the stretching of the C=C bond of lignin. The sample CO_R shows a small peak at 1636, which is found also in literature but not in sample CO_G, and it should be assigned either to the bending of the HOH bonds, or to the stretching of the C=C bonds typical of lignin. CO_R also presents a peak at 1428, indicated in the reference spectra with the assignment to either the bending of the CH bond, the CH₂ scissoring, or to the bending in plane of the COH group, but which is very poorly pronounced on the raw cotton sample CO_G. The peaks at 1094, 1161, 1020, and 1050 corresponds to the stretching of the CO bond in COC and COH fragments. The remaining signals included in the region between 700 and 500 correspond, instead, to the out of plane bending of the OH bond. (Peets et al., 2017a) (Ding et al., 2021)(Geminiani et al., 2022)

RAMAN spectra of cotton (cm^{-1})

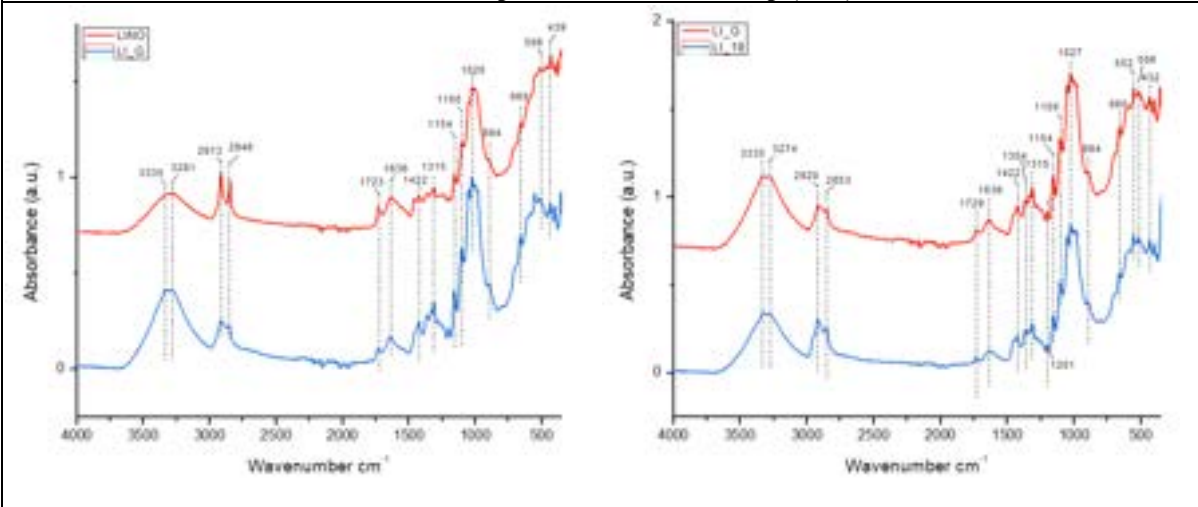


The well-defined peak at 2900 corresponds to the stretching of the CH bond; the signal at 1615, which appears very pronounced in raw cotton (CO_G), stands for the stretching of the C=C bond. The bending of the CH₂ and COH bonds of the 1° and 2° alcohol groups is located at 1469 and is more pronounced in sample CO_R rather than in CO_G. The peaks at 1375 and 1286 corresponds to the bending of the CH₂, while the signal at 1098 could correspond to the stretching of the COC group. The peak at 382 corresponds instead to the stretching of the CCC group (Puchowicz & Cieslak, 2022b)(Kavkler et al., 2011a)

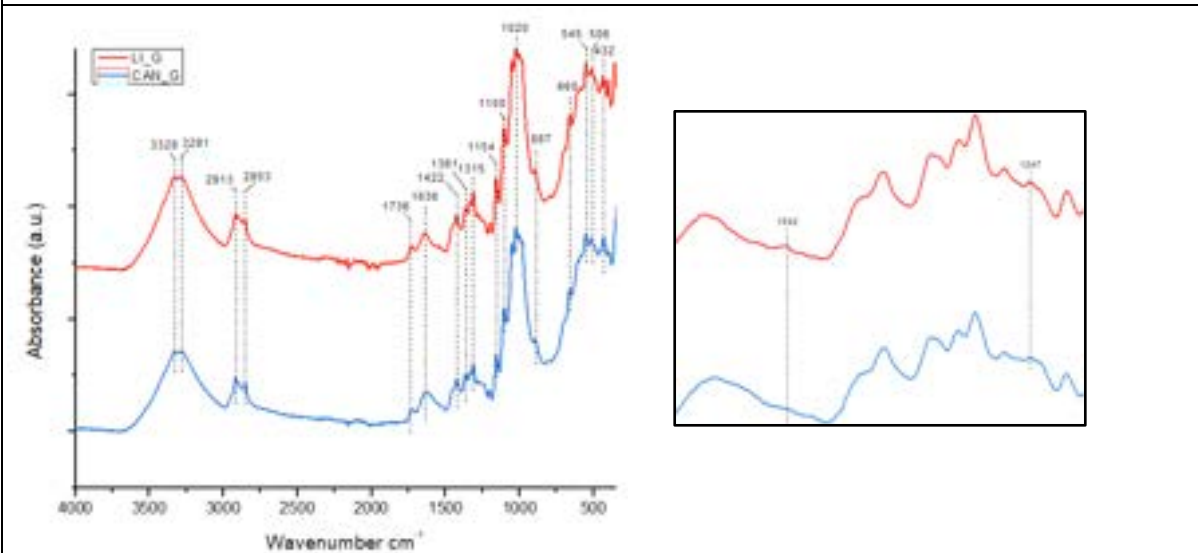


A characteristic peak of cotton that is highlighted through FORS is at 1218 and corresponds to the stretching of the CH and CH₂ bonds in cellulose. Another characteristic feature of cotton is the signal at 1490, which corresponds to the 1st overtone of the OH stretching typical of cellulose; the band at 2274, instead, corresponds to the stretching of the CO bond combined to the OH stretching and both bending and stretching of the CH₂ group. (Maynez-Rojas et al., 2017b) (Delaney et al., 2016) (Quintero Balbas et al., 2022b)

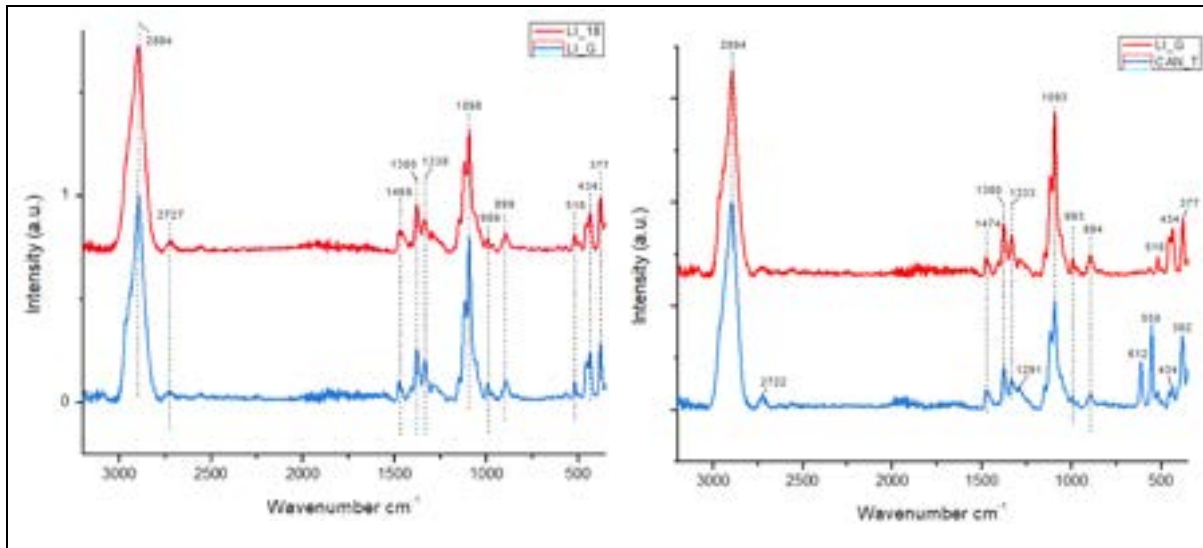
ATR-FTIR spectra of linen and hemp (cm^{-1})



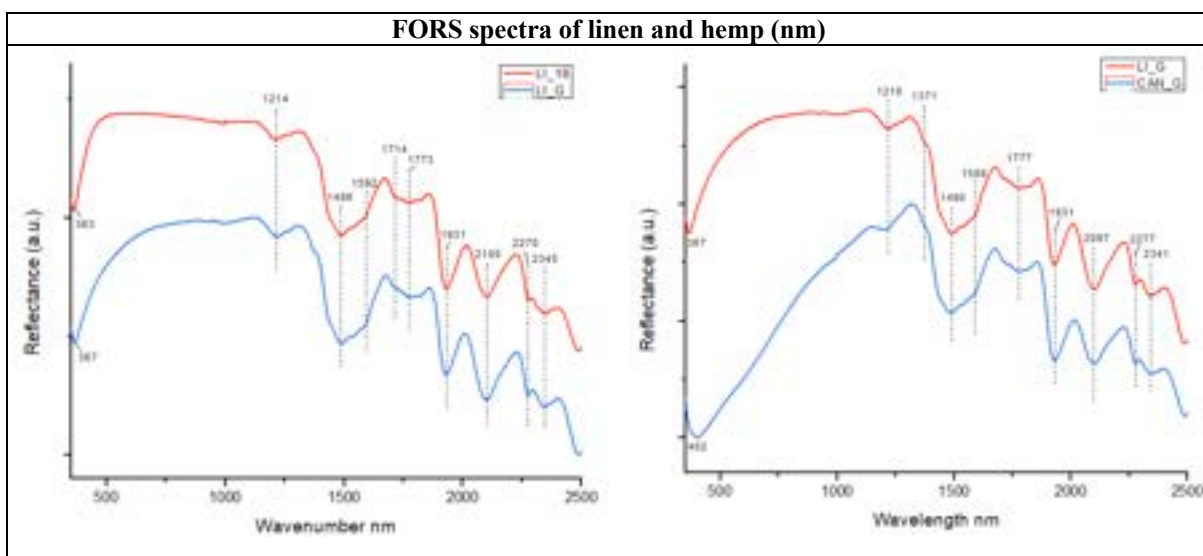
The band at 3335 corresponds to the OH stretching, while the one at around 2853 to the symmetric stretching of the CH bond. At 2920, peak located at 2930 in reference (Geminiani et al., 2022), the stretching of the CH bond is visible, this signal is typical of lignin. The peak at 2853 is found in the study of Geminiani et al., at 2849 and it could be assigned to the presence of wax in the cell wall of linen. The signal at around 1636 can be assigned to the bending of the OH bond, while the peak at 1422 to either the bending of the CH bond, the scissoring of the CH_2 group, or the in plane bending of the COH group. The signal at 1154 corresponds to the stretching of the CO bond in cellulose and to the stretching of the COH bond in secondary alcohols. The broad peak at 1027 corresponds to the stretching of the CO of alcoholic groups characteristic of wax. Another characteristic feature of cellulose is the small peak at 894, which corresponds to the stretching of the glucose ring, to the COC group. The region between 700 and 500 corresponds instead to the OH out of plane bending. (Peets et al., 2017a) (Ding et al., 2021) (Kavkler et al., 2011b)



RAMAN spectra of linen and hemp (cm^{-1})



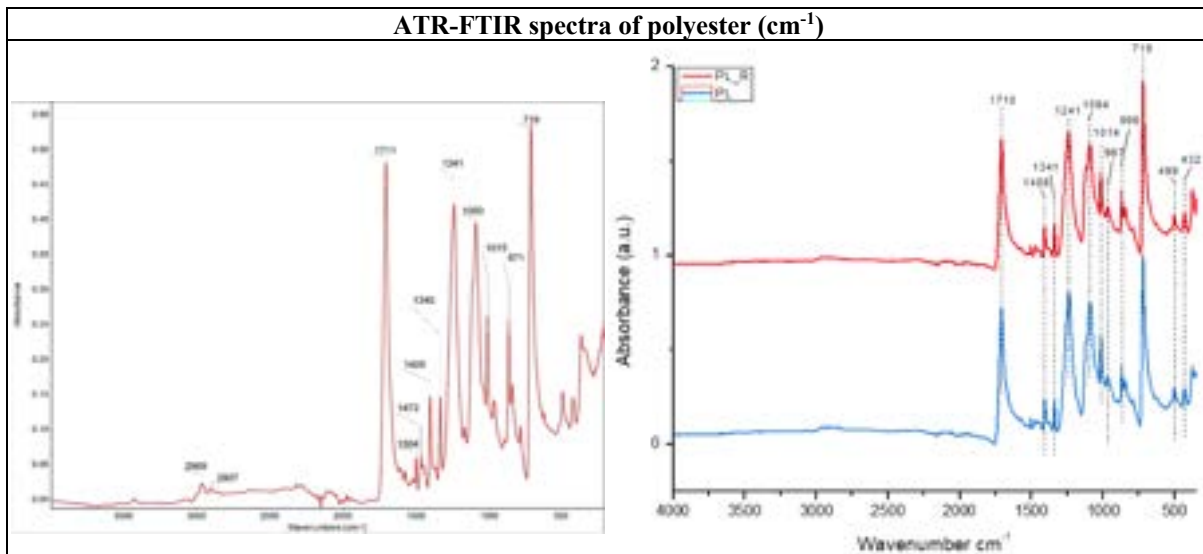
The most defined peak at 2894 is assigned to the stretching of the CH bond. The band at 1469 instead, which in literature is found at 1478, and the peak at 1380 correspond to the bending of the CH₂ bond. The signal at 1338, in literature indicated at 1335, is characteristic of lignin, more specifically to the wagging vibrations of the CH₂ and to the bending of the COH group. The signal at 1098 is assigned to the glycosidic symmetric stretching of the COC group, a skeletal vibration. The peak at 899 corresponds to the bending of the HCC and HCO groups, while the signal at 518 is assigned to the bending of the glycosidic linkage of the COC bonds. The last signals at 434 and 377 correspond to the bending of the CCO and CCC groups respectively. There appear to be no differences in the Raman spectra of raw linen (LI_G) and bleached linen (LI_18). (Kavkler & Demšar, 2011b)(Puchowicz & Cieslak, 2022b) Again, the Raman spectral responses of linen and hemp are very similar. Differences are clearly visible in hemp (CAN_T) in the region between 610-380, with well-defined peaks at 610, 551, and 381 which are not present in linen. (Kavkler & Demšar, 2011b; Puchowicz & Cieslak, 2022b)



The peak at around 1214/1218 in both linen samples and hemp is a characteristic signal of cellulose, indicating the CH bonds of the polymer. The signal at 1490 is another typical signal of cellulose assigned to the stretching of the OH overtone of crustalline cellulose, and is present in both linen and hemp; while the peak at around

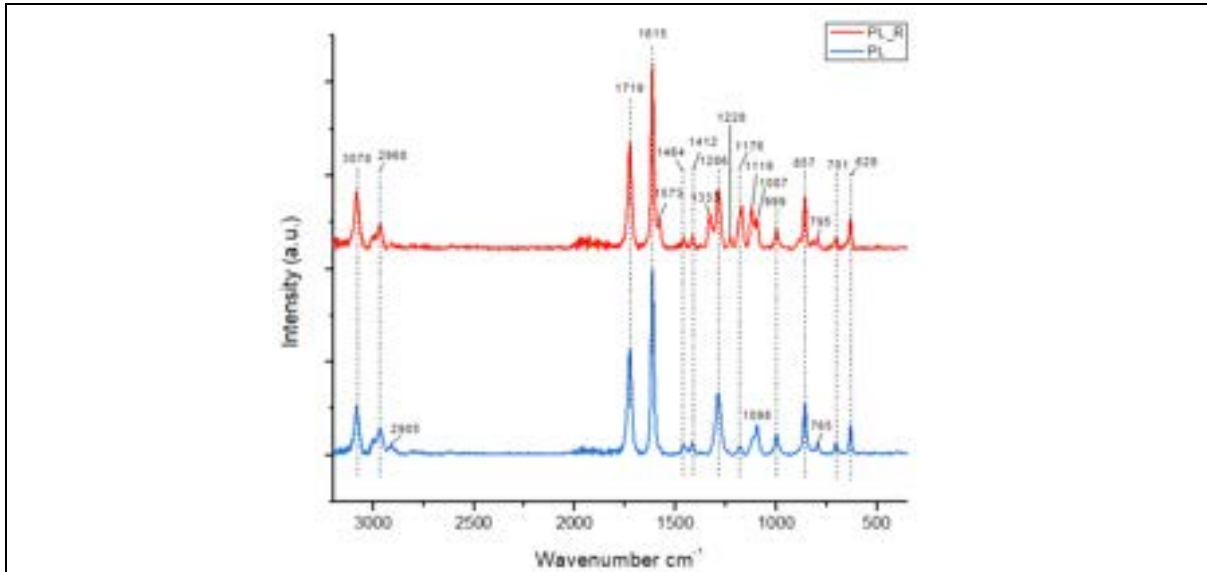
2100 corresponds to the OH and CH deformation modes of cellulose, this being a major feature of this compound. The narrow peak at around 2270/2277 correspond to the stretching and bending of CH₂. The main differences between bleached and row linen, LI_18 and LI_G respectively, is the inflection trend: in both specimens the signal increases its intensity from ca 363, but while in raw linen LI_G the spectrum has a curvilinear trend, in LI_18 the signal's intensity increases sharply from 363, giving the spectra a **denified angular trend**. Also regarding the differences between linen and hemp can be found in the inflection area, which in hemp starts at 402 and shows a less steep trend. The rest of the spectral features appear identical between linen and hemp. (Maynez-Rojas et al., 2017b) (Quintero Balbas et al., 2022b)(Delaney et al., 2016)

Polyester

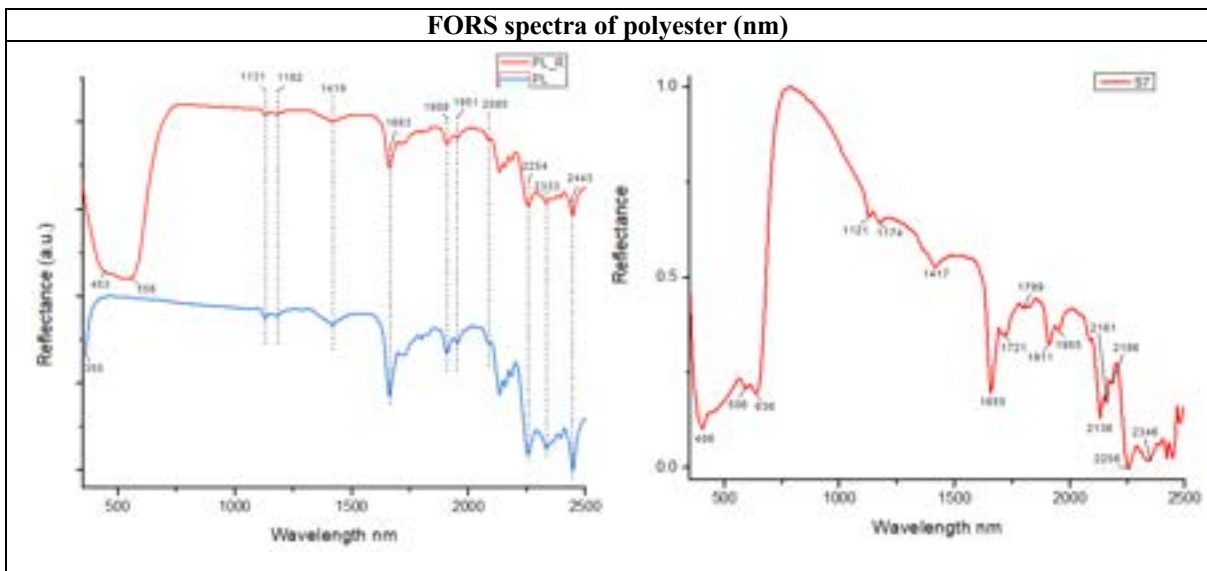


The ATR-FTIR spectra of the polyester samples (PL and PL_R) show well-defined peaks, a typical behavior of synthetic fibers, and there seem to be no differences between the dyed (PL_R) and undyed sample (PL). The peak at 1711 corresponds to the stretching of the C=O bond, while the small signal at 1504 is assigned to the stretching of the aromatic ring C=C. The peaks 1408 and 1340, instead, correspond to the bending of the CH bond. The peak at 1241, present also in the reference peak of the study of Peets et al., corresponds to the ester's stretching of the CO bond. The signal at 1094 is assigned to the stretching of the CO bond, while the sharp peak at 719 to the bending of the CH bond. (Peets et al., 2017a)(Ding et al., 2021)(Ueland et al., 2017)

RAMAN spectra of polyester (cm⁻¹)



The peak at 1615 corresponds to the ring deformation caused by the symmetric stretching of the C=C. The signal at 1286 could be assigned to the stretching of the CC ring and to the stretching of the CO bond. The signal at 1087 in PL_R and at 1098 in PL could correspond to both the asymmetric stretching of the COC group and the stretching of the CC bond. The well-defined signal at 857 can be assigned to the stretching of the COC group, while the peak at 795 in PL_R, which in PL is found at 765, to a deformation of the ring. The differences between the polyester samples PL_R and PL are minimal but well-defined. The PL_R spectrum appears more saturated by signals, such as the peaks at 1573, 1333, 1228, 1087, and 1087. Some of these signals result shifted from one spectrum to another; the peak at 1087 in PL_R, for instance, could correspond to the 1098 signal in PL. The peak at 795 in PL_R, again, could correspond to the same vibration of the signal at 765 in PL. (Cho, 2002) (Hager et al., 2018)



Not enough reference was found in literature regarding the spectral response of polyester against FORS analysis, therefore this discussion will be based on the principal spectral features encountered on multiple polyester samples. In samples PL and PL_R the resemblance of the spectral trend is clear, with the main features at 1663, 2254, 2443, and the scale of values at circa 1130, 1180, 2130, 2160, and 2180 are present in both specimens. The only difference appears to be in the visible region, where the red-dyed sample PL_R shows a broad band between 453 and 556, showing then an inflection trend. Sample PL, instead, presents an inflection that starts at 335. Confronting these two polyester samples and the S7 polyester fabric, some differences are clearly visible especially in the visible region. The light-blue colored textile presents, in fact, peaks at 406, 506,

and 636 which are not present in samples PL_R and PL. Moreover, after the signal at 636, the inflection of the spectrum appears very steep, declining significantly at around 800/850. The rest of the characteristic spectral features are almost identical to the above mentioned ones in samples PL and PL_R.

ER-FTIR spectroscopy: a comparison between the fiber species

The use of ER-FTIR on the analyses of textiles is still limited, therefore the information found in literature was not adequate for a complete interpretation of the spectral information. The analysis performed will be here discussed based on the comparison of the spectral features of each typology of fiber presented in this study.

Proteinaceous materials

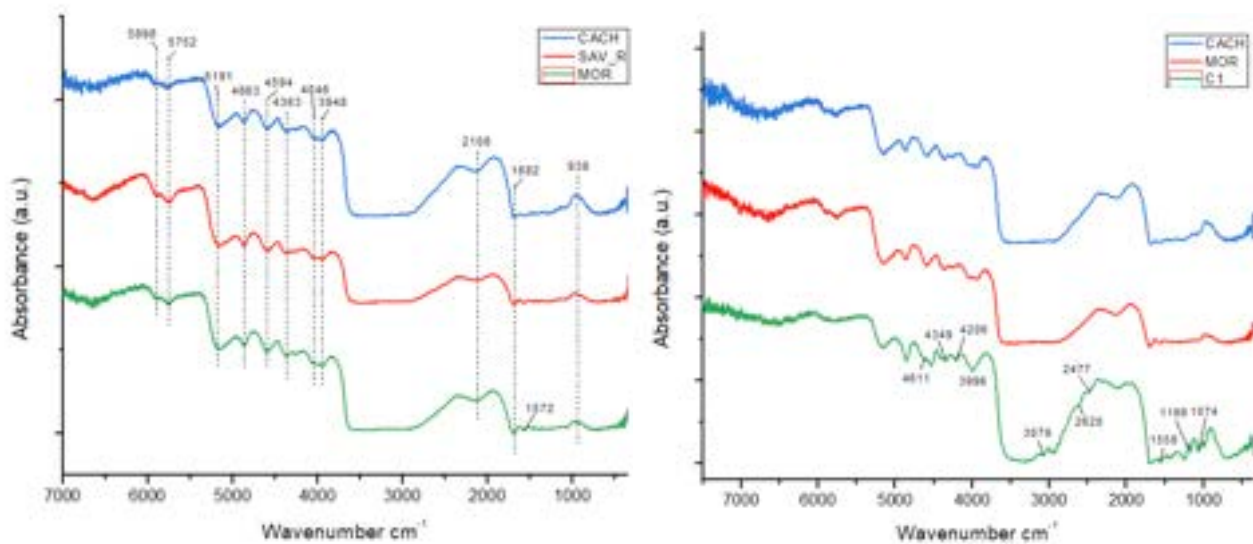


Figure XX shows the comparison between the ER-FTIR spectra of some of the proteinaceous fibers under study. From the comparison between wool textiles (Figure XX A) the deep similarity between different species of wool, including fine (CACH), coarse (MOR), and dyed wool (SAV_R). In fact, the spectra of the three specimens appears identical in every spectral feature, with the only difference being the small peak in sample MOR at 1572. Figure XX B shows, instead, the comparison between wool and silk. Here, the overall trend of the spectra is again very similar, but silk (C1) presents peaks which are not present in the CACH and MOR wool samples, especially in the regions between 4600-3990, 3790-2470, and 1558-500 circa.

Cellulosic materials

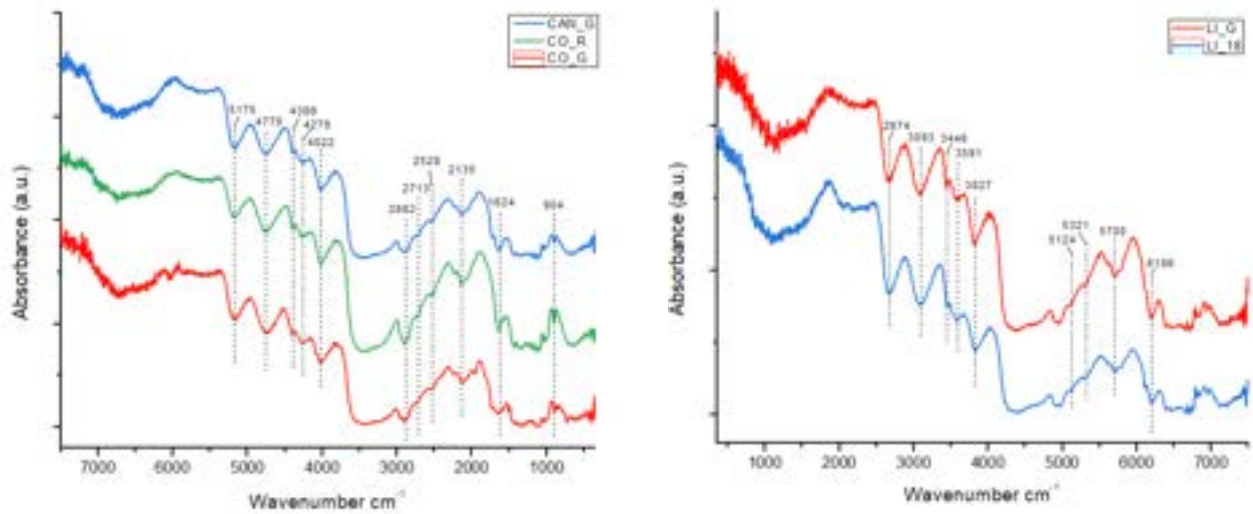


Figure XX shows the comparison of the ER-FTIR spectra of some of the cellulosic fibers included in this research. The overall trend of the spectra seems very similar within fibers of cellulosic origin, the only noticeable differences appear in the intensity of some of the signals. This comparison includes also the treated and dyed cotton fabric CO_G, which shows the same spectral features of CO_G apart from the small peak at ca 6000, which is not present in the dyed specimen.

Synthetic material

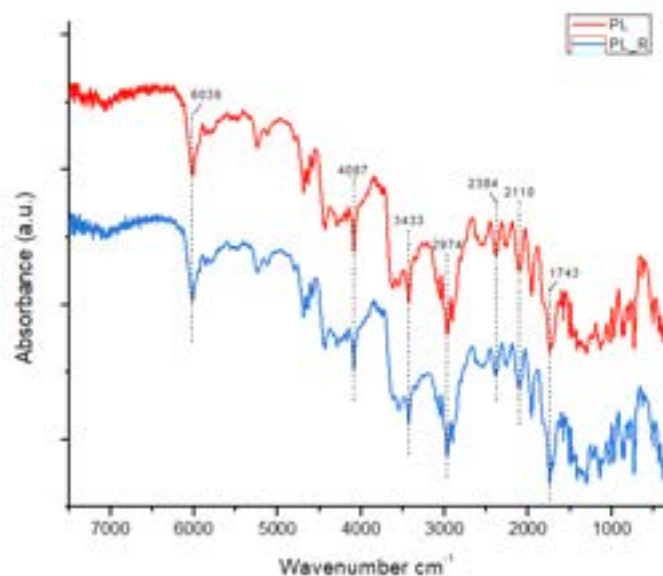


Figure XX shows the ER-FTIR spectra of two polyester samples of the Rubelli set. The difference between these synthetic fibers and both proteinaceous and cellulosic is clear. In the 6000 regions, for example, there is already a well-defined signal (6039), which in the other

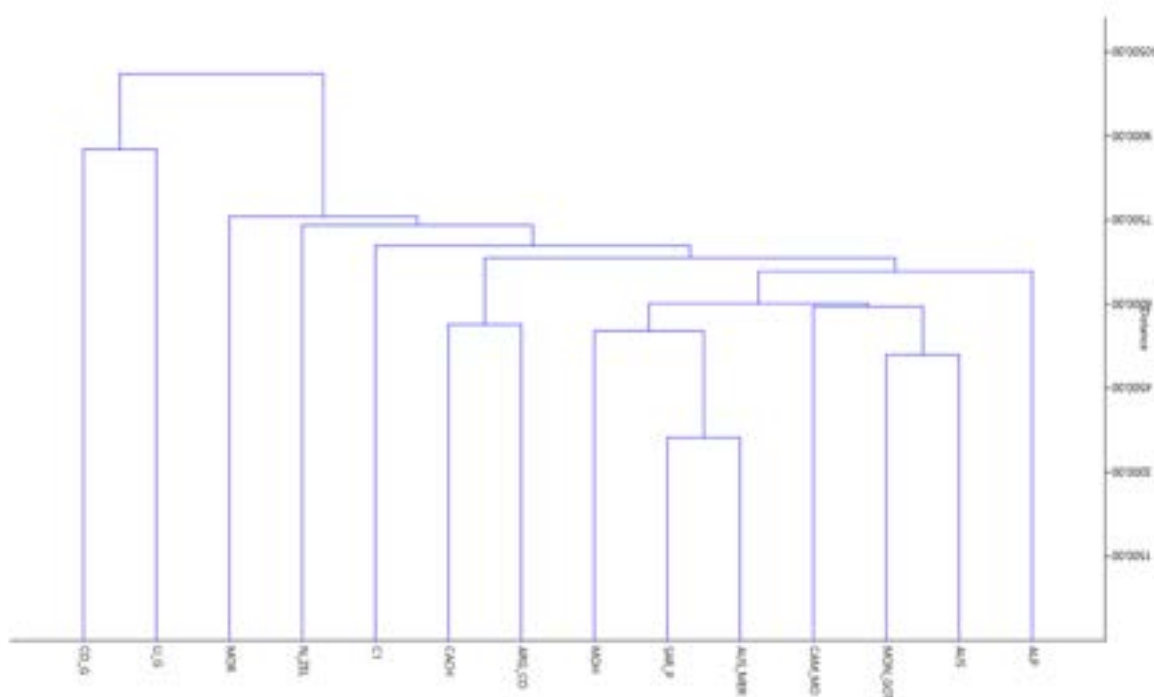
natural based fibers is only slightly pronounced or, even, not present, for example in proteinaceous textiles. A general difference emphasized by ER-FTIR between synthetic and natural fibers is the morphology of the peaks. The signals in the polyester samples PL and PL_R are very narrow and numerous, while the peaks in the spectra of natural fibers, both proteinaceous and cellulosic, are less in number and in narrowness.

Principal Component and Cluster analyses

As previously mentioned in the Materials and Methods chapter, the spectral data of each sample, coming from the four techniques used, was analyzed through the software Past4.0 to understand the capabilities and limitations of the non-invasive techniques for the identification of textiles.

ATR-FTIR

Figure XX shows the dendrogram of the reference animal and vegetable fibers.



Two main families form at the maximum distance (10500), one containing the vegetable fibers cotton and linen (CO_G and LI_G), the other one containing the animal fibers of wool and silk. Within the animal cluster it is possible to notice how some wool types are more related to each other with respect to others, i.e., AUS and MON_GOT form an individual cluster at 5000 ca, which joins with CAM_MO at 6000.

At the distance of 7500 a sub family inside the animal fibers' cluster forms, putting in relation the Moretta wool (MOR) with another sub-family, formed by N_ZEL in relation with silk (C1) which, at the same time, is related to another sub-group. This cluster is formed by the family that includes the relation of Cashmere (CACH) to Argentina Corrientes wool (ARG_CO), which is at the same time related to the remaining wool types, with Alpago wool (ALP) being

related externally to this sub-family. Inside this family it's possible to distinguish the direct relationship between Sarda Piemontese wool (SAR_P) and Australia Merinos wool (AUS_MER), which are then related to Mohair wool (MOH). Australia (AUS) and Mongolian Greyorn form another directly related family, which is related to the Mongolian Camel wool (CAM_MO).

PCA

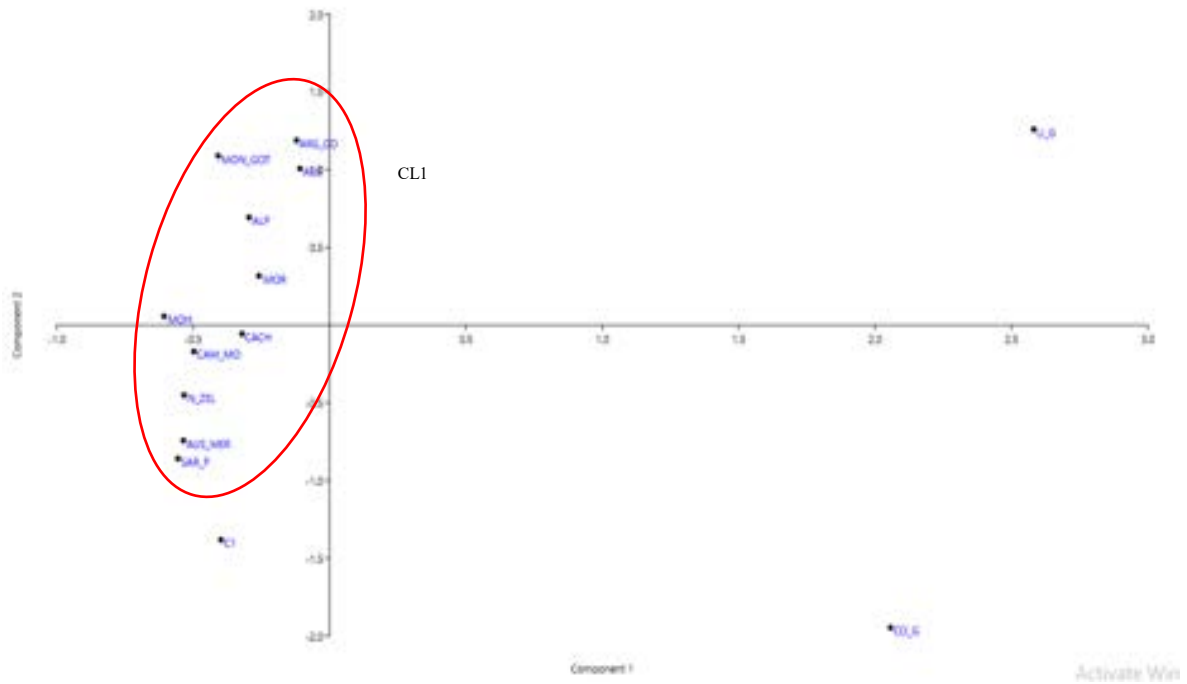
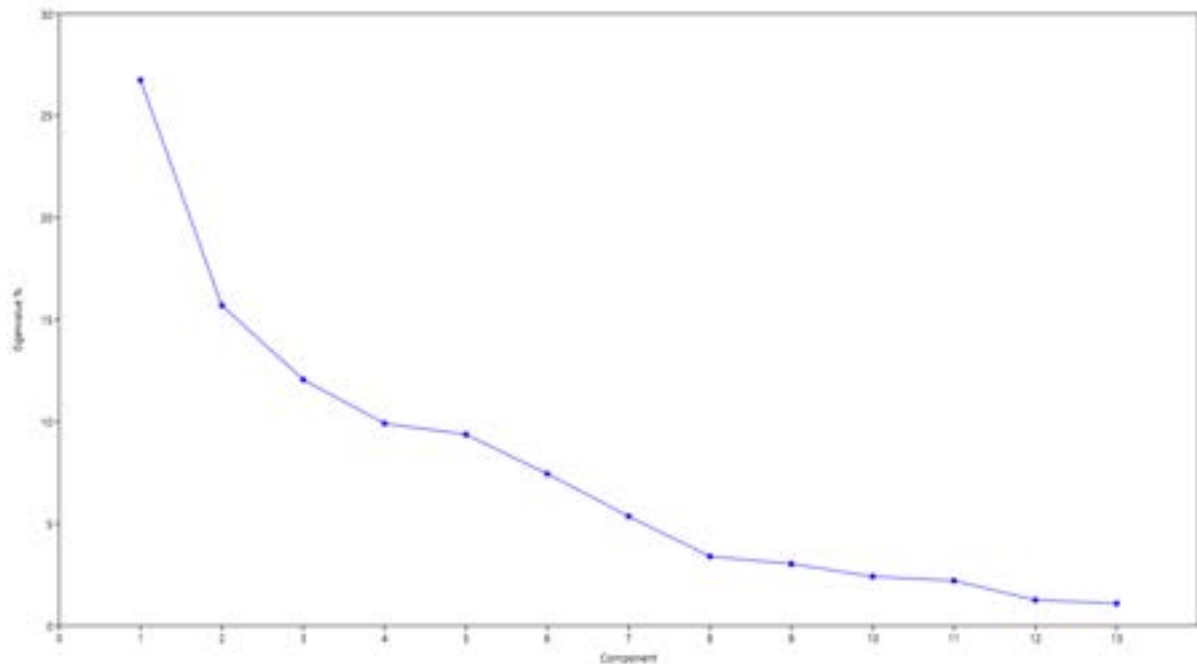


Figure XX shows the scatter plot of animal and vegetable reference fibers (Eigenvalue scale). Animal fibers form a cluster (CL1) at the negative values of the PC2 and both negative and positive values of the PC1, with silk (sample C1) laying outside CL1 and towards the negative



values of PC1. Its position depicts the common protein origin of wool and silk but underlines that the two fiber species show dissimilarities in their compositions. Vegetable fibers are located at the opposite side of the PCs, linen showing that the positive values of both PC1 and PC2 weight more on this fiber, while cotton at positive values of PC1 and negative values of PC2 meaning that, in this case, the negative component of the PC2 and the positive component of the PC1 weight more on cotton. One would expect to find the vegetable fibers inside the same cluster but, instead, the analysis enhances the fact that, despite being both vegetal fibers and showing high correspondence to most of the spectral features, the two fibers differ greatly.

From the scree plot it is possible to deduce that only the first two Principal Components give relevant information about the correlation of the data.

Wool samples

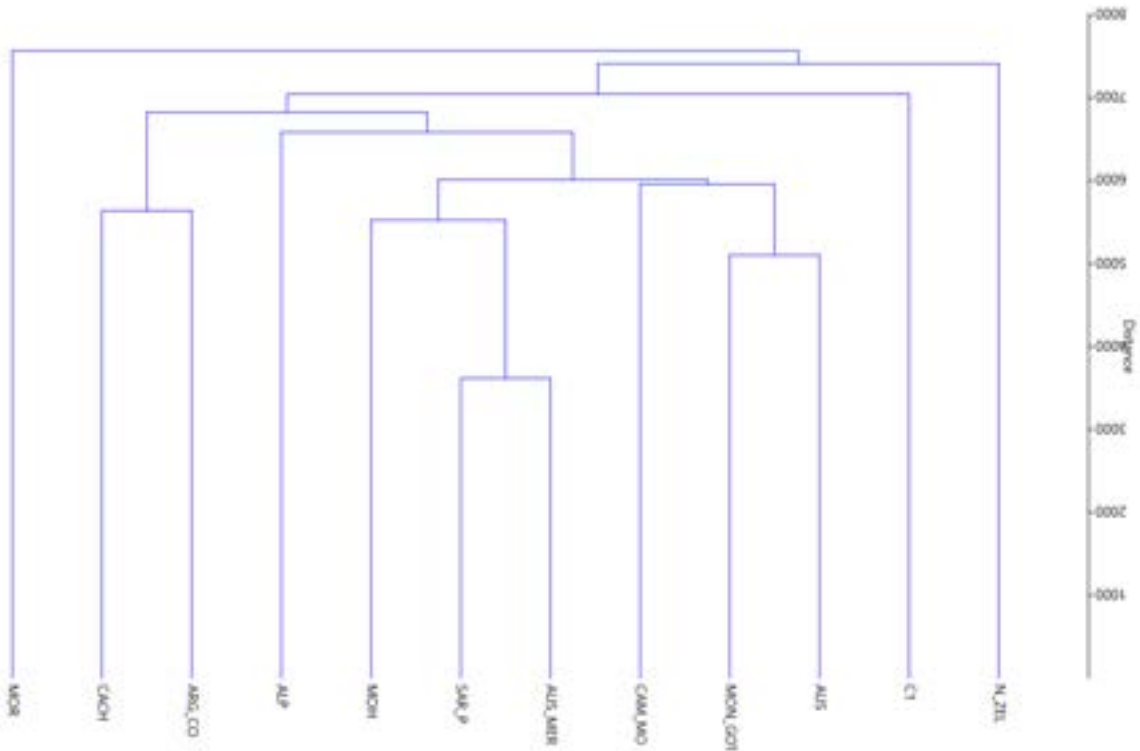


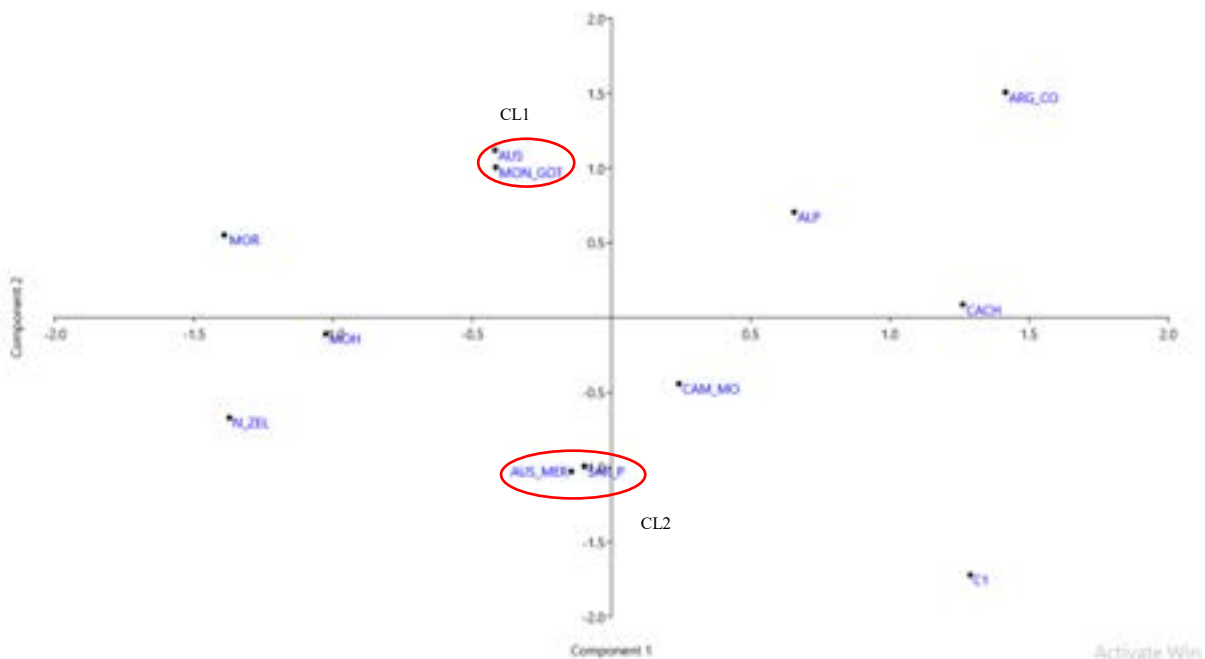
Figure XX shows the dendrogram of the wool species. Moretta (MOR) seems to be isolated from the other species; Moretta, in fact, links to the main family at the furthest distance (8000 ca). The main family is related to MOR, and it is made of the relation between New Zealand wool (N_ZEL) with the rest of the wool types at 7000, which are included in a sub-family.

In this sub-family it's possible to see that silk (C1) is related to the wool types, but it's not included in the sub-group that includes them all. In fact, C1 is linked to the cluster that includes the direct relation between Cashmere (CACH) and Argentina Corrientes (ARG_CO), confirmed in the previous dendrogram. In this sub-family it is also possible to notice how Alpago (ALP), which in the overall reference dendrogram was not directly related to any of the wool types and was, instead, connected externally to the rest, is now included in the main sub-family.

Other direct relationships in this dendrogram are between Sarda Piemontese (SAR_P) and Australia Merinos (AUS_MER) at 3500 ca, and Australia (AUS) and Mongolia Greyhorn (MON_GOT) at 5000; both relations are confirmed also in the overall reference dendrogram.

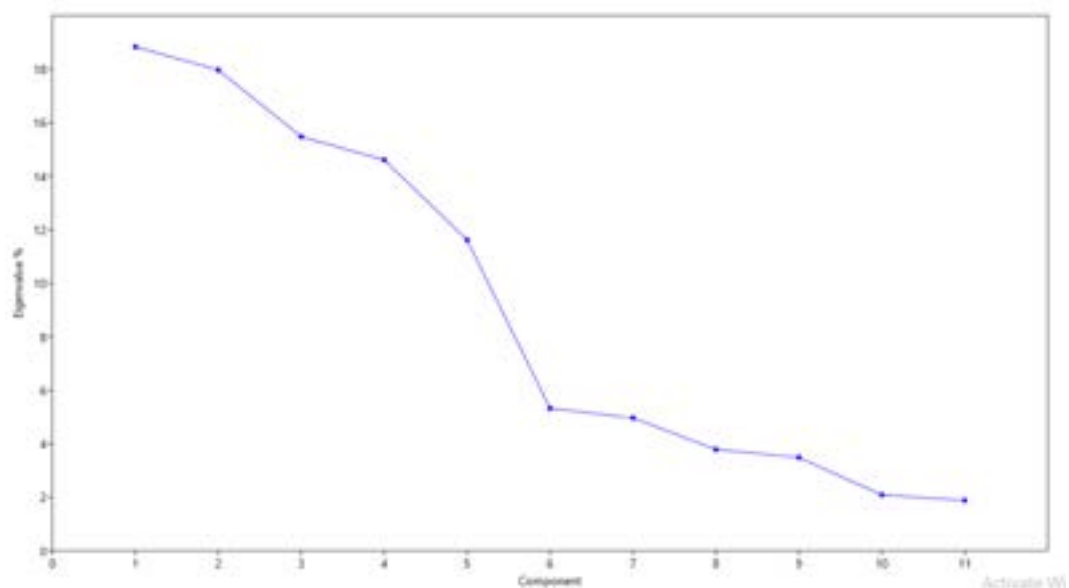
It is interesting to notice the proximity of the Australians, Mongolians, and Piemontese wool types, probably due to similarities in their compositions despite deriving from areas geographically located far from each other (8.561 km Mongolia-Australia, 6.935 km Mongolia-Piemonte).

Figure XX shows the scatter plot of the reference wools (Eigenvalue scale). Unlike in the previous scatter plot, showing both animal and vegetable fibers, this graph underlines the presence of sub-clusters within the family of wools.



As confirmed in both dendrograms, the Australian, Mongolian, and Piemontese types of wool form two well defined clusters, one with AUS and MON_GOT (CL1) and one with AUS_MER and SAR_P (CL2); in the first one the positive components of PC1 and the negative components of PC2 weight more, while in the latter the negative components of both PC1 and PC2 weight substantially. The two clusters are located almost on the same values, although with opposite signs, of both PC1 and PC2. The other wool types are spread on the whole scatter plot, without depicting any specific relational patterns. Silk (C1) is, instead, very distinguished from the wools and can almost be considered as an outlier in this case.

The scree plot of the animal reference fibers (Figure XX) shows that the principal components that should be considered for the PCA are PC1, PC2, PC3, PC4, PC5, and PC6.



FORS

PCA

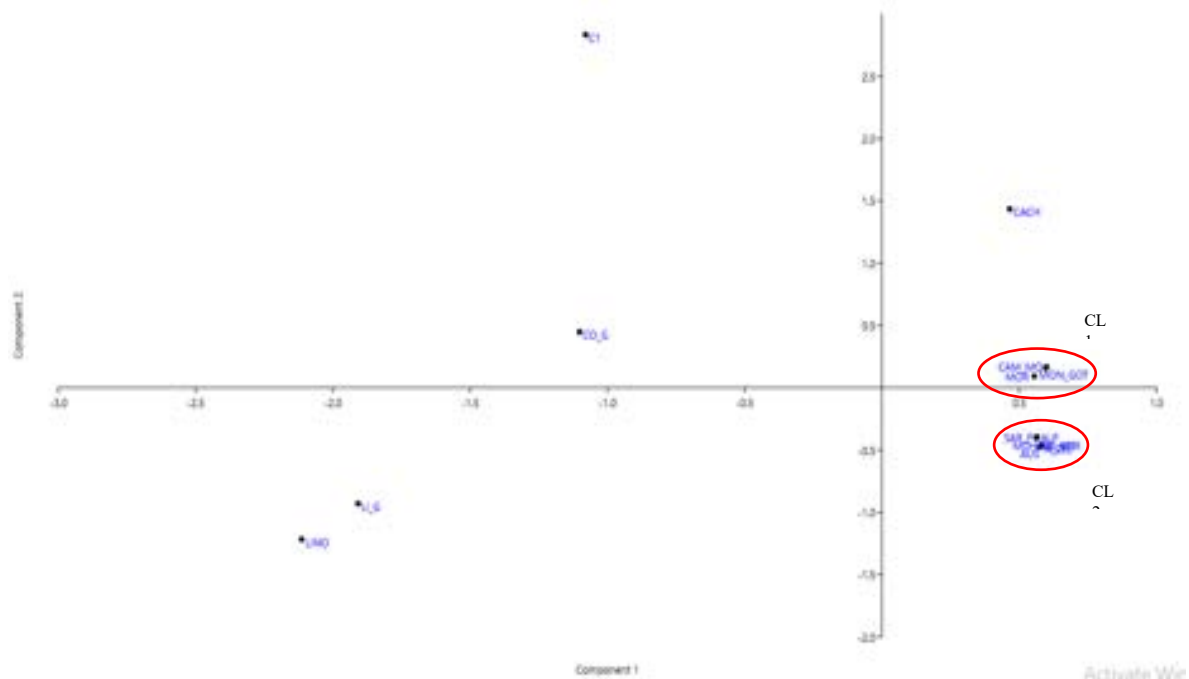


Figure XX shows the scatter plot of the animal and vegetable reference fibers (Eigenvalues scale). A very clear distinction between the families of vegetable fibers, silk, and wool is visible. Wools are divided into two clusters, the first (CL1) formed by Mongolian Camel (CAM_MO), Moretta (MOR), and Mongolian Greyhorn (MON_GOT) in which the positive components of both PC1 and PC2 have a significant weight; the second family (CL2) includes ARG_CO, SAR_P, MOH, ALP, AUS, N_ZEL, and AUS_MER in which the weights of the positive components of the PC1 and the negative components of the PC2 have a significance influence on the data. Cashmere (CACH) is not part of these two wool clusters, it is also influenced by the same weights of the positive components of PC1 but the weights of the PC2, also positive, have a difference influence on the data with respect to the previously mentioned cluster. Silk (C1) does not belong to the wool clusters; it is in fact placed at a great distance from them, influenced by the weights of the positive components of PC2 and negative components of PC1.

Vegetable fibers, namely cotton (CO_G) and linen (LI_G, LINO), form two separate clusters far from wool. Although being separated, they both lie within the negative values of PC1 probably due to their vegetal origin. The two families consist of the linen cluster (LINO + LI_G) at negative values of both PC1 and PC2, and cotton influenced by negative values of PC1 and positive values of PC2.

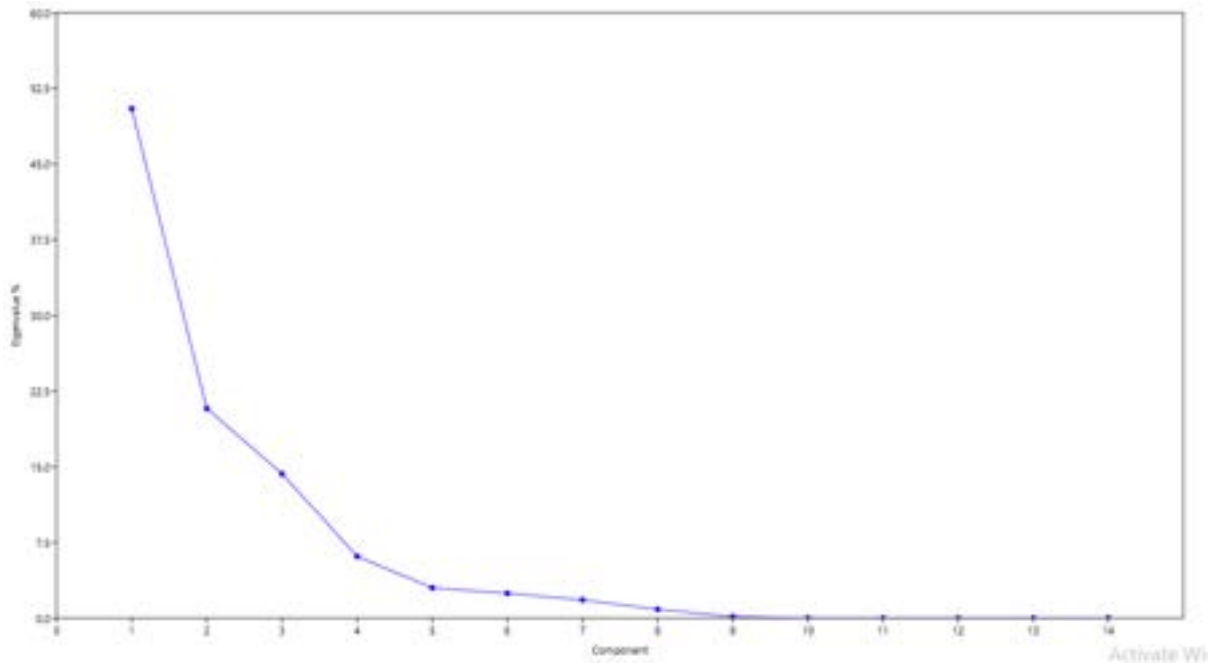
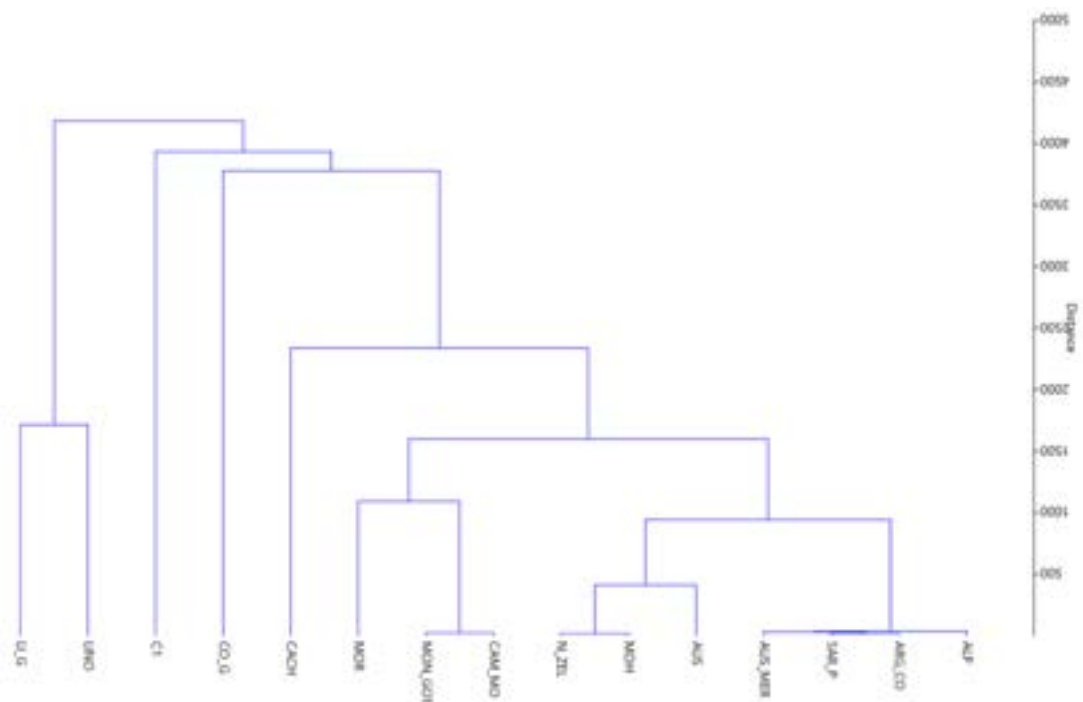


Figure XX shows the Scree plot of the animal and vegetable reference fibers. The scree plot of both animal and vegetable reference fibers shows that the components with the lowest variance are PC1, PC2, PC3, and PC4.

CLUSTER ANALYSIS

Figure XX shows the dendrogram of the animal and vegetable reference fibers.

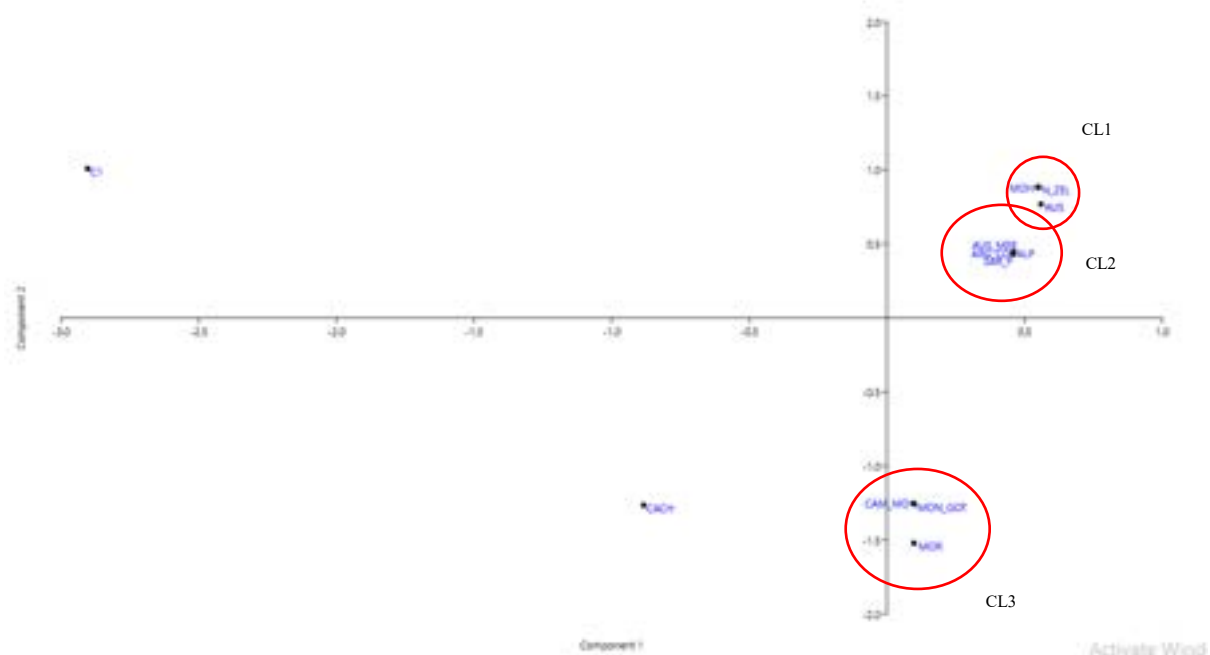


As one would expect, the two linen samples (LI_G and LINO) form a separate family at the distance of 1500. Cotton (CO_G) is, instead, not directly linked to linen, as was expected since their common vegetal origin. Cotton is, in fact, related to silk (C1) at 4000, and is also related to the sub-family that consists of Cashmere (CACH) related to the remaining wool samples, which are themselves divided into sub-groups. In particular, the Mongolian Camel (CAM_MO) and Mongolian Greyhorn (MON_GOT) form a cluster at a very low distance, almost 0, and are then correlated to the Moretta wool (MOR) at 1000. Other close relations at 0 appear in the Mohair and New Zealand cluster (MOH and N_ZEL), which is then related to the Australia wool, and in the cluster that includes the Australia Merinos, Sarda Piemontese, Argentina Corrientes, and Alpago (AUS_MER, SAR_P, ARG_CO, and ALP).

Unlike the statistical analysis of the ATR-FTIR data showed, the Mongolian (CAM_MO and MON_GOT) wools appear strictly related in the FORS data.

WOOL

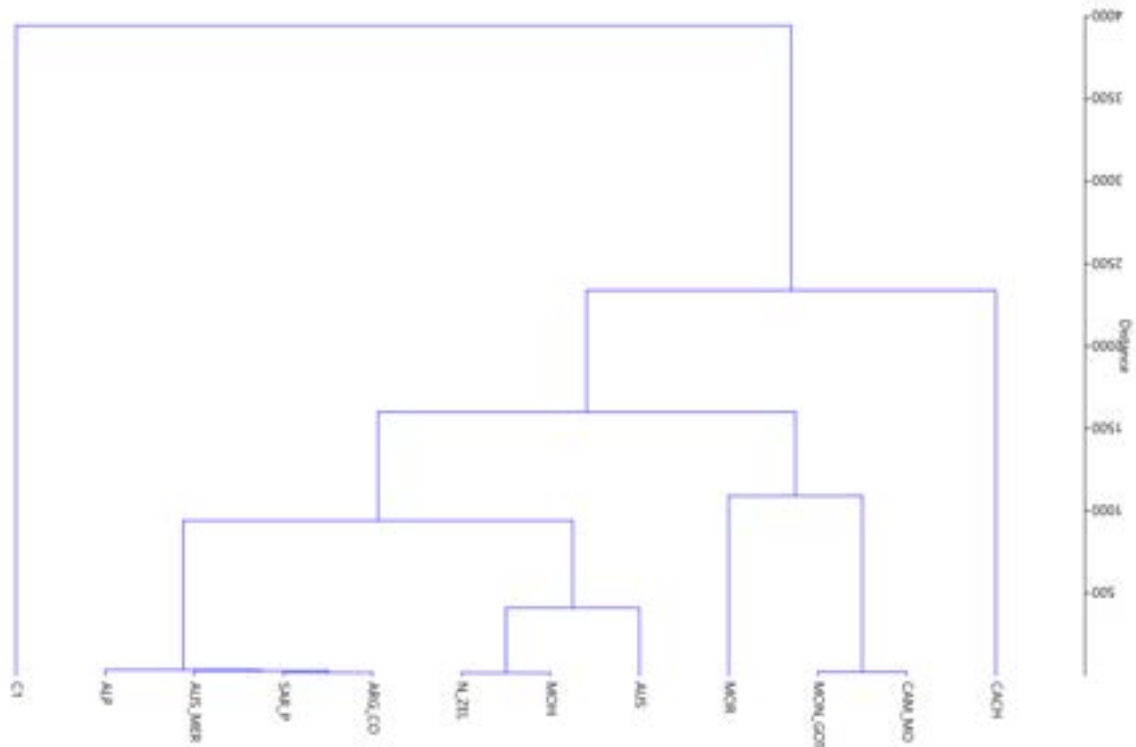
PCA



The scatter plot of the reference animal fibers (Eigenvalue scale). The graph shows the presence of three main clusters. Two families are influenced by the positive components of both PC1 and PC2, one (CL1) consisting of AUS_MER, ARG_CO, SAR_P, and ALP; the latter (CL2) instead includes MOH, N_ZEL, and AUS. The third family (CL3) is made of CAM_MO, MON_GOT, and MOR and shows the influence of the weights of the negative components of PC2 and the positive components of PC1.

Cashmere (CACH) and silk (C1) can be considered outliers since they don't belong to any of the wool clusters. Their placement at positive (C1) and negative (CACH) values for the PC2, which is the same placement on the PC2 of the three clusters, proves that there is at least a small similarity between wool, silk, and cashmere probably due to their protein origin.

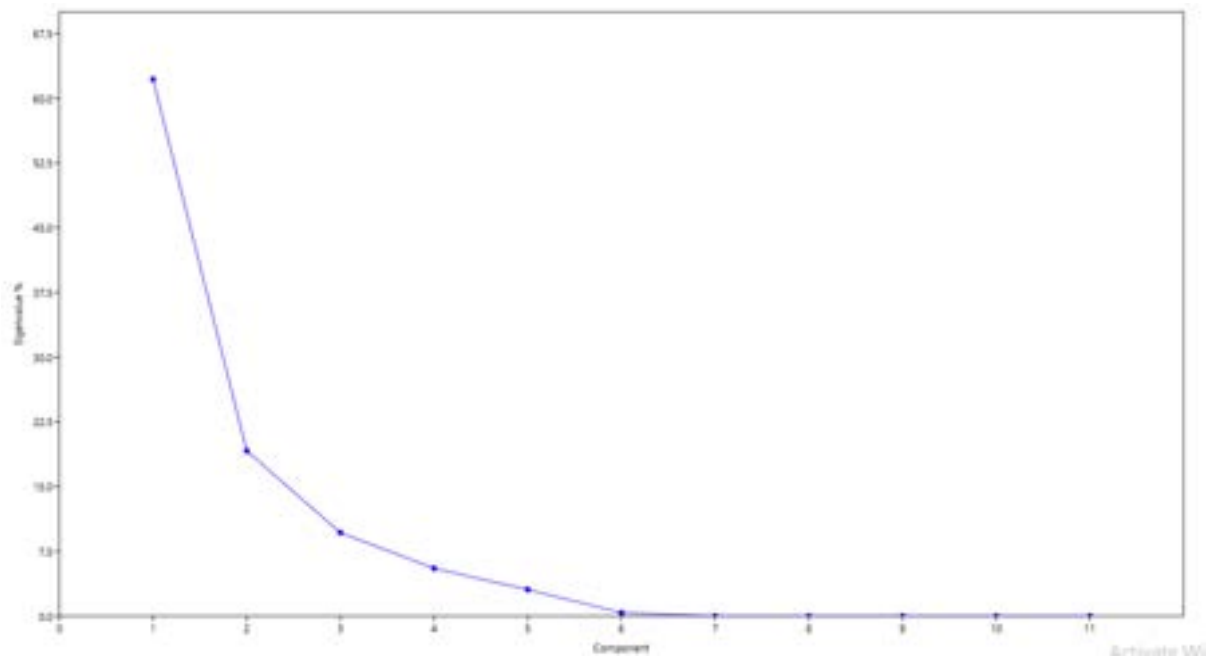
CLUSTER ANALYSIS



The dendrogram of the reference animal fibers. Silk (C1) again behaves as an outlier, relating at the furthest distance of 4000 to all the other animal fibers, while Cashmere (CACH) links to the other samples at 2500. The behavior of both C1 and CACH is confirmed in the scatter plot of the PCA analysis.

The remaining wools form a sub-family at 1500, which is divided in other sub-groups respectively at 1000, 900 ca, and 400 ca. Many wool species appear to be strictly related at the distance of 0, such as the Mongolian wools (CAM_MO and MON_GOT) which are related to the Moretta wool (MOR) at 1000, Mohair and New Zealand (MOH, N_ZEL), then related to the Australia wool (AUS) at 500. Finally, the Argentina Corrientes and Sarda Piemontese wools (ARG_CO and SAR_P), which are related to Australia Merinos and Alpago (AUS_MER and ALP). These sub-divisions are confirmed in the scatter plot of the PCA analysis, in which CAM_MO, MON_GOT, and MOR form the cluster CL3; AUS, MOH, and N_ZEL form the cluster CL2 and the remaining ARG_CO, SAR_P, AUS_MER, and ALP form the cluster CL1.

Figure XX shows the scree plot of the reference animal fibers. The scree plot of the animal reference fibers shows that the principal components to consider should be the PC1, PC2, and PC3.



Raman

ER - FTIR

Conclusions

This study focuses over the identification of the characteristic chemical features of different types of textiles. The non-invasive analyses were performed with Attenuated Total Reflectance and External Reflection FTIR (ATR and ER-FTIR), Raman spectroscopy, and Fiber Optics Reflectance Spectroscopy (FORS). Optical Microscopy was also used for a preliminary investigation of the morphology of the samples and allowed the identification of the characteristic features of the specimens, for instance the scaled surface that characterizes wool fibers, or the ribbon-like twists visible on the surface of a cotton fabric. The use of the non-invasive spectroscopic techniques allowed for the identification of the composition of the specimens and their differentiation based on the principal chemical groups characterizing their structure. The spectral data was then treated with statistical methods, namely Principal Component Analysis (PCA) and Cluster Analysis. This manipulation allowed to distinguish the identification capacities of the techniques. From the observation of the data, it can be deduced that each technique can distinguish animal and cellulosic fibers very clearly. But for what concerns the wool samples, the distinction does not include the differentiation between fine and coarse fibers.

Appendix XX

Table XX: reference ATR-FTIR peaks of wool

<i>Cm⁻¹</i>	<i>Assignments</i>
3272	OH / NH stretching Amide A / abs water (region 3000-4000)(Peets et al.) (Ding Li et al.)
2908	CH asymmetric stretching (Peets et al.)
1720	C=O bond (Zanini et al.)
1626	1643 in ref, Amide (-CONH-), C=O stretching (Peets et al.)
1516	C-N-H bending (combined C-N and N-H) (Peets et al.)
1445	C-H bending (Peets et al.)
1228	Amide III band (Zanini et al.) / C-N stretching (Peets et al.)
1037	C-O-C symmetric stretching (Peets et al.)

Table XX: reference ATR-FTIR peaks of silk

<i>Cm⁻¹</i>	<i>Assignments</i>
3271	N-H/O-H stretching Amide A (Peets et al.) (Ding Li et al.)
2918	C-H stretching (Peets et al.)
1720	C=O bond (Zanini et al.)

1616	Amide (-CONH-), C=O stretching (Peets et al.), Amide I band (F. Vilaplana et al.)
1515	C-N-H bending, combined C-N and N-H (Peets et al.), Amide II bands (F. Vilaplana et al.)
1439	C-H bending (Peets et al.)
1225	C-N stretching (Peets et al.) /Amide III (F. Vilaplana et al.)
1175	CH bending (F. Vilaplana et al.)
1061	C-O-C stretching (Peets et al.)
996-976	skeletal stretching (F. Vilaplana et al.)

Table XX: reference ATR-FTIR peaks of cotton

<i>Cm⁻¹</i>	<i>Assignments</i>
Band 3328-3283	3328 (ref 3323) O-H stretching (Peets et al.)
3334	O-H stretching (Ding Li et al.)
2905	C-H stretching (Ding Li et al.)
2899	C-H symmetric stretching (Peets et al.)
1620	HOH bending (Ding Li et al.)
1428	C-H bending (Peets et al.) / CH ₂ scissoring (K. Kavkler et al.) / COH bending in plane (1428, 1354) (Ding Li et al.)
1363	C-H bending (Peets et al.)
1372, 1335	COH and HCC bending of crystalline cellulose (K. Kavkler et al.)
1280	Indication of crystalline cellulose (K. Kavkler et al.)
1159	C-O stretching in C-O-C and C-O-H fragments (Peets et al.)
1098	C-O stretching in C-O-C and C-O-H fragments (Peets et al.)
1029	C-O stretching in C-O-C and C-O-H fragments (Peets et al.)
1157, 1098, 1025, 1050, 993	C-O stretching in C-O-C and C-O-H fragments (Peets et al.) (Ding Li et al.)
872	C-O stretching in C-O-C and C-O-H fragments (Peets et al.)
721	700-500 O-H out of plane bending (Peets et al.)
664	700-500 O-H out of plane bending (Peets et al.)
556	700-500 O-H out of plane bending (Peets et al.)
504	700-500 O-H out of plane bending (Peets et al.)

Table XX: reference ATR-FTIR peaks of linen

<i>Cm⁻¹</i>	<i>Assignments</i>
Band 3323	O-H stretching (Peets et al.)
3334	O-H stretching (Ding Li et al.)
2905	C-H stretching (Ding Li et al.)
2848	C-H symmetric stretching (Peets et al.)

1632	O-H bending (Peets et al.)
1620	HOH bending (Ding Li et al.)
1428	C-H bending (Peets et al.) / CH ₂ scissoring (K. Kavkler et al.) / COH bending in plane (1428, 1354) (Ding Li et al.)
1372, 1335	COH and HCC bending of crystalline cellulose (K. Kavkler et al.)
1363	C-H bending (Peets et al.)
1281	CH ₂ vibration (K. Kavkler et al.)
1157, 1098, 1025, 1050, 993	C-O stretching in C-O-C and C-O-H fragments (Peets et al.) (Ding Li et al.)
1025	C-O stretching in C-O-C and C-O-H fragments (Peets et al.)
661	700-500 O-H out of plane bending (Peets et al.)
555	700-500 O-H out of plane bending (Peets et al.)

Table XX: reference ATR-FTIR peaks of polyester

<i>Cm⁻¹</i>	<i>Assignments</i>
2969, 2907	C-H stretching (Peets et al.)
1711	C=O stretching (Peets et al.) (Ding Li et al.)
1504	Aromatic ring C=C stretching (Peets et al.)
1472, 1405, 1340	C-H bending (Peets et al.)
1241	Ester's C-O stretching (Peets et al.)
1093	C-O stretching (Peets et al.)
871	Aromatic ring C-H bending (Peets et al.)
718	C-H bending (C-H rocking in C-CH ₂ – fragment) (Peets et al.)

Table XX: reference ATR-FTIR peaks of viscose

<i>Cm⁻¹</i>	<i>Assignments</i>
3321	O-H stretching (Peets et al.)
2890	C-H symmetric stretching (Peets et al.)
1640	O-H bending (Peets et al.)
1366	C-H bending (Peets et al.)
1157, 1017, 895	C-O stretching in C-O-C and C-O-H fragments (Peets et al.)
700-500	O-H out of plane bending (Peets et al.)

Table XX: reference ATR-FTIR peaks of acetate

<i>Cm⁻¹</i>	<i>Assignments</i>
3490	O-H stretching (Peets et al.)
2942, 2888	C-H stretching (Peets et al.)
1735	C=O stretching (Peets et al.)
1431, 1366	C-H bending (Peets et al.)

1014	Acetate C-O-C stretching (Peets et al.)
1030, 899	C-O stretching (C-O-H/C-O-C) (Peets et al.)

Table XX: reference ATR-FTIR peaks of hemp

<i>Cm⁻¹</i>	<i>Assignments</i>
3490	O-H stretching (Peets et al.)
2942, 2888	C-H stretching (Peets et al.)
1735	C=O stretching (Peets et al.)
1372, 1335	COH and HCC bending of crystalline cellulose (K. Kavkler et al.)
1430	CH ₂ scissoring of cellulose (K. Kavkler et al.)
1160	C-O stretching (K. Kavkler et al.)

Table XX: reference Raman peaks of wool

<i>Cm⁻¹</i>	<i>Assignments</i>
2931	C-H stretching (D. Puchowicz, M. Cieslak)
1665	Amide I, C=O and COO stretching (D. Puchowicz, M. Cieslak)
1463	COO bending (D. Puchowicz, M. Cieslak)
1311	C-H bending (D. Puchowicz, M. Cieslak)
1210	N-H deformation, CN elonging (D. Puchowicz, M. Cieslak)

Table XX: reference Raman peaks of silk

<i>Cm⁻¹</i>	<i>Assignments</i>
2935	C-H stretching (D. Puchowicz, M. Cieslak)
1665	Amide I, C=O and COO stretching (D. Puchowicz, M. Cieslak)
1611	C=C stretching (D. Puchowicz, M. Cieslak)
1449	CH ₂ bending scissors (D. Puchowicz, M. Cieslak)
1402	CH ₂ bending (D. Puchowicz, M. Cieslak)
1226	Amide III, CH ₂ bending (D. Puchowicz, M. Cieslak)
1083	CC skeletal (D. Puchowicz, M. Cieslak)
976	CH ₂ (D. Puchowicz, M. Cieslak)
853	C-C skeletal tyrosine (D. Puchowicz, M. Cieslak)

647	Amide IV, NCH bending (D. Puchowicz, M. Cieslak)
499	CCC deformation, combination of backbone deformations with pendant chains (D. Puchowicz, M. Cieslak)

Table XX: reference Raman peaks of cotton

<i>Cm⁻¹</i>	<i>Assignments</i>
2903	C-H stretching band (D. Puchowicz, M. Cieslak)
1460	$\delta(\text{CH}_2)$ scissor, $\delta(\text{COH})$ 1° and 2° alcohol groups (K. Kavler, A. Demsar)
1611	C=C stretching (D. Puchowicz, M. Cieslak)
1377	$\delta(\text{CH}_2)$ (K. Kavler, A. Demsar)
1288	$\delta(\text{CH}_2)$ twisting, long chain (K. Kavler, A. Demsar)
1117	$\nu(\text{COC})$ symmetric, glycosidic (K. Kavler, A. Demsar)
1095	$\nu(\text{COC})$ asymmetric, glycosidic, ring breathing, skeletal (K. Kavler, A. Demsar)
999	$\rho(\text{CH}_2)$ (rotating) (K. Kavler, A. Demsar)
460	$\delta(\text{CCO})$, $\delta(\text{CCC})$, ring (K. Kavler, A. Demsar) / 460 CCO band deformation and skeletal band (D. Puchowicz, M. Cieslak)
437	$\delta(\text{CCO})$, $\delta(\text{CCC})$, ring deformation (K. Kavler, A. Demsar) (D. Puchowicz, M. Cieslak)
382	$\delta(\text{CCC})$, symmetric, ring deformation (K. Kavler, A. Demsar)

Table XX: reference Raman peaks of linen

<i>Cm⁻¹</i>	<i>Assignments (K. Kavkler, A. Demsar) (D. Puchowicz, M. Cieslak)</i>
2894	2903 in ref, CH stretching band
1478	$\delta(\text{CH}_2)$ scissors
1410	$\delta(\text{CH}_2)$
1380	$\delta(\text{CH}_2)$
1335	$\delta(\text{CH}_2)$ wagging, $\delta(\text{COH})$, lignin
1289	$\delta(\text{CH}_2)$ twisting, long-chain hydrocarbons (wax) (?)
1145	$\nu(\text{CC})$, $\nu(\text{CO})$ asymmetric, ring breathing (glucopyranose)
1120	$\nu(\text{COC})$ symmetric, glycosidic, ring breathing, skeletal
1095	$\nu(\text{COC})$ symmetric, glycosidic, ring breathing, skeletal
994	$\rho(\text{CH}_2)$ / 1001 in ref, HCO skeletal rotating
969	
896	$\delta(\text{HCC})$, $\delta(\text{HCO})$; cluster of peaks – primary methine bending
519	$\delta(\text{COC})$, glycosidic linkage/CCC ring deformation
456	$\delta(\text{CCO})$, $\delta(\text{CCC})$, ring deformation, skeletal bending
436	$\delta(\text{CCO})$, $\delta(\text{CCC})$, ring deformation
380	$\delta(\text{CCC})$, symmetric, ring deformation
329	$\delta(\text{CCC})$, symmetric, ring deformation, skeletal bending

Table XX: reference Raman peaks of polyester

<i>Cm⁻¹</i>	<i>Assignments (Li-Ling Cho, 2007)</i>
1737/1728	C=O stretching, CCC bending (ring)
1624	C=C stretching
1615	Ring deformation, symmetric stretching C=C
1288	CC stretching ring, CO stretching
1108	Combination of ring C-C stretching (crystallinity of PET)
1095	Stretching COC asymmetric, stretching CC
858	Stretching COC
795	Ring deformation
633	Ring deformation
274	CC stretching, CCC bending

Table XX: reference Raman peaks of viscose

<i>Cm⁻¹</i>	<i>Assignments (Li-Ling Cho, 2007)</i>
2906	CH, CH ₂ stretching cellulose
1478	H-C-H and H-O-C bending cellulose
1108	C-C and C-O stretching cellulose
910	C-O-C in plane, symmetric cellulose
516-379	Skeletal C-O-C, C-C-C, O-C-C and O-C-O bending cellulose
650	C-S-C stretching

Table XX: reference Raman peaks of hemp

Table XX: reference FORS peaks of wool

<i>Wavelengths (nm)</i>	<i>Assignments</i>
2179	2100-2400 region in ref, alpha helix structure of wool (J.K Delaney et al.)
2289	2275 in ref, CO stretching + OH stretching ad CH ₂ bending and stretching
2350	2100-2400 region in ref, alpha helix structure of wool (J.K Delaney et al.)
1578	overtone and combination amide features (J.K Delaney et al.)
1503	alpha-helix structure of wool, OH overtone (J.K Delaney et al.)
1186	3rd overtone CH (D. Quintero Balbas et al.), CH bonds of proteinaceous origin (M.A. Maynez-Rojas et al.)

Table XX: reference FORS peaks of silk

<i>Wavelength (nm)</i>	<i>Assignments</i>
1507	1502 in ref, NH stretching from the Amide A crystalline and 1st overtone stretching of the Amide II; Amide group in beta-sheet (D. Quinter Balbas et al.)
1539	Amide group of silk's beta-sheet and OH overtone (J.K. Delaney et al.)
1578	Amide group in beta-sheet, OH and NH overtones and combination bands (D. Quinter Balbas et al.), Amide group of silk's beta-sheet (J.K. Delaney et al.)
2203	2205 in ref, vibrational features of beta-sheet (J.K. Delaney et al.)

Table XX: reference FORS peaks of cotton

<i>Wavelength (nm)</i>	<i>Assignments</i>
1219	CH bonds in cellulose (M.A. Maynez-Rojas et al)
1219	CH bonds in cellulose (M.A. Maynez-Rojas et al), 2nd overtone CH, stretching CH and CH2 from cellulose (D. Quintero Balbas et al.)
1490	OH overtone of cellulose and water (J.K. Delaney et al.), stretching from semi-crystalline cellulose; the band at 1490 ca from the 1st overtone of the OH stretching is characteristic of cotton (D. Quintero Balbas et al.)
2098	2103 in ref, major feature of cellulose = OH and CH deformation modes and OH stretching (J.K. Delaney et al.)
2274	narrow feature, CO stretching + OH stretching and CH2 bending and CH2 stretching (J.K. Delaney et al.)

Table XX: reference FORS peaks of linen

<i>Wavelength (nm)</i>	<i>Assignments</i>
1219	CH bonds in cellulose (M.A. Maynez-Rojas et al)
1490	OH overtone of cellulose and water (J.K. Delaney et al.)
2098	2103 in ref, major feature of cellulose = OH and CH deformation modes and OH stretching (J.K. Delaney et al.)
2274	narrow feature, CO stretching + OH stretching and CH2 bending and CH2 stretching (J.K. Delaney et al.)

Bibliography

- Bacci, M., Casini, A., Cucci, C., Picollo, M., Radicati, B., & Vervat, M. (2003). *Non-invasive spectroscopic measurements on the Il ritratto della figliastra by Giovanni Fattori: identification of pigments and colourimetric analysis*. <https://doi.org/10.1016/j.culher.2003.09.003>
- Bergfjord, C., & Holst, B. (2010). A procedure for identifying textile bast fibres using microscopy: Flax, nettle/ramie, hemp and jute. *Ultramicroscopy*, *110*, 1192–1197. <https://doi.org/10.1016/j.ultramic.2010.04.014>
- Campagnol, I. (2007). Venice 1870-1930: The rediscovery of textile arts. *Dress*, *34*(1), 33–47. <https://doi.org/10.1179/036121107805252935>
- Cho, L.-L. (2002). Identification of textile fiber by Raman microspectroscopy. In *FORENSIC SCIENCE JOURNAL SINCE* (Vol. 6, Issue 1). <https://www.researchgate.net/publication/237772459>
- Delaney, J. K., Ricciardi, P., Glinsman, L. D., Facini, M., Thoury, M., Palmer, M., & De La Rie, E. R. (2014). Use of imaging spectroscopy, fiber optic reflectance spectroscopy, and X-ray fluorescence to map and identify pigments in illuminated manuscripts. [Http://Dx.Doi.Org/10.1179/2047058412Y.0000000078](http://Dx.Doi.Org/10.1179/2047058412Y.0000000078), *59*(2), 91–101. <https://doi.org/10.1179/2047058412Y.0000000078>
- Delaney, J. K., Ricciardi, P., Glinsman, L., Palmer, M., & Burke, J. (2016). Use of near infrared reflectance imaging spectroscopy to map wool and silk fibres in historic tapestries. *Analytical Methods*, *8*(44), 7886–7890. <https://doi.org/10.1039/c6ay02066f>
- Derrick, M. R., & Landry, J. M. (1999). *Scientific Tools for Conservation Infrared Spectroscopy in Conservation Science*.
- Ding, L., Gong, T., Yang, qin, Wu, N., Wang, B., Zhao, Z., & Lu, X. (2021). Non-destructive fiber type identification in ancient textiles using portable near-infrared fiber optic reflectance spectroscopy. *Sciences of Conservation and Archaeology*.
- Favaro, B., Balliana, E., Rigoni, F., & Zendri, E. (2021). A preliminary evaluation of chemical interaction between sanitizing products and silk. *Journal of Cultural Heritage*, *51*, 1–13. <https://doi.org/10.1016/j.culher.2021.06.012>
- Geminiani, L., Campione, F. P., Canevali, C., Corti, C., Giussani, B., Gorla, G., Luraschi, M., Recchia, S., & Rampazzi, L. (2023). Historical Silk: A Novel Method to Evaluate Degumming with Non-Invasive Infrared Spectroscopy and Spectral Deconvolution. *Materials*, *16*(5). <https://doi.org/10.3390/ma16051819>
- Geminiani, L., Campione, F. P., Corti, C., Luraschi, M., Motella, S., Recchia, S., & Rampazzi, L. (2022). Differentiating between Natural and Modified Cellulosic Fibres Using ATR-FTIR Spectroscopy. *Heritage*, *5*(4), 4114–4139. <https://doi.org/10.3390/heritage5040213>
- Greaves, P., & Saville, B. (n.d.). *Microscopy of Textile Fibres*.
- Hager, E., Farber, C., & Kurouski, D. (2018). Forensic identification of urine on cotton and polyester fabric with a hand-held Raman spectrometer. *Forensic Chemistry*, *9*, 44–49. <https://doi.org/10.1016/j.forc.2018.05.001>
- Handke, M., Milosevic, M., & Harrick, N. J. (1990). *External reflection Fourier transform infrared spectroscopy: theory and experimental problems* (Vol. 1, Issue 2).

- Kavkler, K., & Demšar, A. (2011a). Examination of cellulose textile fibres in historical objects by micro-Raman spectroscopy. *Spectrochimica Acta - Part A: Molecular and Biomolecular Spectroscopy*, 78(2), 740–746. <https://doi.org/10.1016/j.saa.2010.12.006>
- Kavkler, K., & Demšar, A. (2011b). Examination of cellulose textile fibres in historical objects by micro-Raman spectroscopy. *Spectrochimica Acta - Part A: Molecular and Biomolecular Spectroscopy*, 78(2), 740–746. <https://doi.org/10.1016/j.saa.2010.12.006>
- Kavkler, K., Gunde-Cimerman, N., Zalar, P., & Demšar, A. (2011a). FTIR spectroscopy of biodegraded historical textiles. *Polymer Degradation and Stability*, 96(4), 574–580. <https://doi.org/10.1016/j.polymdegradstab.2010.12.016>
- Kavkler, K., Gunde-Cimerman, N., Zalar, P., & Demšar, A. (2011b). FTIR spectroscopy of biodegraded historical textiles. *Polymer Degradation and Stability*, 96(4), 574–580. <https://doi.org/10.1016/j.polymdegradstab.2010.12.016>
- Kirmizi, B., Colomban, P., & Blanc, M. (2010). On-site analysis of Limoges enamels from sixteenth to nineteenth centuries: An attempt to differentiate between genuine artefacts and copies. *Journal of Raman Spectroscopy*, 41(10), 1240–1247. <https://doi.org/10.1002/JRS.2566>
- Leona, M., & Winter, J. (2013). *Fiber optics reflectance spectroscopy: a unique tool for the investigation of Japanese paintings*. <https://doi.org/10.1179/sic.2001.46.3.153>
- Luo, J., Lu, K., Chen, Y., & Zhang, B. (2021). Automatic identification of cashmere and wool fibers based on microscopic visual features and residual network model. *Micron*, 143, 103023. <https://doi.org/10.1016/j.micron.2021.103023>
- Markova Ivana. (2019). *Textile Fiber Microscopy*.
- Mather, R. R., & Wardman, R. H. (2015). *The chemistry of textile fibres*.
- Maynez-Rojas, M. A., Casanova-González, E., & Ruvalcaba-Sil, J. L. (2017a). *Identification of natural red and purple dyes on textiles by Fiber-optics Reflectance Spectroscopy*. <https://doi.org/10.1016/j.saa.2017.02.019>
- Maynez-Rojas, M. A., Casanova-González, E., & Ruvalcaba-Sil, J. L. (2017b). Identification of natural red and purple dyes on textiles by Fiber-optics Reflectance Spectroscopy. *Spectrochimica Acta - Part A: Molecular and Biomolecular Spectroscopy*, 178, 239–250. <https://doi.org/10.1016/j.saa.2017.02.019>
- Nodari, L., & Ricciardi, P. (2019). Non-invasive identification of paint binders in illuminated manuscripts by ER-FTIR spectroscopy: a systematic study of the influence of different pigments on the binders' characteristic spectral features. *Heritage Science*, 7(1). <https://doi.org/10.1186/S40494-019-0249-Y>
- Notayi, M., Hunter, L., Engelbrecht, J. A., Botha, A. F., Minnaar, E. G., Lee, M. E., & Erasmus, R. (2022a). The Application of Raman Spectroscopic Ratiometric Analysis for Distinguishing between Wool and Mohair. *Journal of Natural Fibers*, 19(15), 11536–11546. <https://doi.org/10.1080/15440478.2022.2028212>
- Notayi, M., Hunter, L., Engelbrecht, J. A., Botha, A. F., Minnaar, E. G., Lee, M. E., & Erasmus, R. (2022b). The Application of Raman Spectroscopic Ratiometric Analysis for Distinguishing between Wool and Mohair. *Journal of Natural Fibers*, 19(15), 11536–11546. <https://doi.org/10.1080/15440478.2022.2028212>

- Oras, E., Anderson, J., Tõrv, M., Vahur, S., Rammo, R., Remmer, S., Mölder, M., Malve, M., Saag, L., Saage, R., Teearu-Ojakäär, A., Peets, P., Tambets, K., Metspalu, M., Lees, D. C., Barclay, M. V. L., Hall, M. J. R., Ikram, S., & Piombino-Mascali, D. (2020). Multidisciplinary investigation of two Egyptian child mummies curated at the University of Tartu Art Museum, Estonia (Late/Graeco-Roman Periods). *PLoS ONE*, *15*(1). <https://doi.org/10.1371/journal.pone.0227446>
- Peets, P., Leito, I., Pelt, J., & Vahur, S. (2017a). Identification and classification of textile fibres using ATR-FT-IR spectroscopy with chemometric methods. *Spectrochimica Acta - Part A: Molecular and Biomolecular Spectroscopy*, *173*, 175–181. <https://doi.org/10.1016/j.saa.2016.09.007>
- Peets, P., Leito, I., Pelt, J., & Vahur, S. (2017b). Identification and classification of textile fibres using ATR-FT-IR spectroscopy with chemometric methods. *Spectrochimica Acta - Part A: Molecular and Biomolecular Spectroscopy*, *173*, 175–181. <https://doi.org/10.1016/j.saa.2016.09.007>
- Puchowicz, D., & Cieslak, M. (2022a). Raman Spectroscopy in the Analysis of Textile Structures. In *Recent Developments in Atomic Force Microscopy and Raman Spectroscopy for Materials Characterization*. IntechOpen. <https://doi.org/10.5772/intechopen.99731>
- Puchowicz, D., & Cieslak, M. (2022b). Raman Spectroscopy in the Analysis of Textile Structures. In *Recent Developments in Atomic Force Microscopy and Raman Spectroscopy for Materials Characterization*. IntechOpen. <https://doi.org/10.5772/intechopen.99731>
- Quintero Balbas, D., Lanterna, G., Cirrincione, C., Fontana, R., & Striova, J. (2022a). Non-invasive identification of textile fibres using near-infrared fibre optics reflectance spectroscopy and multivariate classification techniques. *European Physical Journal Plus*, *137*(1). <https://doi.org/10.1140/epjp/s13360-021-02267-1>
- Quintero Balbas, D., Lanterna, G., Cirrincione, C., Fontana, R., & Striova, J. (2022b). Non-invasive identification of textile fibres using near-infrared fibre optics reflectance spectroscopy and multivariate classification techniques. *European Physical Journal Plus*, *137*(1). <https://doi.org/10.1140/epjp/s13360-021-02267-1>
- Ravindran, T. R., Arora, A. K., Ramya, S., Subba Rao, R. V., & Raj, B. (2011). Raman spectroscopic study of medieval Indian art of 17th century. *Journal of Raman Spectroscopy*, *42*(4), 803–807. <https://doi.org/10.1002/JRS.2776>
- Rousaki, A., & Vandenabeele, P. (2021). In situ Raman spectroscopy for cultural heritage studies. *Journal of Raman Spectroscopy*, *52*(12), 2178–2189. <https://doi.org/10.1002/JRS.6166>
- Rubelli. (2023). *Rubelli, la nostra storia* . <https://www.rubelli.com/it/storia>
- Shahid, M., Wertz, J., Degano, I., Aceto, M., Khan, I., & Quye, A. (2019). *Analytical methods for determination of anthraquinone dyes in historical textiles: A review*. <https://doi.org/10.1016/j.aca.2019.07.009>
- Śmigielska-Kamińska, D., Kumirska, J., Wąs-Gubała, J., & Stepnowski, P. (2020). The Identification of Cotton Fibers Dyed with Reactive Dyes for Forensic Purposes. In *Molecules* (Vol. 25, Issue 22). MDPI. <https://doi.org/10.3390/molecules25225435>
- Stuart H. Barbara. (2007). *Analytical Techniques in Materials Conservation*.
- Tessitura Luigi Bevilacqua. (2020, January 27). *Le origini dei tessuti pregiati a Venezia* .
- Timar-Balazsy, A., & Eastop, D. (2011). *Chemical Principles of Textiles Conservation*. Routledge.

- Tournié, A., Prinsloo, L. C., Paris, C., Colomban, P., & Smith, B. (2011). The first in situ Raman spectroscopic study of San rock art in South Africa: procedures and preliminary results. *Journal of Raman Spectroscopy*, *42*(3), 399–406. <https://doi.org/10.1002/JRS.2682>
- Ueland, M., Howes, J. M., Forbes, S. L., & Stuart, B. H. (2017). Degradation patterns of natural and synthetic textiles on a soil surface during summer and winter seasons studied using ATR-FTIR spectroscopy. *Spectrochimica Acta - Part A: Molecular and Biomolecular Spectroscopy*, *185*, 69–76. <https://doi.org/10.1016/j.saa.2017.05.044>
- Vetter, W., Frühmann, B., Cappa, F., & Schreiner, M. (2021). Materials and techniques used for the “Vienna Moamin”: multianalytical investigation of a book about hunting with falcons from the thirteenth century. *Heritage Science*, *9*(1). <https://doi.org/10.1186/S40494-021-00553-W>
- Vetter, W., Latini, I., & Schreiner, M. (2019). Azurite in medieval illuminated manuscripts: a reflection-FTIR study concerning the characterization of binding media. *Heritage Science*, *7*(1). <https://doi.org/10.1186/S40494-019-0262-1>
- Vilaplana, F., Nilsson, J., Sommer, D. V. P., & Karlsson, S. (2015). Analytical markers for silk degradation: comparing historic silk and silk artificially aged in different environments. *Analytical and Bioanalytical Chemistry*, *407*(5), 1433–1449. <https://doi.org/10.1007/s00216-014-8361-z>
- Wojciechowska, E., Rom, M., Włochowicz, A., Wysocki, M., & Wesełucha-Birczyńska, A. (2004). The use of Fourier transform-infrared (FTIR) and Raman spectroscopy (FTR) for the investigation of structural changes in wool fibre keratin after enzymatic treatment. *Journal of Molecular Structure*, *704*(1–3), 315–321. <https://doi.org/10.1016/j.molstruc.2004.03.044>
- Zanini, S., Citterio, A., Leonardi, G., & Riccardi, C. (2018). Characterization of atmospheric pressure plasma treated wool/cashmere textiles: Treatment in nitrogen. *Applied Surface Science*, *427*, 90–96. <https://doi.org/10.1016/j.apsusc.2017.07.280>
- Zhao, H., Wang, Y., Liu, S., Li, K., & Gao, W. (2019a). Spectral reflectance characterization and fiber type discrimination for common natural textile materials using a portable spectroradiometer. *Journal of Archaeological Science*, *111*. <https://doi.org/10.1016/j.jas.2019.105026>
- Zhao, H., Wang, Y., Liu, S., Li, K., & Gao, W. (2019b). Spectral reflectance characterization and fiber type discrimination for common natural textile materials using a portable spectroradiometer. *Journal of Archaeological Science*, *111*. <https://doi.org/10.1016/j.jas.2019.105026>